LIST OF PUBLICATIONS

PUBLICATIONS **[32, Citations > 829, h-Index: 14, i10-Index: 16]**

- **Research/Review Articles**

30) Yadav, Amit K; Verma, Damini; Solanki, Pratima. Structuring two-dimensional MoS2 nanosheets @reduced graphene oxide interface for high throughput electrochemical biosensing of cancer biomarker in serum samples. **ACS Applied Biomaterials [Accepted for publication]**.

29) Yadav, A.K., Verma, D., Kumar, A., Bhatt, A.N. and Solanki, P.R., 2023. Biocompatible epoxysilane substituted polymer-based nano biosensing platform for label-free detection of cancer biomarker SP17 in patient serum samples. **International Journal of Biological Macromolecules**, p.124325. [**IF- 8.025**] doi.org/10.1016/j.ijbiomac.2023.124325

28) Verma, A.K., Noumani, A., **Yadav, A.K.** and Solanki, P.R. FRET Based Biosensor: Principle Applications Recent Advances and Challenges. **Diagnostics.** 2023 April. ***[IF-3.992]*** https://doi.org/10.3390/diagnostics13081375

27) Sen RK, Prabhakar P, Mayandi V, Dwivedi N, **Yadav AK**, Solanki PR, Gupta A, Gowri VS, Lakshminarayanan R, Verma NK, Mondal DP. Metal mediated high performance antimicrobial hydrogel films for wound infection management: Zn, Cu, and Mg versus Ag and Au. **Materials Chemistry and Physics**. 2023 Jan 10:127365. ***[IF-4.778]*** *doi.org/10.1016/j.matchemphys.2023.127365*

26) Kumar, A., Sah, D.K., Khanna, K., Rai, Y., **Yadav, A.K.,** Ansari, M.S. and Bhatt, A.N., 2022. A calcium and zinc composite alginate hydrogel for pre-hospital hemostasis and wound care. **Carbohydrate Polymers**, p.120186. ***[IF-10.723]*** *doi.org/10.1016/j.carbpol.2022.120186*

25) Prabhakar P, Sen RK, Patel M, Dwivedi N, Singh S, Chouhan M, **Yadav AK**, Mondal DP, Solanki PR, Srivastava AK, Dhand C. Development of Copper Impregnated Bio-Inspired Hydrophobic Antibacterial Nanocoatings for Textiles. **Colloids and Surfaces B: Biointerfaces**. 2022 Oct 10:112913. ***[IF-5.999]*** *doi.org/10.1016/j.colsurfb.2022.112913*

24) Yadav AK, Verma D, Dalal N, Kumar A, Solanki PR. Molecularly imprinted polymer-based nanodiagnostics for clinically pertinent bacteria and virus detection for future pandemics**. Biosensors and Bioelectronics: X. 2022 Oct 8:100257. *[Cite score-7.3]*** *doi.org/10.1016/j.biosx.2022.100257*

23) Shekhar S, **Yadav, A.K.,** Khosla A, Solanki PR. Interleukins Profiling for Biosensing Applications: Possibilities and the Future of Disease Detection. **ECS Sensors Plus**. 2022 Sep 15. **[Equal contribution]** *doi.org/10.1149/2754-2726/ac9227*

22) Yadav AK, Verma D, Sajwan RK, Poddar M, Yadav SK, Verma AK, Solanki PR. Nanomaterial-Based Electrochemical Nanodiagnostics for Human and Gut Metabolites Diagnostics: Recent Advances and Challenges. **Biosensors**. 2022 Sep;12(9):733. ***[IF- 5.743]*** *doi.org/10.3390/bios12090733*

21) Verma D, **Yadav AK,** Chaudhary N, Mukherjee MD, Kumar P, Kumar A, Solanki PR. Recent Advances in Understanding SARS-CoV-2 Infection and Updates on Potential Diagnostic and Therapeutics for COVID-19. **Coronavirus**. 2022. **[Equal contribution]** *10.2174/2666796703666220302143102*

20) Bisht, N., Dwivedi, N., Kumar, P., Venkatesh, M., **Yadav, A.K.,** Mishra, D., Solanki, P., Verma, N.K., Lakshminarayanan, R., Ramakrishna, S. and Mondal, D.P., 2022. Recent Advances in Copper and Copper-Derived Materials for Antimicrobial Resistance and Infection Control. **Current Opinion in Biomedical Engineering**, p.100408. ***[IF- 4.164]*** *doi.org/10.1016/j.cobme.2022.100408*

19) Verma, D., Singh, K.R., **Yadav, A.K.**, Nayak, V., Singh, J., Solanki, P.R. and Singh, R.P., 2022. Internet of things (IoT) in nano-integrated wearable biosensor devices for healthcare applications. **Biosensors and Bioelectronics: X**, p.100153. ***[Cite score- 7.3]*** *doi.org/10.1016/j.biosx.2022.100153*

18) Yadav, A.K., Gulati, P., Sharma, R., Thakkar, A. and Solanki, P.R., 2022. Fabrication of alkoxysilane substituted polymer-modified disposable biosensing platform: Toward sperm protein 17 sensing as a new cancer biomarker. ***Talanta***, p.123376. ***[IF- 6.556]*** *doi.org/10.1016/j.talanta.2022.123376*

17) Verma, D., **Yadav, A.K.,** Rathee, G., Dhingra, K., Mukherjee, M.D. and Solanki, P.R., 2022. Prospects of Nanomaterial-Based Biosensors: A Smart Approach for Bisphenol-A Detection in Dental Sealants. ***Journal of The Electrochemical Society***. **[Equal contribution; IF- 4.316]** *doi.org/10.1149/1945-7111/ac51fc*

16) Yadav, A.K., Verma, D., Chaudhary, N., Kumar, A. and Solanki, P.R., 2022. Aptamer based switches: A futuristic approach for Helicobacter pylori detection. ***Materials Letters***, *308*, p.131239. **[IF- 3.574]** *doi.org/10.1016/j.matlet.2021.131239*

15) Sen, R.K., Prabhakar, P., Bisht, N., Patel, M., Mishra, S., **Yadav, A.K**., Venu, D.V., Gupta, G.K., Solanki, P.R., Ramakrishnan, S. and Mondal, D., 2021. 2D Materials-Based

Aptamer Biosensors: Present Status and Way Forward. ***Current medicinal chemistry*****. [IF- 4.740]** *10.2174/0929867328666211213115723*

14) Yadav, A.K., Verma, D. and Solanki, P.R., 2021. Electrophoretically deposited L-cysteine functionalized MoS2@MWCNT nanocomposite platform: a smart approach toward highly sensitive and label-free detection of gentamicin. ***Materials Today Chemistry***, *22*, p.100567. **[IF- 7.613]** *doi.org/10.1016/j.mtchem.2021.100567*

13) Chaudhary, N., **Yadav, A.K.,** Sharma, J.G. and Solanki, P.R., 2021. Designing and characterization of a highly sensitive and selective biosensing platform for ciprofloxacin detection utilizing lanthanum oxide nanoparticles. ***Journal of Environmental Chemical Engineering***, *9*(6), p.106771. **[IF- 7.968]** *doi.org/10.1016/j.jece.2021.106771*

12) Yadav, A.K., Verma, D., Lakshmi, G.B.V.S., Eremin, S. and Solanki, P.R., 2021. Fabrication of label-free and ultrasensitive electrochemical immunosensor based on molybdenum disulfide nanoparticles modified disposable ITO: An analytical platform for antibiotic detection in food samples. ***Food Chemistry***, *363*, p.130245. **[IF- 9.231]** *doi.org/10.1016/j.foodchem.2021.130245*

11) Sharma, M., Kumari, M., Rani, S., **Yadav, A.K.,** Solanki, P.R. and Mozumdar, S., 2021. Influence of pH, β-Cyclodextrin, and Metal Ions on the Solubility and Stability of the Medicinally Competent Isoxazole Derivative of Curcumin: A Photophysical Study. ***ACS Applied Bio Materials***, *4*(12), pp.8407-8423. **[Cite score- 4.9]** *doi.org/10.1021/acsabm.1c00957*

10) Dalal, N., Jalandra, R., Bayal, N., **Yadav, A.K.,** Sharma, M., Makharia, G.K., Kumar, P., Singh, R., Solanki, P.R. and Kumar, A., 2021. Gut microbiota-derived metabolites in CRC progression and causation. ***Journal of Cancer Research and Clinical Oncology***, *147*(11), pp.3141-3155. **[IF- 4.332]** *doi.org/10.1007/s00432-021-03729-w*

9) Jalandra, R., Dalal, N., **Yadav, A.K.,** Verma, D., Sharma, M., Singh, R., Khosla, A., Kumar, A. and Solanki, P.R., 2021. Emerging role of trimethylamine-N-oxide (TMAO) in colorectal cancer. ***Applied Microbiology and Biotechnology***, *105*(20), pp.7651-7660. **[IF- 5.560]** *doi.org/10.1007/s00253-021-11582-7*

8) Verma, D., **Yadav, A.K.,** Mukherjee, M.D. and Solanki, P.R., 2021. Fabrication of a sensitive electrochemical sensor platform using reduced graphene oxide-molybdenum trioxide nanocomposite for BPA detection: An endocrine disruptor. ***Journal of Environmental Chemical Engineering***, *9*(4), p.105504. **[IF- 7.968]** *doi.org/10.1016/j.jece.2021.105504*

7) Yadav, A.K., Verma, D., Kumar, A., Kumar, P. and Solanki, P.R., 2021. The perspectives of biomarker-based electrochemical immunosensors, artificial intelligence and the Internet of Medical Things towardáCOVID-19 diagnosis and management. ***Materials Today Chemistry***, *20*, p.100443. **[IF- 7.613]** *doi.org/10.1016/j.mtchem.2021.100443*

6) Vashistha, V., Bhardwaj, S., Kumar, A., Yadav, A.K., Yadav, B.K., Yadav, A.K., 2021. HnRNPA1 isoform bring diversity in glioma cell survival. **Global Journal for Research Analysis. [IF-5.956]** *10.36106/gjra*

5) Chauhan, D., **Yadav, A.K**. and Solanki, P.R., 2021. Carbon cloth-based immunosensor for detection of 25-hydroxy vitamin D3. ***Microchimica Acta***, *188*(4), pp.1-11. **[IF- 6.408]** *doi.org/10.1007/s00604-021-04751-y*

4) Verma, D., Chauhan, D., Das Mukherjee, M., Ranjan, K.R., **Yadav, A.K**. and Solanki, P.R., 2021. Development of MWCNT decorated with green synthesized AgNps-based electrochemical sensor for highly sensitive detection of BPA. ***Journal of Applied Electrochemistry***, *51*(3), pp.447-462. **[IF- 2.925]** *doi.org/10.1007/s10800-020-01511-3*

3) Lakshmi, G.B.V.S., **Yadav, A.K**., Mehlawat, N., Jalandra, R., Solanki, P.R. and Kumar, A., 2021. Gut microbiota derived trimethylamine N-oxide (TMAO) detection through molecularly imprinted polymer-based sensor. ***Scientific reports***, *11*(1), pp.1-14. **[equal contribution; IF- 4.996]** *doi.org/10.1038/s41598-020-80122-6*

2) Jalandra, R., **Yadav, A.K.,** Verma, D., Dalal, N., Sharma, M., Singh, R., Kumar, A. and Solanki, P.R., 2020. Strategies and perspectives to develop SARS-CoV-2 detection methods and diagnostics. ***Biomedicine & Pharmacotherapy***, *129*, p.110446. **[equal contribution; IF- 7.419]** *doi.org/10.1016/j.biopha.2020.110446*

1) Yadav, A.K., Dhiman, T.K., Lakshmi, G.B.V.S., Berlina, A.N. and Solanki, P.R., 2020. A highly sensitive label-free amperometric biosensor for norfloxacin detection based on chitosan-yttria nanocomposite. ***International journal of biological macromolecules,*** *151*, pp.566-575. **[IF- 8.025]** *doi.org/10.1016/j.ijbiomac.2020.02.089*

Submitted Manuscripts

6) Vidhi Vashishtha, Sachin Bhardwaj, Sanjay Kumar, Sindhu Nair, **Amit Yadav**, Avinash Kumar, Markus Bredel, Ramin Massoumi, and Ajay Yadav. hnRNPA1 and SF2/ASF1 co-existence favor's therapeutic resistance in glioma cells. **Molecular Cancer Research [under review).**

5) Navneet Chaudhary, **Amit K. Yadav**, Damini Verma, Jai Gopal Sharma, Pratima R. Solanki. Electrochemical Immunosensor based on Nanostructured Lanthanum oxide

substituted reduced graphene oxide Interface for Ultralow Ciprofloxacin Detection in Milk Samples. **RSC Materials Advances. [In-peer review].**

4) Payal Gulati, Avinash Kumar Singh, **Amit K. Yadav**, Kiran Pasbola, Prerna Pandey, Rinu Sharma, Alok Thakar, Pratima R. Solanki. Nano-modified Screen-Printed Electrodes based Electrochemical Immunosensors for Oral Cancer Biomarkers Detection in Undiluted Human Serum and Saliva Samples. **RSC Nanoscale Advances [In-peer review].**

3) Abhishek Kumar, Dhananjay Kumar Sah, Yogesh Rai, **Amit Kumar Yadav**, Pratima R. Solanki, Mohd Saquib Ansari, Anant Narayan Bhatt. A granular hemostatic composite of alginate, calcium, and zinc for rapid and effective management of post-traumatic hemorrhage. **Advanced Functional Materials [Submitted].**

2) Damini Verma, N. Dubey, **Amit K. Yadav**, R. Sharma, Pratima R Solanki. Disposable Paper based Screen Printed Electrochemical Immunoplatforms for Dual Detection of Esophageal Cancer Biomarkers in Patients' Serum samples. **RSC Materials Advances [Under review].**

1) Navneet Chaudhary, Damini Verma, **Amit K. Yadav**, Jai Gopal Sharma, Pratima R. Solanki Rational hydrothermal-assisted green synthesis of blueish emitting carbon dots as an optical sensing platform for antibiotic detection in the milk sample. **Talanta Open [Under review]**.

Book Chapters

7) Mishra A, Nair N, **Yadav AK**, Solanki P, Majeed J, Tripathi V. Coronavirus Disease 2019 (COVID-19): Origin, Impact, and Drug Development. **Intechopen.** *10.5772/intechopen.98358*

6) Yadav AK, Verma D, Solanki PR. Introduction to numerous diseases of the livestock. Nanobiotechnology for the Livestock Industry: Animal Health and Nutrition. ***Elsevier***. 2023 Jan 15:141. *doi.org/10.1016/B978-0-323-98387-7.00020-3*

5) Verma D, **Yadav AK**, Solanki PR. Prospects of nanobiotechnological applications for the livestock industry. In Nanobiotechnology for the Livestock Industry 2023 Jan 1 (pp. 475-493). **Elsevier**. *doi.org/10.1016/B978-0-323-98387-7.00015-X*

4) Verma, D., **Yadav, A.K.,** Solanki, P.R. Enzymatic Bio-sensing Platforms for Gut Diseases. **SpringerNature** [***accepted for publication***].

3) Verma, D., **Yadav, A.K.,** Solanki, P.R. Nanocomposites Applications in Wound Management. ***Elsevier***. **(Equal contribution)** [***Under Revision***].

2) Amit K. Yadav, Damini Verma, Pratima R Solanki. Approaches/Modification strategy to fight against Medical Device associated Biofilms. ***Elsevier (under review)***

1) Amit K. Yadav, Damini Verma, Pratima R Solanki. Electrospun fiber-based mats as anti-microbial coatings for medical devices and implant. ***Elsevier (under review)***

PATENTS

1) **Amit K. Yadav,** Pratima R. Solanki, Renu Sharma. ***"A novel electrochemical detection platform for cancer biomarker: Sp17"***. **Indian Patent Granted**. [Application. No. 202211005455; February 01, 2022].

International Journal of Biological Macromolecules 239 (2023) 124325

Contents lists available at ScienceDirect

International Journal of Biological Macromolecules

journal homepage: www.elsevier.com/locate/ijbiomac

Biocompatible epoxysilane substituted polymer-based nano biosensing platform for label-free detection of cancer biomarker SP17 in patient serum samples

Amit K. Yadav [a], Damini Verma [a], Abhishek Kumar [b], Anant Narayan Bhatt [b], Pratima R. Solanki [a,*]

[a] Nano-Bio Laboratory, Special Center for Nanoscience, Jawaharlal Nehru University, New Delhi 110067, India
[b] Institute of Nuclear Medicine and Allied Sciences, Defence Research and Development Organization, New Delhi, India

ARTICLE INFO

Keywords:
3-Glycidoxypropyltrimethoxysilane
Self-assembled monolayers
Indium tin oxide
Sperm protein 17
Cancer biomarker
Differential pulse voltammetry

ABSTRACT

Herein, we report the results of the studies relating to developing a simple, sensitive, cost-effective, and disposable electrochemical-based label-free immunosensor for real-time detection of a new cancer biomarker, sperm protein-17 (SP17), in complex serum samples. An indium tin oxide (ITO) coated glass substrate modified with self-assembled monolayers (SAMs) of 3-glycidoxypropyltrimethoxysilane (GPTMS) was functionalized *via* covalent immobilization of monoclonal anti-SP17 antibodies using EDC(1-(3-(dimethylamine)-propyl)-3-ethyl-carbodiimide hydrochloride) - NHS (N-hydroxy succinimide) chemistry. The developed immunosensor platform (BSA/anti-SP17/GPTMS@SAMs/ITO) was characterized *via* scanning electron microscopy (SEM), atomic force microscopy (AFM), contact angle (CA), Fourier transform infrared (FT-IR) spectroscopic, and electrochemical techniques such as cyclic voltammetry (CV), differential pulse voltammetry (DPV), and electrochemical impedance spectroscopy (EIS) techniques. The fabricated BSA/anti-SP17/GPTMS@SAMs/ITO immunoelectrode platform was used to measure changes in the magnitude of the current of the electrodes through an electrochemical CV and DPV technique. A calibration curve between current and SP17 concentrations exhibited a broad linear detection range of (100–6000 & 50–5500 pg mL^{-1}), with enhanced sensitivity (0.047 & 0.024 μA pg mL^{-1} cm^{-2}), limit of detection (LOD) and limit of quantification (LOQ) of 47.57 & 142.9 pg mL^{-1} and 158.58 & 476.3 pg mL^{-1}, by CV and DPV technique, respectively with a rapid response time of 15 min. It possessed exceptional repeatability, outstanding reproducibility, five-time reusability, and high stability. The biosensor's performance was evaluated in human serum samples, giving satisfactory findings obtained *via* the commercially available enzyme-linked immunosorbent assay (ELISA) technique, proving the clinical applicability for early diagnosis of cancer patients. Moreover, various *in vitro* studies in murine fibroblast cell line L929 have been performed to assess the cytotoxicity of GPTMS. The results demonstrated that GPTMS has excellent biocompatibility and can be used for biosensor fabrication.

1. Introduction

Cancer has recently become one of the leading causes of death worldwide. According to the World Health Organization (WHO) 2018 report, cancer kills almost 10 million people worldwide [1]. The world's population is expected to reach 8.3 billion by 2025, with >20 million new cases of cancer recorded each year [2,3]. Current research focuses on detecting cancer biomarkers in human fluids to aid in the early detection of cancer [4–6]. In this regard, the predictive importance of the Sperm protein 17 (SP17) in cancer patients has piqued researchers' curiosity. SP17 is a highly conserved mammalian protein found in the testis as well as spermatozoa which belongs to the cancer testis antigen (CTA) family and has been recognized as a tumor-linked antigen in several cancers occurring in humans, such as non-small cell lung cancer immunotherapy, neck, and head squamous cell carcinoma (HNSCC), multiple myeloma, and ovarian cancer. SP17 is composed of 151 amino acids (the full-length amino acid sequence has been shown in Fig. S7) and has an apparent 24.5 kDa molecular mass. Though the function of

* Corresponding author.
E-mail address: partima@mail.jnu.ac.in (P.R. Solanki).

https://doi.org/10.1016/j.ijbiomac.2023.124325
Received 16 December 2022; Received in revised form 30 March 2023; Accepted 31 March 2023
Available online 11 April 2023

SP17s is not clear; however, it is assumed to play a role in egg zona pellucida interactions during the process of fertilization regulating sperm acrosomal response, capacitation, and maturation, but display high expression in cancer [7]. Thus, SP17 has been proposed as a potential biomarker for several cancers when its cancer-specific expression is combined. Traditional methods for cancer detection, such as biopsy, laparoscopy, hepatic angiography, CT-scan, ultrasonography, and enzyme-linked Immunosorbent Assay (ELISA), might take several hours/days from the time of testing and take days for result findings [8–10]. These procedures are unpleasant and long as well as sometimes necessitate expensive equipment and special care. This led to problems in the diagnosis of cancer in patients suffering from it and admitted to an emergency division. Therefore, a more sensitive, selective, user-friendly, and quick platform is urgently needed to meet the immediate diagnosis demands for detecting cancer markers at the initial disease stage. Sensors are important because they can provide real-time and accurate data in situations where current methods may have gaps or limitations. This can be especially valuable in healthcare monitoring, where timely and precise information is essential for making informed decisions. Sensors can also help identify previously undetectable patterns and trends, leading to improved understanding and better problem-solving [11–13].

Electrochemical biosensors have gained appealing attention as an alternative to aid in quick diagnosis, giving improved intervention, and lowering the dissemination test time, which is very advantageous to reduce patient stress [14–16]. This is due to their high sensitivity, low cost, and portability. Further, a biosensing platform is critical for detecting target analytes with high sensitivity and specificity. Indium tin oxide (ITO) is an outstanding substrate in electrochemical and optical biosensors. In addition, compared to typical electrodes like glassy carbon electrodes, platinum, as well as gold, ITO is a cheap, stable, robust, and superb transparent conductive material. ITO-coated electrodes exhibit poor electro-catalytic activity, with a flat and low background current, which is advantageous to reduce noise in the case of an electrochemical biosensor [17]. Many studies have been conducted using ITO electrodes for their usage in electro-chemiluminescence, electrochemical nucleic acid biosensors, optical as well as electrical sensors analysis [18–20].

Various techniques have been used to modify ITO electrodes, including self-assembled monolayers (SAMs) creation [21], electropolymerization [22], direct physical adsorption [23], electrophoretic deposition [24], and polymer thin film development [25]. Among them, SAMs are commonly used in biosensor production and play a vital role in developing electrochemical biosensors [26]. Self-assembling of silane molecules occurs with greater stability on the hydroxylated surface of ITO, allowing for efficient biomolecule coupling [27]. As a result, silanization-based SAMs formation may deliver a homogeneous layer on a specified surface for getting pre-determined surface attributes. Demirel et al. developed a DNA sensor utilizing a poly(N-isopropyl acrylamide) layer deposited on a silicon (Si) wafer [28]. 3-glycidoxypropyltrimethoxy silane (GPTMS) is an epoxy silane molecule used to create SAMs on oxide surfaces without needing a secondary cross-linker between the silane molecule and target antibodies. GPTMS is a bifunctional organ silane with three methoxy groups on one side and an epoxy ring on the other with the chemical formula $C_9H_{20}O_9Si$ [The 2D and 3D molecular structure of GPTMS has been given in Fig. S1(a and b)] [29,30]. In aqueous environments, epoxy groups are highly reactive to nucleophiles like acids, thiols, and amines and are relatively stable at neutral pH [29]. Yang and co-workers fabricated a SAM-based epoxysilane biosensing platform for *Escherichia coli* (*E. coli*) O157: H7 detection based on the immobilization of affinity-purified antibodies [31].

In this study, we invented an amperometric immunosensor created on disposable ITO thin films utilizing biocompatible SAMs of GPTMS to detect a novel SP17 cancer biomarker for the first time. The GPTMS was self-assembled on the cleaned and activated surface of a hydroxyl-functionalized ITO electrode, forming an epoxy-functionalized highly structured SAMs layer at room temperature (RT). Subsequently, the anti-SP17 antibodies were covalently attached to this 3-glycidoxypropyltrimethoxy silane@ self-assembled monolayers (GPTMS@SAMs) layer without a cross-linker, providing a bio-recognition layer for SP17 biomarker detection. Cyclic voltammetry (CV), differential pulse voltammetry (DPV) and electrochemical impedance spectroscopy (EIS) techniques are vital for monitoring interface information between the electrode and the electrolyte solution and are thus used for electrochemical characterization. The immunosensor had good sensitivity and specificity in detecting the SP17 biomarker and was effectively utilized to measure SP17 concentrations in human serum samples, indicating the method's effectiveness. The results were then validated through the standard gold method, *i.e.*, ELISA, for analysis of protein molecules. This immunosensor offers numerous advantages, including a simple production procedure, a low limit of detection

(LOD), and minimal interference from other components found in real samples (human serum). Furthermore, the fabricated immunosensor was reusable five times, lowering the cost of the biosensor. The biocompatibility of nanomaterials is a critical consideration in the development of biosensors for biomedical applications. Thus, to the best of our knowledge, for the first time, the GPTMS was examined for its cytotoxicity in human lymphocyte cells using hemolysis and biocompatibility utilizing various *in vitro* studies in murine fibroblast cell line L929.

2. Materials and methods

2.1. Reagents and instruments

2.1.1. Chemicals

N-hydroxysuccinimide (NHS, $C_4H_5NO_3$, ≥98 %); 3-glycidoxypropyltrimethoxysilane (GPTMS: molecular weight- 236.34; density- 1.07 g mL^{-1} at 25 °C; Chemical formula- CO[Si](CCCOCC1CO1)(OC)OC; bp-120 °C/2 mmHg); N-ethyl-N′-(3-dimethyl aminopropyl) carbodiimide hydrochloride (EDC, $C_8H_{17}N_3$, ≥97.0 %); and bovine serum albumin (BSA, ≥ 96 %) were brought from Sigma-Aldrich, India. Potassium hexacyanoferrate trihydrate [$(K_4[Fe(CN)_6)]$, ≥99.95 %]; potassium ferricyanide(III) [$(K_3[Fe(CN)_6)]$, 99 %]; acetone (CH_3COCH_3, 100); hydrogen peroxide (H_2O_2, 200); ethanol (CH_3CH_2OH, 99.9 %); and sodium hydroxide pellets (NaOH, ≥97.0 %) were purchased from Fisher Scientific. Sodium chloride (NaCl, 99.9 %); uric acid ($C_5H_4N_4O_3$, 99 %); urea (NH_2CONH_2, 99.5 %); oxalic acid ($(COOH)_2.2H_2O$, 99.5 %); ascorbic acid ($C_6H_8O_6$, 99.7 %); disodium hydrogen phosphate dihydrate (Na_2HPO_4, ≥99.5 %) and sodium dihydrogen phosphate dihydrate (NaH_2PO_4, 99.5 %) were procured from SRL India Pvt. Ltd. Antibodies of SP17 (anti-SP17), tumor necrosis factor-alpha (TNF-α), interleukin-8 (IL-8), cytokeratin 19 fragment (CYFRA-21-1), and SP17 were brought from My BioSource, USA. Various SP17 antigens, and an anti-SP17 antibody, were prepared in 20 mM Tris, 150 mM NaCl buffer (pH 8.0), and PBS having pH 7.4, respectively. ELISA KIT (Catalog No.- CSB-EL022451HU) of human sperm surface protein SP17 (SPA 17) was brought from CUSABIO. NaH_2PO_4 and $NaHPO_4$ were mixed well in Millipore water (Milli-Q) to prepare 0.2 M PBS, *i.e.*, electrolyte solution with pH = 7.0, and kept in the refrigerator for further use. The ITO-coated glass substrate was purchased from Blazers, UK. Every chemical was utilized without any treatment and of analytical grade. Milli-Q (18.2 MΩ/cm) was employed for the whole experiment. Murine Fibroblast cells (L929) were retrieved from National Centre for Cell Sciences, Pune, India. The cells were propagated in High glucose Dulbecco's Modified Essential Medium (Sigma, USA), followed by 10 % Fetal bovine Serum (Gibco, USA), and incubated at 37 °C with 5 % CO_2.

2.1.2. Instruments

The elemental mapping, composition, and surface morphologies of GPTMS@SAMs/ITO, as well as BSA/anti-SP17/GPTMS@SAMs/ITO electrode surfaces, were characterized using energy-dispersive X-ray (EDX) spectroscopy and scanning electron microscopy (SEM, JSM-IT

200, JEOL), functioned at an acceleration voltage of 5 k, respectively. In addition, atomic force microscopy (AFM) with commercial silicon (Si) tip having a tip radius of <10 nm of the WITEC system in the tapping mode (applied in the standard cantilevers) was utilized for analyzing the surface modification steps of electrode fabrications. The images were taken at a scan rate of 5 μm s^{-1}, having a resolution of 256 × 256. To monitor surface end groups in different fabricated electrodes, Fourier transform infrared spectroscopy (FT-IR, Perkin Elmer, ATR Model, USA) for analyzing the chemical bonds from 4000 to 400 cm^{-1} wavenumber range was utilized. The dispersive Raman measurements were performed using EnSpectr R532, USA (laser of WITEC system having confocal microscope with 3 objectives) and excitation laser (780 nm) ranging from 500 to 2000 cm^{-1}. Moreover, for studying the water contact angle, the drop shape analyzer [KRUSS, Germany] was utilized to detect the hydrophobic/hydrophilic nature of fabricated electrodes. The SP17 concentrations in cancer patients' serum samples were estimated employing the ELISA plate reader of Biotek 800 TS microplate reader.

2.2. In vitro biocompatibility studies of GPTMS

The biocompatibility of GPTMS-based nanomaterials was estimated using a case-by-case procedure in accordance with the International Standards ISO 10993-5 Third Edition 2009-06-01 "Biological Evaluation of Medical Devices – Part 5: Tests for *in vitro* Cytotoxicity. For determining the viability of GPTMS as a biocompatible nanomaterial for biosensor development, the cytotoxicity and biocompatibility of GPTMS were examined using an *in vitro* cell proliferation study as well as its interactions between the human cells at *v*arious time points by employing an inverted optical microscope.

2.2.1. Cellular viability and cytotoxicity

The percent cellular proliferation of the cells treated with various concentrations of GPTMS (5 μg to 2.5 mg mL^{-1}) *w/v* in culture medium was determined using 3-(4,5-dimethylthiazol-2-yl)-2,5-diphenyl tetrazolium bromide (MTT) assay as described earlier with slight modifications [32]. The cells were seeded in 96 well culture plates (5 × 10^3 cells per well, 200 μL) as well as incubated overnight, followed by the addition of GPTMS. The cells were allowed to propagate for 48 h, and a further 20 μL of MTT (5 mg mL^{-1}) was added with 2 h incubation in the dark. The wells were then aspirated, and formazan crystals were dissolved by adding dimethyl sulfoxide (DMSO) (200 μL/well), followed by spectrophotometric determination at 540/630 nm.

The morphology and viability assessment in the adhesive form of the fibroblast cells was determined with the implementation of Calcein-acetoxymethyl (Calcein-AM) / Propidium Iodide (PI) (Live/Dead) fluorescent staining [33]. The cells were plated in 24 well culture plates (25 × 10^3 cells per well, 500 μL) as well as subjected to various concentrations of GPTMS (5 μg - 50 μg) for 24 h. After incubation, the media was aspirated and incubated with Calcein-AM & PI (3 μM each), followed by fluorescence image acquisition using (Olympus CH30, Japan).

2.2.2. Clonogenicity and migration potential

The reproductive potential of the fibroblast cells incubated with various concentrations of GPTMS was determined using a Macro colony assay as described earlier [34]. The cells were first seeded in 60 mm cell culture Petri Dishes (PDs) (0.5 × 10^6 cells/PD), and PDs were treated with GPTMS (5 μg - 2.5 mg mL^{-1}) for 24 h. The cells of each treatment group were then trypsinated and seeded in fresh 60 mm PDs (200 cells/PD) and left undisturbed for 7–9 days until colonies formed (50–100 cells/colony). The number of colonies was enumerated in both treatment and control groups by implementing crystal violet staining.

The *in vitro* cellular scratch assay model was adapted to determine the migration potential of GPTMS-treated fibroblast cells. The cells were seeded in 24 well culture plates (25 × 10^3 cells/well) overnight in a carbon dioxide (CO_2) incubator. A sterile pipette tip generated a scratch in the middle of the cell monolayer to mimic a wound. A single wash with PBS was given to remove the cellular debris, and GPTMS (5 μg - 50 μg) was added to the wells. Images of the scratch area were captured at 0 h, 12 h, and 24 h by 4× objective and 10× eyepiece (Olympus CH30, Japan), and the total cells migrated to the wound area were counted in both the treatment and control groups [35].

2.2.3. Hemolysis rate

The varying concentrations of GPTMS (10 μg - 1 mg mL^{-1}, 500 μL) samples diluted in phosphate buffer silane (PBS) were prepared in 1.5 mL microcentrifuge tubes, and 2 % red blood cells (RBC) cell suspension (500 μL) was then added to the tubes, followed by incubation at 37 °C on a water bath. The mixture was then centrifuged at 100 *g* for 2 min, and the supernatant was further transferred to a 96-well plate and read at 540 nm to determine the extent of hemolysis [35]. PBS was used as a negative control, while distilled water was taken as a positive control. Hemolysis rate was calculated as Eq. (1):

$$\text{Hemolysis rate } (\%) = \frac{\left(\text{OD}_{\text{sample}} - \text{OD}_{\text{negative control}}\right)}{\left(\text{OD}_{\text{positive control}} - \text{OD}_{\text{negative control}}\right)} \times 100 \quad (1)$$

2.3. Fabrication of biocompatible GPTMS@SAMs-based immunosensor

As reported in the literature, the GPTMS@SAMs were made on a precleaned ITO glass plate with slight modification [36]. Before the immunosensor fabrication, the surface of the ITO electrode was cleaned by ultrasonication in ethanol and Milli-Q for 5 min. After drying, the cleaned ITO electrodes were firstly treated with a mixed solution of water: hydrogen peroxide: ammonium hydroxide ($H_2O/H_2O_2/NH_4OH$) in a 5:1:1 ratio for 60 min at 80 °C to get a uniform layer of hydroxyl (-OH) groups on the surface of ITO, followed by rinsing with water and drying protocol [37,38]. Next, the 1 % (*v*/v) solution of GPTMS in toluene was drop casted over the hydroxylated ITO electrodes overnight at RT (25 °C) to form a monolayer of epoxy silane comprising several active tails of epoxy groups to react rapidly with amino protein groups. This stage was essential as the silanization agent was coupled with the ITO electrode's hydroxylated terminals forming a Si-O-Si bonds monolayer [39]. The ITO electrode shape was made rectangular, having an active surface area of 0.5 cm × 0.5 cm, *i.e.*, 0.25 cm^2, which is modified with GPTMS. Thus, all the electrodes were made under similar conditions. The SAMs formed electrode (GPTMS@SAMs/ITO) was then washed with water and toluene for removing other epoxysilane molecules from the surface and dried in the air at RT.

Following that, a stock solution of antibodies (anti-SP17 having 50 μg mL^{-1}) in PBS of pH 7.0 solution was prepared. The carboxyl (–COOH) terminal of the Fragment crystallizable (Fc) region of the antibody biomolecule was then activated utilizing the coupling chemistry of heterobifunctional cross-linkers such as EDC-NHS. Then, a solution of anti-SP17, EDC having 0.4 M (a coupling agent) and NHS having 0.1 M (an activator), was prepared in a 2:1:1 ratio and stored at 4 °C for 45 min to activate the carbonyl group of antibody molecules. Furthermore, 30 μL of antibody solution (activated) was drop casted onto the platform of GPTMS@SAMs/ITO as well as incubated at 25 °C in a humified chamber for 6 h to form an amide bond (-$CONH_2$) between –COOH ends of anti-SP17 and epoxy ends of GPTMS@SAMs through the EDC-NHS mechanism as displayed in Scheme S1 (Supplementry data). The fabricated platform (anti-SP17/GPTMS@SAMs/ITO) was then washed thrice with PBS of pH 7.4 for removing any extra anti-SP17 molecules. Lastly, 20 μL of 2 mg mL^{-1} bovine serum albumin (BSA) was drop casted to block the non-specific active areas of the prepared immunoelectrode. The developed immunosensing platform (BSA/anti-SP17/GPTMS@SAMs/ITO) was rinsed with PBS and kept in 4 °C until used again. Scheme 1(b) depicts a schematic representation of the fabrication of SAMs of a biocompatible GPTMS-based immunosensing platform for SP17 detection in serum samples. The whole immunosensor construction pathway, principle, and chemical interactions of the biosensor are schematically

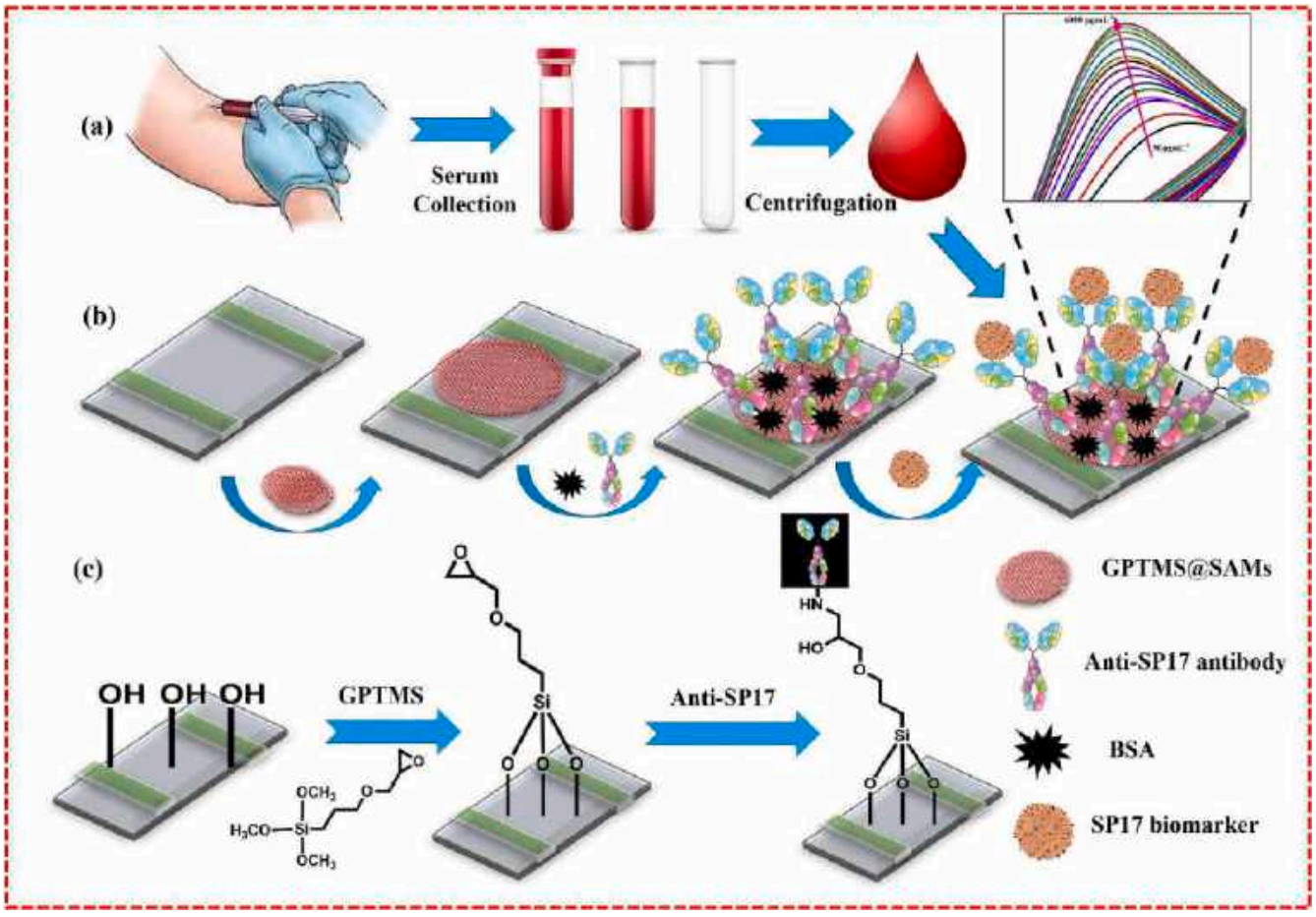

Scheme 1. A schematic representation for the formation and step-wise fabrication of an immunosensing platform for SP17 cancer biomarker detection in cancer patients' samples based on biocompatible and non-toxic SAMs of GPTMS.

displayed in Scheme 1(c).

2.4. Collection of patient blood samples

The Jawaharlal Nehru University (JNU), New Delhi, and the All-India Institute of Medical Sciences (AIIMS), New Delhi, gave all the necessary ethical permissions for the collection of patient samples. All cancer patient samples were received by following the procedure of AIIMs. Patients filled out the consent form during the collection of the blood sample. Before processing, these serum samples were taken in a pre-sterilized vial and stored undisturbed in the refrigerator for 20 min to allow coagulation of blood. Serum was then shifted in 5 mL centrifuge tubes as well as centrifuged (3000 rpm) for 15 min at 4 °C. To avoid freeze-thaw cycles, extraction of serum from the supernatant was done as well as its aliquots were made and kept at −80 °C until needed. The schematic representation of serum collection from cancer patients has been displayed in Scheme 1(a).

2.5. Sample preparation of target analyte SP17

The stock solution of SP17 protein was prepared in 150 mM sodium chloride (NaCl) and 20 mM Tris buffer having pH 7.0, and its different concentrations were made from 100 pg mL^{-1} to 6000 pg mL^{-1} in PBS buffer (pH 7.4). The fabricated immunosensor was performed utilizing the CV and DPV technique in PBS of pH 7.0 with 5 mM $[Fe(CN)_6]^{3-/4-}$. The practical utility of the developed immunosensor was done by validating the sensor in real samples such as blood.

2.6. Electrochemical measurements

The electrochemical response was investigated through cyclic voltammetry (C*V*), differential pulse voltammetry (DPV) as well as electrochemical impedance spectroscopy (EIS) techniques utilizing Autolab Potentiostat/ Galvanostat electrochemical analyzer (EcoChemie, The Netherlands). The CV measurements were performed at a 50 mVs^{-1} scan rate from −0.8 to +0.8 V potential. The EIS was measured at 0 voltage having a frequency ranging from 100 kHz to 10 Hz in the absence and presence of redox species *i.e.*, $[Fe(CN)_6]^{3-/4-}$. The impedimetric signals were fitted to Randles equivalent circuit by using NOVA software. The studies were conducted to investigate the immobilization process and to monitor the interaction between anti-SP17 antibody and SP17 antigen in PBS (pH 7.0), which is made up of 0.9 % NaCl, 0.2 M $Na_2HPO_4.2H_2O$, and 0.2 M $NaH_2PO_4.2H_2O$ in Milli-Q, with 5 mM $[Fe(CN)_6]^{3-/4-}$ as the redox species. For the electrochemical analysis, a three-electrode system involving silver/silver chloride (Ag/AgCl), platinum (Pt), and GPTMS-modified ITO glass acted as a reference, counter, and working electrodes, respectively. The complete electrochemical analysis was performed in triplicate ($n = 3$). Moreover, the reference electrode (Ag/AgCl) used to monitor and control the oxygen level in the solution, which measured the potential of the electrochemical cell. By monitoring the potential, any changes due to oxygen interference has been detected and corrected [40,41].

3. Results and discussion

3.1. Analytical characterization

3.1.1. FTIR analysis

The Fig. 1A illustrates the FTIR curves of the anti-SP17 antibody immobilized ITO as well as GPTMS-modified ITO electrodes. FTIR spectra of each electrode were recorded in ATR mode in 4000–400 cm^{-1} wavenumber range at the resolution and scan of 4 cm^{-1} and 16, respectively. The findings depict the characteristic band of the epoxy group present in GPTMS at 847 cm^{-1} and 910 cm^{-1} [Fig. 1D] [42]. The bending and stretching vibrations were due to alkyl hydrogen at around 1563 cm^{-1} and 2941 cm^{-1}, respectively (Figs. 1C and 1B). The asymmetric stretching vibration of Si–O–Si gave a strong, broad band at 1080 cm^{-1}. The 814 and 910 cm^{-1} bands occur due to Si–O–Si symmetric and Si-OH asymmetric stretching vibrations, respectively. Also, the O–Si–O vibrations occurred at 448 and 533 cm^{-1}. A weak band appeared at 678 cm^{-1} due to the out-of-plane bending vibrations of the C–OH groups [36] (Fig. 1E). After the immobilization of the anti-SP17 antibody, the distinctive bands of -NH bending and C═O stretching were seen at 1077 cm^{-1} and 1644 cm^{-1}, respectively. The occurrence of the band at 1077 cm^{-1} corresponding to –CO stretching was reported, produced between the anti-SP17 –COOH group and GPTMS –NH_2 group, thus affirming the binding of anti-SP17 to the surface of silane-modified ITO electrode.

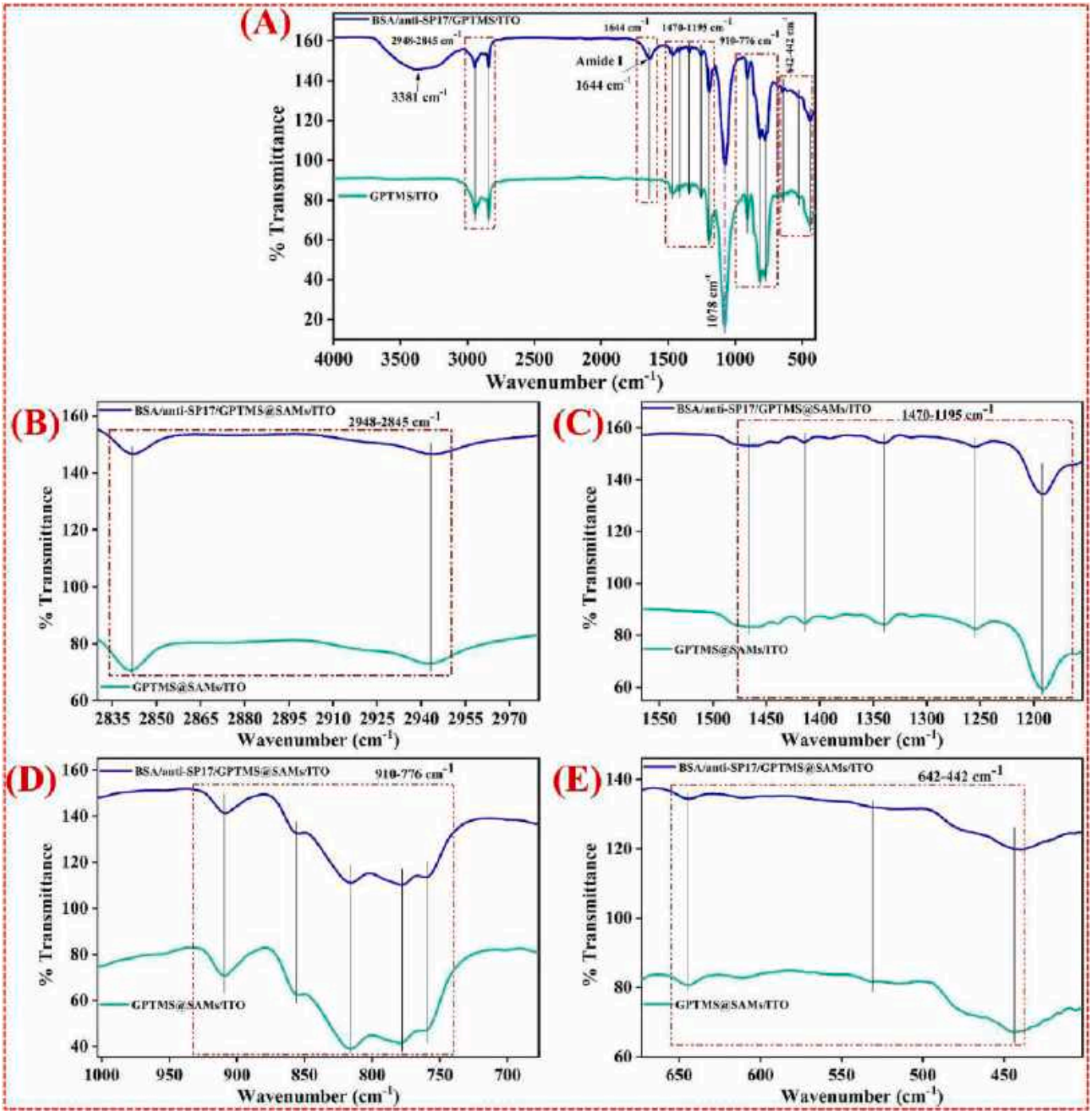

Fig. 1. (A) FT-IR spectra of GPTMS@SAMs/ITO electrode and BSA/anti-SP17/ GPTMS@SAMs/ITO immunoelectrode; (B) details of 2948–2845 cm^{-1} band; (C) details of the 1470–1195 cm^{-1} band; (D) details of the 910–776 cm^{-1} band; and (E) details of the 642–439 cm^{-1} band.

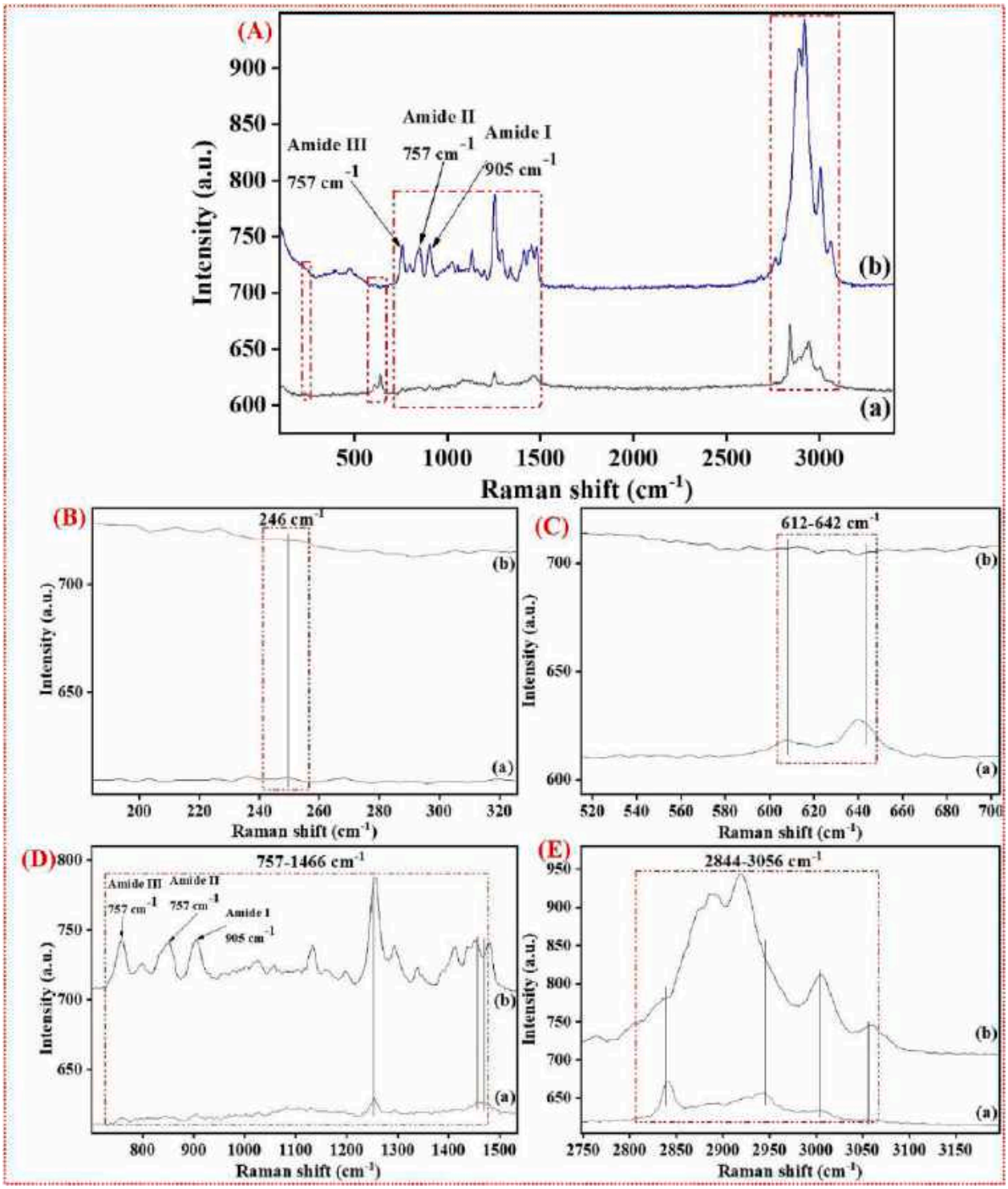

Fig. 2. (A) Raman spectra of (a) GPTMS@SAMs/ITO electrode and (b) BSA/anti-SP17/ GPTMS@SAMs/ITO immunoelectrode; (B) details of the 246 cm^{-1} band; (C) details of the 612–642 cm^{-1} band; (D) details of the 757–1466 cm^{-1} band; and (E) details of the 2844–3056 cm^{-1} band.

These bands confirm the amide formation between the anti-SP17 antibody terminal amino groups and GPTMS epoxy groups. Additionally, Fig. 1A also depicts a broad band ranging from 3000 to 3400 cm^{-1}, which is due to the –OH and –NH bond stretching vibrations of water molecules. The amide groups in the protein backbone of antibodies, such as the primary amine group ($-NH_2$) and the carboxylic acid group (-COOH) of the amino acids, contribute to the characteristic peaks in the amide I (1650–1700 cm^{-1}) and amide II (1550–1630 cm^{-1}) regions of the FTIR spectra [43]. In addition, antibodies also contain hydroxyl (-OH) groups in the side chains of some amino acids, such as serine, threonine, and tyrosine. The hydroxyl groups contribute to the broad peak in the 3200–3600 cm^{-1} region of the FTIR spectra. On the other hand, GPTMS is a silane coupling agent containing no hydroxyl (-OH) groups, thus not showing the band at 3000 to 3400 cm^{-1} in the FTIR spectra.

3.1.2. Raman analysis

The chemical and molecular findings of the working surface

electrode were estimated with the help of Raman spectroscopy. This technique helps in proving the practical data for the particular interactions taking place between different biomolecules and molecules. The relative shift of the Raman band and variation in intensity depicts the chemical communication between biomolecules and SAMs [44]. Therefore, SAMs formation and the immobilization of antibody on the surface of the ITO electrode was performed utilizing this technique. As shown in Fig. 2A(a), bands at 911 cm^{-1} and 852 cm^{-1} were attributed to the epoxy ring stretching of GPTMS. Considering calculated Raman activities, the intensive Raman bands observed at 3056 cm^{-1} and 3006 cm^{-1} are CH_2 and CH stretching modes connected to the epoxy ring. Three bands observed in Raman spectra at 2944 cm^{-1}, 2844 $cm^{-1,}$ and 2839 cm^{-1} are assigned to CH_3 stretching modes of the methoxy groups (Fig. 2E). In the frequency region 1500–1100 cm^{-1}, the fundamentals at 1480 cm^{-1} (υ22), 1389 cm^{-1} (υ35), 1196 cm^{-1} (υ 43) and 1162 cm^{-1} (υ 44) have been assigned as CH_2 group vibrations of propyl chain. A strong Raman band observed at 1256 cm^{-1} is characteristic of the epoxy group [45] (Fig. 2D). A strong IR band observed at 1159 cm^{-1} (υ45) is a pure vibration of methoxy groups that consists of CH_3 rocking combined with CO stretching. The weak Raman bands observed at 1136 cm^{-1} (υ49), 1114 cm^{-1} (υ53), and 1106 cm^{-1} (υ54) are the vibrations of the glycidoxy group. The band at 530 cm^{-1} is assigned as the scissoring vibrations of the CCO valence bond angle in the glycidoxy group (Fig. 2C). Bands observed at 480 cm^{-1} and 443 cm^{-1} are described as COC and SiO_3 symmetrical deformations, respectively. A moderate Raman band observed at 246 cm^{-1} is assigned as SiO_3 rocking, SiOC deformation, CCO, and CCC scissoring connected with SiO_3 asymmetric deformation (Fig. 2B) [46].

Furthermore, this technique is the most suitable for analyzing the amide bonds. The characteristic bands of amide III, II, and I bonds were observed between 1235 and 1350 cm^{-1}; 1480 and 1570 cm^{-1}, as well as 1650 and 1680 cm^{-1}, respectively, on GPTMS-modified ITO electrodes [47] (Fig. 2A(b)). After immobilizing the anti-SP17 antibody, amide III, I, and II bonds were found at 757, 905, and 757 cm^{-1}, respectively, confirming the binding of anti-SP17 on the GPTMS@SAMs/ITO electrode surface (Fig. 2D).

3.1.3. Contact angle analysis

The technique of sessile drop was performed for contact angle (CA) studies for investigating the hydrophilicity or hydrophobicity nature of the SAMs of the GPTMS surface, as well as for every step-wise alteration [Fig. S2(a-d)]. The contact angles of these electrodes were evaluated using water droplets spread onto GPTMS@SAMs films as a qualitative method for assessing the relative variation of hydrophobic/hydrophilic behavior of the ITO, GPTMS@SAMs/ITO, anti-SP17/GPTMS@SAMs/ITO and BSA/anti-SP17/GPTMS@SAMs/ITO immunoelectrodes [48]. The value of CA for ITO was 99.7° as depicted in Fig. S2(a), which decreased to 86.5° [(Fig. S2(b)] showing the GPTMS monolayer fabrication on the hydrolyzed ITO (GPTMS@ SAMs/ITO). The reduced CA value could be ascribed to hydrophilic epoxy group presence in the GPTMS, which establishes a convenient platform for the immobilization of anti-SP17 antibodies. The value of CA was further reduced to 43.2° [Fig. S2(c)] and 25.6° [Fig. S2(d)] after immobilizing the biomolecules such as anti-SP17 antibodies as well as BSA, respectively. The reduction in CA value is due to the hydrophilic nature of electrodes (BSA/anti-SP17/GPTMS@SAMs/ITO and anti-SP17/GPTMS@SAMs/ITO) which proves the covalent attachment of anti-SP17 antibodies as well as BSA on the surface of GPTMS@SAMs/ITO electrode. This immunoelectrode hydrophilicity enhances the increased attachment of antigen (in PBS buffer), thus improving immunosensor sensitivity [7].

3.2. Morphological characterization

Scanning electron microscopy (SEM) and atomic force microscopy (AFM) methods are recognized as powerful techniques for studying the surface morphology of various surfaces of electrodes. The images of SEM, as well as AFM of the GPTMS@SAMs/ITO and anti-SP17/GPTMS@SAMs/ITO immunoelectrode, are shown in Fig. 3(A and E) and Fig. 3(B-D and F-H), respectively, confirming the step-by-step alteration done on the sensing platform. It could be observed that GPTMS@SAMs/ITO and anti-SP17/GPTMS@SAMs/ITO immunoelectrode surfaces had evidently diverse morphologies. The image of SEM [Fig. 3(A)] and AFM [Fig. 3(B-D)] of the GPTMS@SAMs/ITO electrode shows a dense surface structure revealing SAMs formation. The GPTMS monolayer distribution on the surface of ITO is dense, thick, and uniform, with insufficient homogeneous agglomerates. The average roughness (Ra) value of the GPTMS@SAMs/ITO electrode was −484.4 nm on a 5 × 5 mm scale which confirmed the highly ordered and dense SAMs over the ITO surface. The formed SAMs 3D network layer was appropriate for anti-SP17 antibody immobilization owing to the increased GPTMS layer surface area. The sole assembly of the GPTMS layer can deliver an advantageous microenvironment for the proteins for retaining its good bioactivity. Fig. 3(E) and (F-H) depicts SEM as well as AFM images, respectively, for the anti-SP17 antibody-immobilized ITO electrode surface. It could be observed from the figure that the surface morphology of the electrode was modified in comparison to the GPTMS@SAMs/ITO electrode, followed by the uniform distribution of immobilized antibodies for binding to anti-SP17 antibodies homogenously. The antibodies' homogeneous immobilization offers a reproducible and sensitive response to the electrode. The bigger size and globular structure of anti-SP17 antibodies binded to the GPTMS@SAMs/ITO electrode surface are clearly visible. Therefore, an increase was seen in Ra (0.7 nm) on a 5 × 5 mm scale as compared to GPTMS@SAMs/ITO. Biomolecules' covalent attachment to the GPTMS functional groups in a similar style shows more compactness of anti-SP17 molecules at the GPTMS@SAMs/ITO electrode.

Moreover, Energy-dispersive X-ray spectroscopy (EDX) with elemental mapping studies was also conducted for defining the elemental compositions of ITO surface after modification of SAMs with GPTMs (GPTMS@SAMs/ITO) and anti-SP17 antibodies (anti-SP17/GPTMS @SAMs/ITO), as illustrated in Fig. S3(A) and Fig. S3(B), respectively. The analysis showed that the GPTMS@SAMs/ITO electrode had significant binding energies peaks of Indium (In), Silicon (Si), Oxygen (O), and carbon (C) elements, suggesting the high purity of the SAMs formation. The Si element (orange) could be clearly visible in Fig. S3(E) that arises from molecules of GPTMS epoxysilane as well as its ratio was estimated as 6.77 %. This finding shows GPTMS coating on the surface of ITO. Next, after modification with anti-SP17 antibodies (anti-SP17/GPTMS@SAMs/ITO bioelectrode), it showed C, O, and Si elements [Fig. S3(B)]. Moreover, EDX spectra also represent the N atom, showing successful anti-SP17 antibodies biomolecule immobilization on the GPTMS@SAMs/ITO electrode surface. This peak for the N atom arises due to the amino acids chain of antibodies biomolecules. Thus, these images of EDX demonstrate the presence of anti-SP17 biomolecules on the GPTMS@SAMs/ITO electrode. In addition, the elemental mapping profile of GPTMS@SAMs/ITO [Fig. S3(C-F) and anti-SP17/GPTMS@SAMs/ITO [Fig. S3(G-J)] indicates the homogeneous distribution of C, O, Si, In, and N elements.

3.3. Biocompatibility studies

The biocompatibility of nanomaterials is a critical consideration in the development of biosensors for biomedical applications. The use of nanomaterials in biosensor fabrication has shown great promise in enhancing the sensitivity, selectivity, and stability of biosensors. However, it is essential to ensure that these nanomaterials are biocompatible to avoid any adverse effects on living organisms. Therefore, several studies have been conducted to evaluate the biocompatibility and cytotoxicity of GPTMS in human lymphocyte cells using hemolysis and several *in vitro* studies in murine fibroblast cell line L929 in the current work.

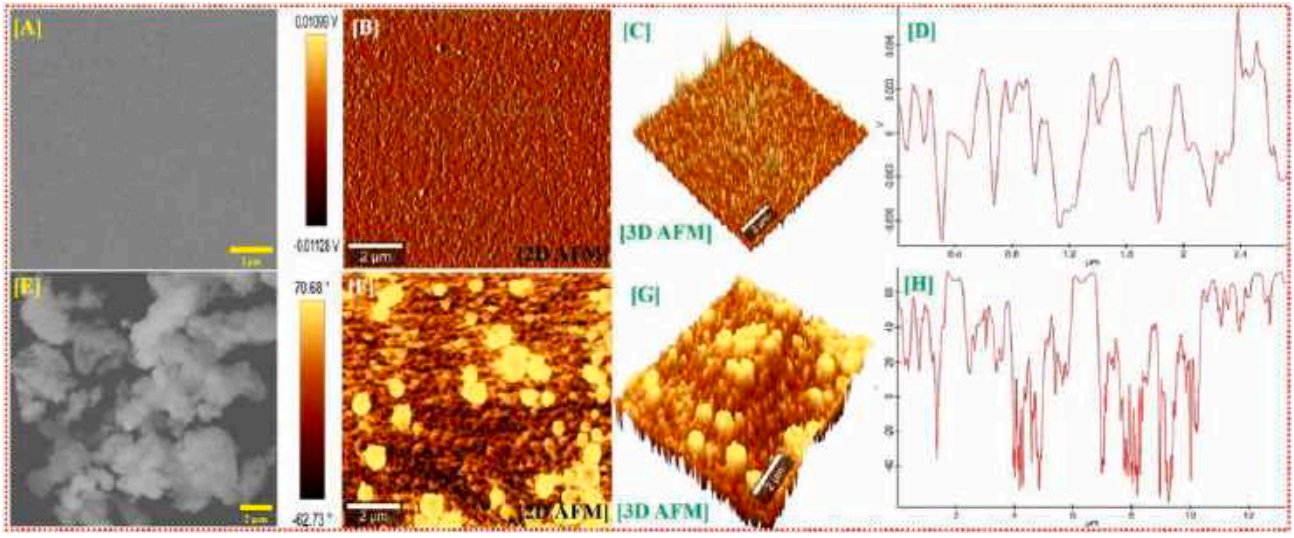

Fig. 3. Scanning electron microscopy images of GPTMS@SAMs/ITO electrode (A) and anti-SP17/GPTMS@SAMs/ITO immunoelectrode (E); 2D AFM (B and F), 3D AFM (C and G), and cross-section line images of GPTMS@SAMs/ITO electrode and anti-SP17/GPTMS@SAMs/ITO immunoelectrode, respectively.

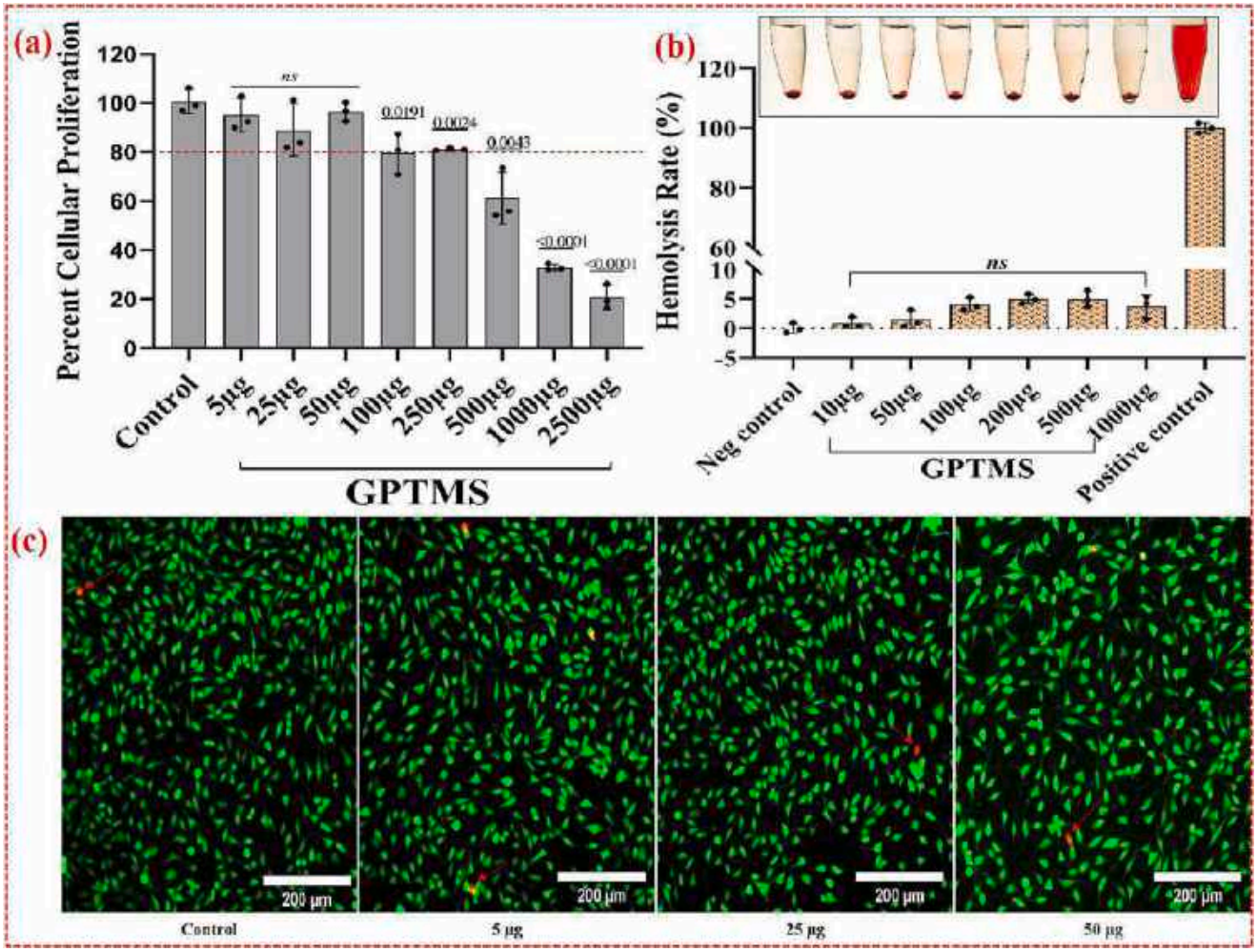

Fig. 4A. (a) Cell viability of murine fibroblast L929 cell lines treated with GPTMS at different concentrations after 48 h. IC50 of GPTMS was found to be >500 µg mL^{-1}; (b) Hemolysis test of blood after centrifugation at different concentrations of GPTMS observed under UV absorbance at 540 nm; and (c) Morphology and viability assessment of L929 cell line in the adherent form Calcein-AM & PI fluorescent staining fluorescence imaging.

3.3.1. In-vitro compatibility and cytotoxicity of GPTMS

The cytotoxicity profiling of the GPTMS, including cellular viability, morphology determination, and live/dead cell assessment, was performed in a murine fibroblast cell line, L929. These cells are highly utilized in cytotoxicity determination studies as they closely resemble human dermal fibroblasts [49]. After incubation, the percent proliferation of cells with various concentrations of GPTMS (5 μg to 2.5 mg mL^{-1}) *w/v* in a culture medium was determined using MTT cellular viability assay. The obtained results showed that the cells treated with 5 μg to 50 μg GPTMS had no significant effect on the cellular viability, but relative cellular proliferation inhibition of up to 20 % (generally considered safe) was observed at conc. 100 μg to 250 μg [Fig. 4A(a)]. Further increasing the conc. of GPTMS from 250 μg to 2500 μg proved cytotoxic to fibroblast cells. The fibroblast cells were then observed for morphological changes induced by the treatment of GPTMS. The morphology was studied by Calcein-AM (Live) and PI (Dead) stained cells observed by fluorescence imaging. The resulting photomicrographs of fibroblast cells treated with GPTMS (5 μg to 50 μg) showed morphology which was comparable with control (untreated) cells, and no significant induction in the dead cell population was observed. [Fig. 4A(c)]. These results indicate the relatively safe nature of GPTMS up to 50 μg mL^{-1} concentration.

3.3.2. Hemolysis analysis of GPTMS

A small tendency for inducing hemolysis is a vital necessity for the fabrication of biocompatible biosensors. The existence of hemolytic material with serum may destroy the red blood cells along with the liberation of free plasma hemoglobin in the supernatant of the test solution, which may affect the transportation of oxygen, inducing stress and toxic effects to other organs or the kidneys [50,51]. The GPTMS solution ranging from 10 μg to 1 mg mL^{-1} (in PBS) was subjected to hemolysis rate analysis in whole human blood for hemocompatibility assessment. The polymer compound was found to be non-hemolytic at all the tested concentrations and was comparable with negative control (PBS), while an apparent rupture of RBCs and release of hemoglobin could be seen in erythrocytes treated with the positive control (distilled water), as shown in Fig. 4A(b) The lower hemolysis rate of the formulation represents the better hemocompatibility of the polymer [35,52].

3.3.3. Reproductive and migration potential of GPTMS

To further substantiate the *in-vitro* cytotoxicity findings, a clonogenic survival assay was performed to estimate the treatment-induced change in cell plating efficiency (PE). The results obtained showed no significant difference in the PE of 5 μg to 100 μg of GPTMS treated cells, but a slightly decreased PE could be observed in 250 μg mL^{-1} GPTMS (55 % PE) treated cells as compared with untreated control cells (69 % PE) [Fig. 4B(a) and (b)]. It could be interpreted from these results that the fibroblast cells treated with GPTMS (up to 100 μg) are not losing any of their reproductive potentials.

From the *in-vitro* findings, the relatively non-toxic GPTMS concentrations 5 μg, 25 μg, and 50 μg mL^{-1} were selected for assessment of cellular migration potential. The cells exposed to 5 μg mL^{-1} GPTMS non-significant increase in the migration potential, while the cells treated with 25 μg mL^{-1} and 50 μg mL^{-1} GPTMS showed 2.5 and 1.7 times ($p < 0.5$) increased migration of fibroblasts inside the scratch area respectively. This points towards the higher biocompatibility of GPTMS at a concentration ranging from 5 to 50 μg mL^{-1}, as illustrated in Fig. 4C(a) and (b).

3.4. Electrochemical studies

The electrochemical analysis was performed through CV, DPV, and EIS during the SP17 immunosensor development. The PBS (0.2 M, pH 7.0) consisting of 0.9 % NaCl and 5 mM $[Fe(CN)_6]^{3-/4-}$ as an inner sphere redox species were utilized for whole experiments to monitor the transfer of electrons between the electrolyte and the developed electrodes. The electrons produced from the electrochemical response were transferred through the Fe (III)/Fe (IV) redox mediator leading to a current signal which depicts the distinct role of the developed electrode. This redox species showed a heterogeneous one-electron transmission, *i.e.*, $n = 1$.

3.4.1. Optimization of analytical parameters

The electrochemical response of the developed immunosensor can be affected by various parameters. Thus, in the present study, for the selection of the ideal binding interactions taking place between SP17 antigens and anti-SP17 antibodies, four distinct parameters such as (i) GPTMS concentration effect, (ii) anti-SP17 antibody concentration, (iii) anti-SP17 antibody incubation time, and (iv) effect of BSA concentration were investigated [the detailed explanation of optimization parameters has been given in supporting information (S1)]. The optimized findings of experimental factors are described in Fig. S4 and Table S1 of the

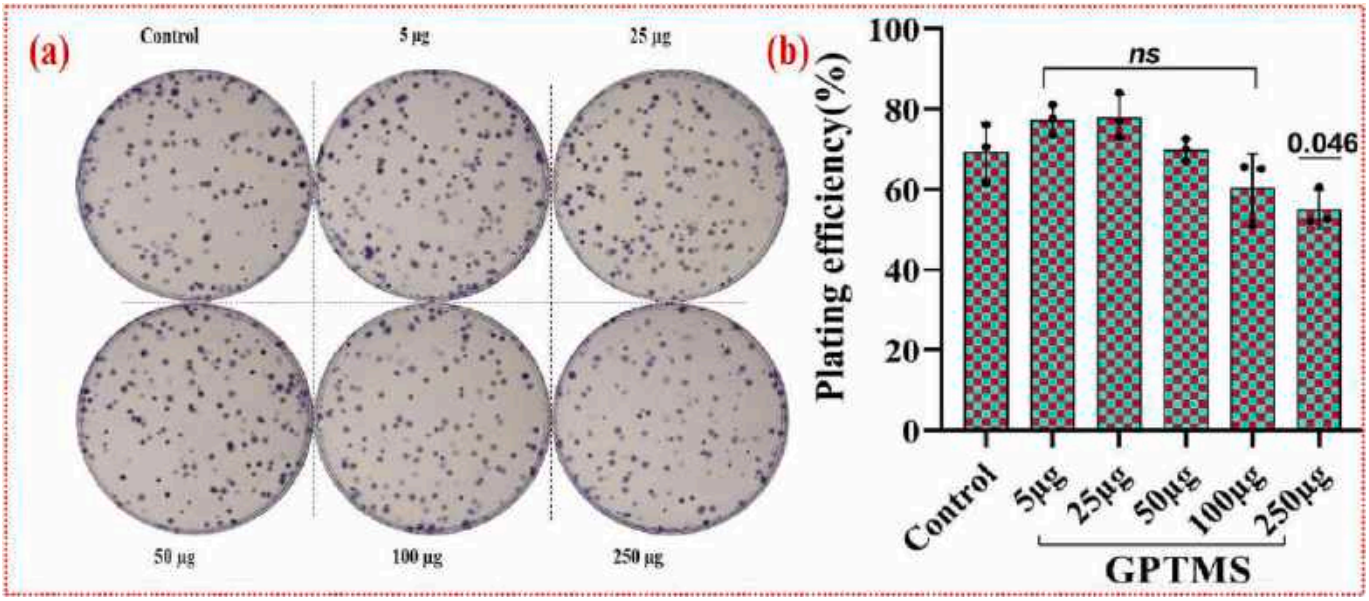

Fig. 4B. (a) and (b) Reproductive potential with various concentrations of GPTMS using Macro colony assay.

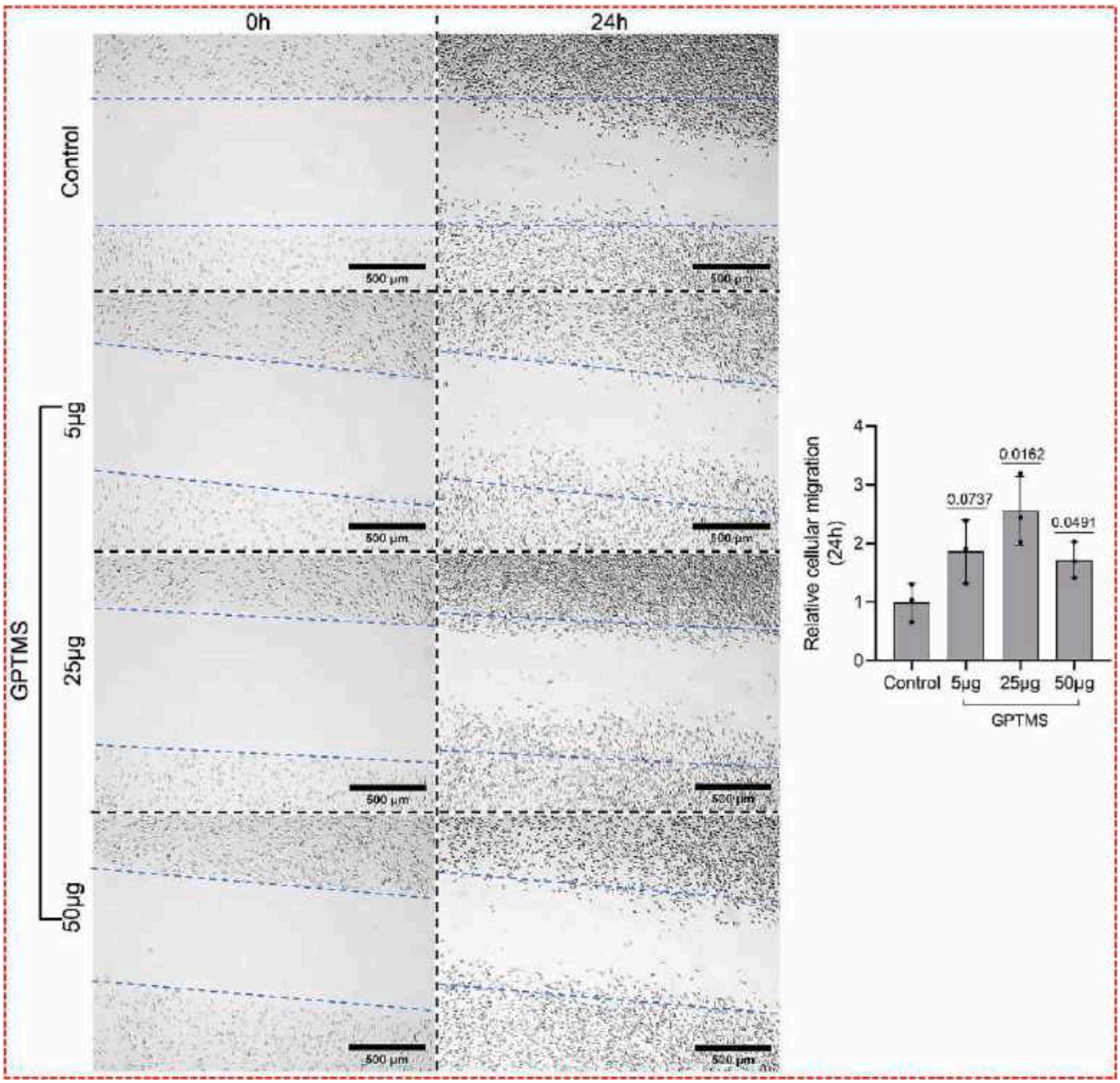

Fig. 4C. (a) and (b) Cellular migration potential of GPTMS.

supporting information file.

3.4.2. *pH study*

The pH analysis has a vital significance as pH variations can impact the microstructure and activity of the proteinaceous biological molecules like BSA and Ab immobilized on the surface of the electrode. Therefore, the first electrochemical experiment that was conducted was the effect of pH for exploring the electrochemical analysis of the fabricated BSA/anti-SP17/GPTMS@SAMs/ITO immunoelectrode in PBS (0.2 mM, 0.9 % NaCl) comprising $[Fe(CN)_6]^{3-/4-}$ as redox mediator at 50 mV s^{-1} with varying pH range (6.0 to 8.0). The results showed that the proteinaceous biological molecule's surface charge is based on the buffer solution pH, affecting the electrochemical response, and thus, the maximum anodic current was obtained at neutral pH = 7.0 [Fig. 5(A)]. The attained results depict that the proteinaceous molecule, *i.e.*, the antibody, is reactive in its native form as well as highly stable at pH = 7.0. The alkaline and acidic pH would cause protein denaturation of biological molecules owing involvement of OH^- or H^+ ions on the antibody's amino acids [53,54]. Hence, viewing all these factors, successive electrochemical responses were performed using a PBS buffer of neutral pH.

3.4.3. *Electrode study*

CV and EIS are efficient methods for providing valuable data on the difference in the current response of the electrode [55]. Due to this, CV and the EIS technique were used to follow the fabrication process of the proposed biosensor and to analyze the interface properties of ITO-modified electrodes. The electrochemical CV studies of the different modified surfaces were investigated at a 50 mV s^{-1} scan rate within a fixed potential window of −0.8 to +0.8 V in 0.2 M PBS comprising the redox species. For all electrodes, a well-defined redox peak current is detected. The peak separation for hydrolyzed bare ITO is >400 mV due

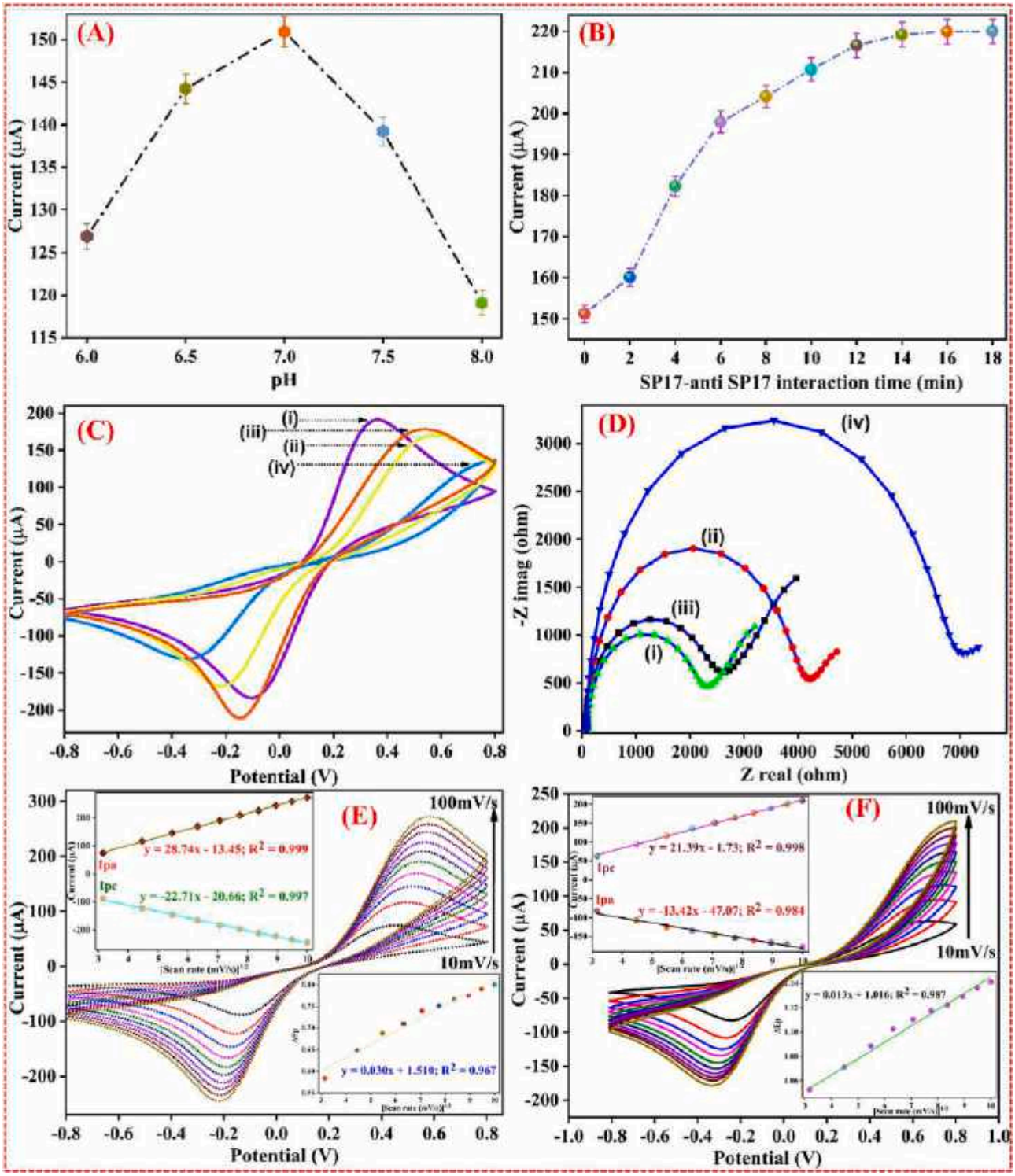

Fig. 5. (A) Effect of different pH (6.0–8.0) on BSA/anti-SP17/GPTMS@SAMs/ITO immunoelectrode; (B) Response time studies of BSA/anti-SP17/GPTMS@SAMs/ITO immunoelectrode as a function of SP17; (C) CV response, and (D) EIS spectra of the step-by-step construction of immunosensor in PBS (0.2 mM; pH 7.0) comprising redox species of hydrolyzed ITO (i), GPTMS@SAMs/ITO (ii), anti-SP17/GPTMS@SAMs/ITO (iii), BSA/anti-SP17/ GPTMS@SAMs/ITO electrodes (iv); CV response of various scan rates from 10 to 100 mVs^{-1}, (E) GPTMS@SAMs/ITO, as well as (F) BSA/anti-SP17/GPTMS@SAMs/ITO immunoelectrode. The upper inset shows the anodic and cathodic peak current magnitude, and the lower inset depicts the difference of oxidation as well as reduction peak potential (ΔEp = Epa − Epc) *versus* the square root of scan rate, respectively.

to a combination of factors, including the surface roughness and heterogeneity of the electrode, the presence of defects and impurities, and the kinetics of the electrochemical reactions occurring at the electrode surface. As observed in Fig. 5(C), the ITO electrode exhibits an increased value of peak currents at 190.88 μA [curve (i)]. However, low peak currents of 170.56 μA [curve (ii)] were observed after modification with GPTMS (GPTMS@SAMs/ITO) owing to the non-conductive nature of the GPTMS layer. The formation of epoxysilane monolayer was a barrier; therefore, diffusion of redox mediator could not occur to the electrode's surface [36,42]. Moreover, the anti-SP17 antibodies' attachment on the

surface of GPTMS@SAMs/ITO instigated mediator-like activity, which increases the transfer of electrons, and thus, an increase in current was seen owing to the small electron tunneling distance between the electrode and antibodies [56]. Therefore, the slight increase in anodic peak currents was recorded at 178.64 μA [curve (iii)]. This also suggests efficient bioconjugation through the Fc region and good orientation of anti-SP17 on the surface of the electrode. Moreover, the electrostatic charge interaction created by Fe^{3-}/Fe^{4-} transformation in the redox probe with the antibody's cationic $-NH_3^+$ terminus (F_{ab} terminal) promotes electron transport across the electrolyte-electrode interface. It may also be inferred that anti-SP17 is immobilized onto the sensor surface without altering their specificity and immunological activity. Then, immobilization of BSA was done by covering the left epoxy ends on the surface of the electrode; hence the electrical conductance decreased drastically to 137.34 μA [curve (iv)] due to the non-conductive property of BSA molecules. This reveals the blockage of unspecific surface sites, which endow the electrode resistant to non-specific adsorption of contaminants and thus resist the permeability of the redox probe $[Fe(CN)_6]^{3-/4-}$ between the electrode surface and the medium. The results show that BSA was immobilized on the anti-SP17/GPTMS@SAMs/ITO electrode.

Further, Electrochemical Impedance Spectroscopy (EIS) studies of ITO, GPTMS@SAMs/ITO, anti-SP17/GPTMS@SAMs/ITO, and BSA/anti-SP17/GPTMS@SAMs/ITO were also performed for characterizing the step-wise modification made on the surface of the ITO electrode in PBS solution containing $[Fe(CN)_6]^{3-/4-}$ in the 100 kHz −10 Hz frequency range at zero (0) potential [Fig. 5(D)]. EIS is an effective way to monitor surface-modified electrode properties and thus allows the understanding of chemical transformation and processes formed on the electrode surface. The semicircle of the Nyquist plot shows the charge transfer resistance (R_{ct}) of various electrodes, which depends on the dielectric features of the electrolyte and the surface of the electrode. Randle's equivalent circuit has been displayed in Fig. S5. Various parameters were estimated, which include time constant (τ), rate constant of heterogeneous electron transfer (K_{ct}) as well as charge transfer resistance (R_{ct}) for ITO, GPTMS@SAMs/ITO, anti-SP17/GPTMS@SAMs/ITO, and BSA/anti-SP17/GPTMS@SAMs/ITO immunoelectrode as described in Table S2 [the detail explained data has been mentioned in Supporting information (S2)]. Moreover, the EIS spectra measurements were also taken in PBS only (pH 7.0) *i.e.*, in the absence of $[Fe(CN)_6]^{3-/4-}$ [Fig. S6] and estimated various parameters (Table S3) to compare the FRA response in PBS having 5 mM $[Fe(CN)_6]^{3-/4-}$ and without 5 mM $[Fe(CN)_6]^{3-/4-}$. The results of EIS spectra in PBS only showed same trend as EIS spectra in presence of redox species for different modified electrodes, however the semicircle Nyquist plot is not same as in presence of redox species. Thus, the CV results were in agreement with the EIS measurements that revealed the excellent immobilization processes on the electrode surface.

3.4.4. Scan rate studies

Interfacial kinetics of the surface of GPTMS@SAMs/ITO and BSA/anti-SP17/GPTMS@SAMs/ITO electrodes were analyzed by differing the scan rate ranging from 10 to 100 mVs^{-1} [Fig. 5(E) and (F)]. In both cases, the cathodic (Ipc) and anodic (Ipa) peak currents magnitudes rise with the increased value of the scan rate, which shows that the electrochemical process is diffusion control [57,58]. Fig. 5(E) and (F) (upper inset) depict the anodic (Ipa) as well as cathodic (Ipc) peak currents as a function of the square root of the scan rate. Both electrodes illustrate the linear rise in current magnitude with the surge in scan rate values. When performing CV, increasing the scan rate increases the current response observed during the experiment. This is because a faster scan rate allows more redox reactions to occur in a shorter span of time, resulting in a higher current. However, increasing the scan rate also leads to an increase in the peak separation, which refers to the difference in potential between the oxidation and reduction peaks in a CV. This is because as the scan rate increases, the time available for the diffusion of species to the electrode surface decreases. This can lead to a greater separation between the oxidation and reduction peaks as the oxidation and reduction processes become more kinetically controlled. Therefore, increasing the scan rate can result in a trade-off between obtaining a higher current response and maintaining a reasonable peak separation. The full description of this study is provided in the Supporting information (S3).

3.5. Analytical performance towards SP17 detection

3.5.1. Incubation studies

For monitoring the time needed for completion of interaction between BSA/anti-SP17/GPTMS@SAMs/ITO immunoelectrode with SP17 antigen and for confirming anti-SP17 antibodies-SP17 antigen immunocomplex formation, the incubation analysis was performed by measuring the variations in anodic peak current repeatedly after adding SP17. Here, measurement of BSA/anti-SP17/GPTMS@SAMs/ITO immunoelectrode was done utilizing the C*V* technique with a particular SP17 concentration, *i.e.*, 4000 pg mL^{-1} for 18 min at 2 min regular intervals. It was seen that after adding a specific concentration, the increase in peak current was reported till 15 min, and after that, flattening of the curve occurs, resulting in saturation of current [Fig. 5(B)]. Thus, 15 min incubation time was given for the complete reaction to occur after adding each concentration of SP17, and therefore, the investigation of the subsequent electrochemical response of the developed immunosensor was done using this procedure.

3.5.2. Electrochemical response studies

To determine the concentration-dependent measurements, the theory of the rate of transportation and charge formation at the surface of the electrode was employed [59]. The analytical response of the developed immunosensor BSA/anti-SP17/GPTMS@SAMs/ITO was conducted by measuring the various SP17 antigens concentrations (100–6000 pg mL^{-1}) under optimum experiment conditions. The electrochemical response of the developed immunosensor was recorded by CV (at 50 mVs^{-1} scan rate within the −0.8 V to +0.8 V potential range) [Fig. 6A] and DPV (−0.8 to +0.8 V) [Fig. 6C] techniques in PBS solution containing redox species. The charge distribution and diffusion of the redox probe towards the electrode surface vary due to the covalent interaction between antigen and antibody. The variations are because antibodies function as polyelectrolytes in solution, and their electrical charge changes when they attach to the electrode surface. Thus, these changes are measured by varying the oxidation peak current of CV and DPV by providing a 15 min incubation period. It was established that after increasing the SP17 concentration from 50 to 6000 pg mL^{-1}, there seems to be a linear rise in peak current that got stable after 6000 pg mL^{-1} concentration addition as shown in Fig. 6A and C (the inset displayed the magnified image showing the peak current). The peak current was gradually increased on adding higher concentrations of SP17 is due to the formation of an antigen–antibody complex by probing the features of the interfacial properties. This complex offers additional electroactive locations for unstrained electron transfer at the surface of electrode and results in the formation of electron transfer layer as well as change the conformational structure [60–62]. Moreover, the sequence of sperm protein 17 (SP17) antigen (Accession: AAK20878.1, sperm protein 17, *Homo sapiens*) is known to contain 3 residues of tyrosine (Y) amino acid molecules (full length amino acid sequence has been shown in Fig. S7). During an electrochemical reaction, these tyrosine amino acid molecules undergo oxidation and release electrons resulting in increased peak current as shown in Scheme 2 [63,64]. The rise in concentration of tyrosine amino acids due to addition of higher concentrations of SP17 antigen is likely to result in enhanced antigen-antibody interaction onto BSA/anti-SP17/GPTMS@SAMs/ITO immunoelectrode leading to gradual increase in peak currents [9,65]. Alternatively, it may perhaps be attributed to both the conformation changes in the BSA/anti-SP17/GPTMS@SAMs/ITO matrix and the strong affinity of SP17 antigen

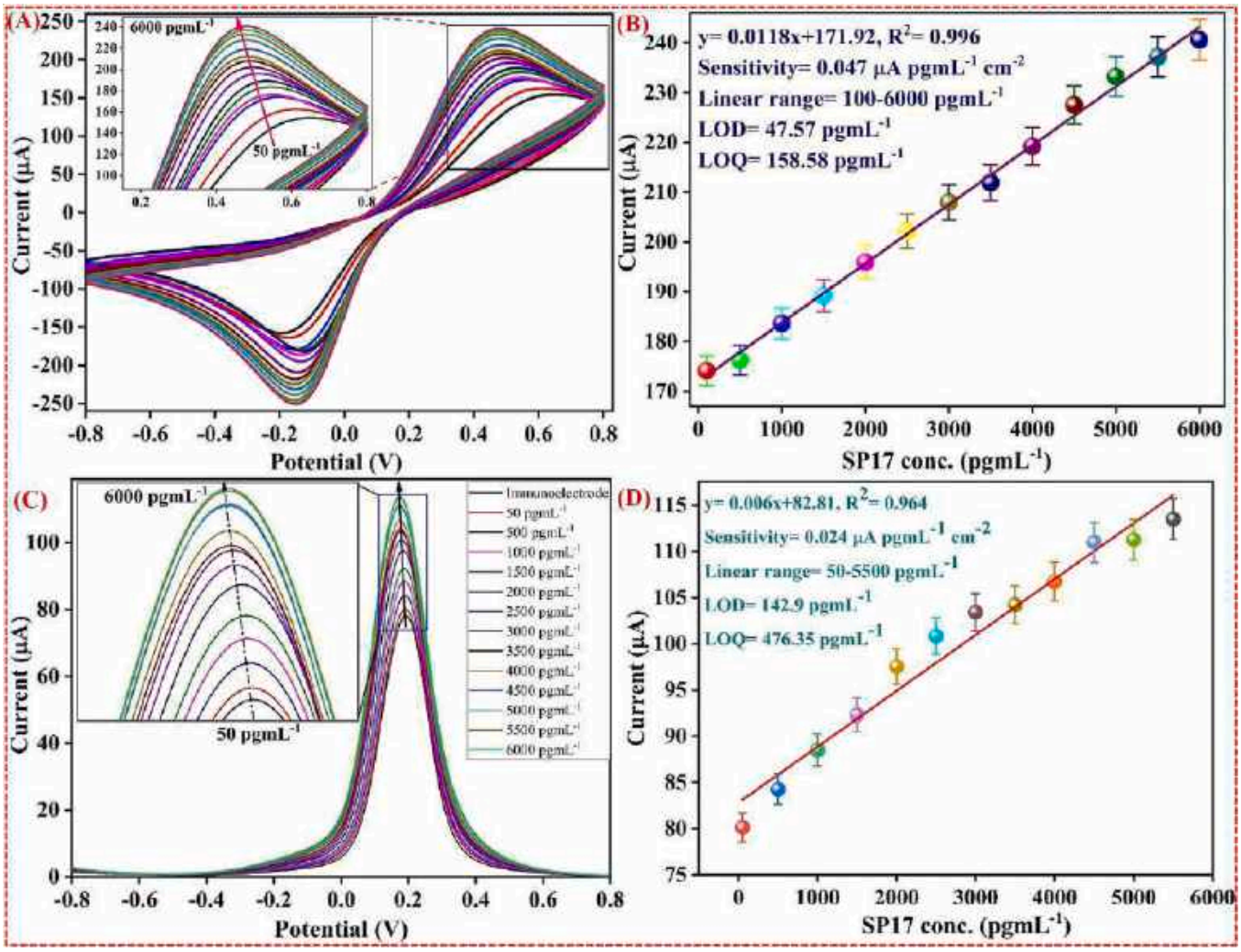

Fig. 6. The electrochemical response of BSA/anti-SP17/GPTMS@SAMs/ITO immunoelectrode as a function of increasing concentrations of SP17 (50–6000 pg mL^{-1}) through (A) CV and (C) DPV techniques and calibration plot of magnitude of anodic peak current against concentration of SP17 through (B) CV (50–6000 pg mL^{-1}) and (D) DPV (50–5500 pg mL^{-1}) techniques [inset shows the magnified image].

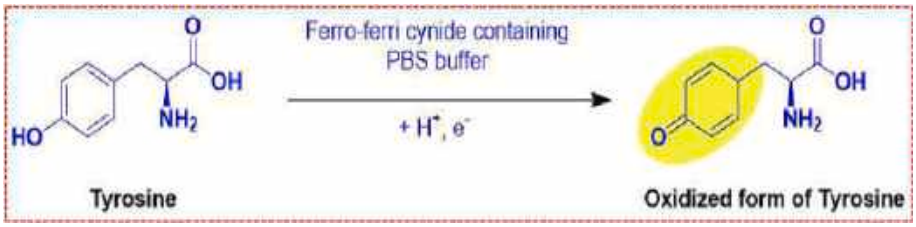

Scheme 2. Schematic illustration of oxidation reaction of Tyrosine molecules.

towards the spatially oriented antibodies that are likely to provide easy conducting paths for electron transfer to the BSA/anti-SP17/GPTMS@SAMs/ITO electrode leading to improved sensing characteristics such as linearity, faster response time and shelf life [66] [63,67]. In addition, GPTMS@SAMs get attached to biomolecules covalently (anti-SP17 antibodies and SP17 antigen) as well as act as a molecular wire between the surface of the electrode and biomolecules. Additionally, a similar trend of increased current has been observed for other biological analytes, such as prostate specific antigen [63], carcinoembryonic antigen [68], CYFRA-21-1 (oral cancer biomarker) [65], Aflatoxin B1 [69], Annexin A2 (liver cancer biomarker) [9], SARS-CoV-2 [70], *Vibrio cholerae* [71], Troponin I [72], *S. aureus* [73], quinolinic acid (neurotoxin) [74] and influenza virus H1N1 [75], in several label-free electrochemical detection studies.

Moreover, when the concentration of the analyte increases, the potential of the electrode shifts towards a more positive direction [Fig. 6A and C]. This phenomenon is known as the Nernst equation, which relates the electrode potential to the analyte concentration in the solution. The Nernst equation states that the potential difference between the two electrodes in an electrochemical cell is proportional to the logarithm of the ratio of the analyte concentrations at the two electrodes. Specifically, the equation is:

$$E = E0 + (RT/nF) \times ln([ox]/[red])$$

where: E is the potential difference between the two electrodes; E0 is the standard electrode potential; R is the gas constant; T is the temperature in Kelvin; n is the number of electrons transferred in the electrochemical reaction; F is Faraday's constant; [ox] and [red] are the concentrations of the oxidized and reduced forms of the analyte, respectively.

As the concentration of the analyte increases, the ratio of [ox]/[red] increases, and the logarithmic term in the Nernst equation becomes more positive. Therefore, the overall potential of the electrode shifts in a more positive direction. In summary, the potential of an electrode shifts towards a more positive direction as the concentration of the analyte increases due to the logarithmic relationship described by the Nernst equation.

After optimizing all the experimental parameters, outstanding linearity was achieved between the current difference (ΔI) and SP17 concentration ranging from 50 to 6000 pg mL^{-1}, as depicted in Fig. 6(B and C). The linear curve between peak current as a function of concentrations of SP17 with positive inclination [Fig. 6(B and D)] gave the following linear Eqs. (2) and (3) with a 0.996 and 0.964 linear regression coefficient (R^2).

$$\mathrm{Ip} = \left[0.0118\ \left(\mu\mathrm{A\ mL\ pg^{-1}}\right) \times \mathrm{SP17\ conc.}\left(\mathrm{pg\ mL^{-1}}\right)\right] + 171.92\ \mu\mathrm{A}, \mathrm{R}^2 = 0.996 \quad (2)$$

$$\mathrm{Ip} = \left[0.0060\ \left(\mu\mathrm{A\ mL\ pg^{-1}}\right) \times \mathrm{SP17\ conc.}\left(\mathrm{pg\ mL^{-1}}\right)\right] + 82.81\ \mu\mathrm{A}, \mathrm{R}^2 = 0.964 \quad (3)$$

The SAMs of GPTMS acted as the outstanding matrix due to the strong non-covalent interactions with the biological molecules having the negative surface charge, which helped in adsorbing the mass anti-SP17 antibodies, therefore achieving a remarkable 0.047 μA mL pg^{-1} cm^{-2} and 0.024 μA mL pg^{-1} cm^{-2} sensitivity along with R^2 of 0.996 and 0.964 as well as the rapid response time of 15 min through CV and DPV, respectively. The sensitivity was calculated from the linear plot' slope/surface area, *i.e.*, 0.25 cm^2. The immunosensor depicted a broad linear detection range (LDR) for SP17 from 100 pg mL^{-1} to 6000 pg mL^{-1} (CV) and 50–5500 pg mL^{-1} (DPV). The limit of quantification (LOQ) and the detection limit was estimated as 158.58 pg mL^{-1} (CV) and 476.35 pg mL^{-1} (DPV) (calculated using = 10σ/m) and 47.57 pg mL^{-1} (CV) and 142.9 pg mL^{-1} (DPV) (calculated using = 3σ/m), respectively, where m depicts the sensitivity, as well as σ, shows the standard deviation of intercept [76]. Henceforth, the developed GPTMS@SAMs biosensor exhibits outstanding biosensing parameters for effectively determining SP17. Table 1A represents the comparative parameters of an earlier published biosensor for detecting SP17. The BSA/anti-SP17/GPTMS@SAMs/ITO immunosensor shows improved sensitivity, LDR value, and response time than our previously reported work [7] (0.013 μA mL pg^{-1} cm^{-2}; 100–6000 pg mL^{-1} and 15 min, respectively) and ELISA kit (64–2400 pg mL^{-1}). GPTMS-SAMs have one molecule thick layer as well as offer facile contact to the SP17 antigen for rapid charge transfer owing to the molecular interaction between the biomolecules in the vicinity of the surface of electrode and analyte, thus leading to broad LDR from 50 to 6000 pg mL^{-1} and low LOD of 47.57 pg mL^{-1}. From this outstanding detection limit, the immunosensor can sense 22 × 10^7 SP17 molecules [detailed calculation for SP17 molecules has been given in supplementary information, S4], hence determining an ultralow SP17 concentration.

Further, the estimation of the association constant, *i.e.*, K_a, was done using the Hens-Wolf plot, which is between the concentration of SP17 and SP17 conc./current for BSA/anti-SP17/GPTMS@SAMs/ITO immunoelectrode as depicted in Fig. 7(a) and the calculated value obtained is 250 pg mL^{-1}. K_a depends on various factors of the developed immunosensor, such as how immobilization of antibodies on the surface of the electrode was done and biomolecules binding areas, that could be the basis of different conformation variations in the structure of antibodies present on the electrode surface. The increased K_a value shows increased BSA/anti-SP17/GPTMS@SAMs/ITO immunoelectrode affinity for SP17 owing to the higher loading and constructive anti-SP17 conformation on the surface of the electrode. The value of K_a was estimated through the inverse slope values achieved from the Hanes-Wolf linear fitting plot.

3.5.3. Control study

Using the CV technique, a control study was performed to determine the SP17 concentrations' effect on the electrochemical response of the GPTMS@SAMs/ITO electrode. It was observed from Fig. 7(b) those negligible variations occurred in anodic peak current against the increasing values of antigen SP17 concentrations from 100 to 6000 pg mL^{-1}. Thus, it was concluded that the fabrication of immunocomplex between anti-SP17 antibodies and SP17 antigen is entirely responsible for the difference in peak current during the electrochemical response study and not because of the interaction between GPTMS@SAMs/ITO and SP17 molecules.

3.5.4. Selectivity studies

Further, selectivity is the standard demand for developing an immunosensor. For evaluating the selectivity/interference of the developed platform towards SP17, some analogous proteins and metabolites [cytokeratin 19 fragment (CYFRA-2-1), TNF-α, uric acid, oxalic acid, ascorbic acid, interleukin-8 (IL-8), urea, and glucose] present in human serum were selected as interference biomarkers. These biomarkers are successively added to measure the electrochemical response of BSA/anti-SP17/GPTMS@SAMs/ITO immunoelectrode. As seen from Fig. 7(c), the difference in current occurred only after SP17 addition. This is caused owing to the specific recognition between SP17 antigen and anti-SP17 antibody, as no variation was seen on adding other interferents. Therefore, the fabricated biosensor depicted high selectivity for the detection of SP17. Furthermore, the interference from analytes is estimated using Eq. (4) to calculate the selectivity coefficient (SC).

$$SC = \frac{I_{c+i}}{I_c} \quad (4)$$

where Ic and (Ic + i) correspond to the current value in the presence of SP17 and interfering molecules, respectively. The calculated SC for the tested analytes is found to be significantly low (SC ~ 1), indicating the minimal effect of the interfering molecules on the immunosensor response.

3.6. Reusability, reproducibility, repeatability, and shelf-life studies

Repeatability and reproducibility are two main parameters of immunosensors development for practical utility. To observe the reproducibility response of the fabricated immunosensor, 8 diverse

Table 1A
Comparative biosensing parameters of earlier reported biosensors for SP17 detection.

Immunoelectrode	Method	Sensitivity (μA mL^{-1} pg^{-1} cm^{-2})	Linear range (pg mL^{-1})	LOD (pg mL^{-1})	LOQ (pg mL^{-1})	Response Time (min)	Regeneration	Shelf-life (week)	Ref.
BSA/anti-SP-17/APTMS/ITO	DPV	0.013	100–5000	70.07	233.57	30	5 (90 %)	5	[7]
BSA/anti-SP17/GPTMS@SAMs/ITO	CV DPV	0.047 0.024	100–6000 50–5500	47.57 142.9	158.58 476.35	15	5 (95 %)	8	Present work

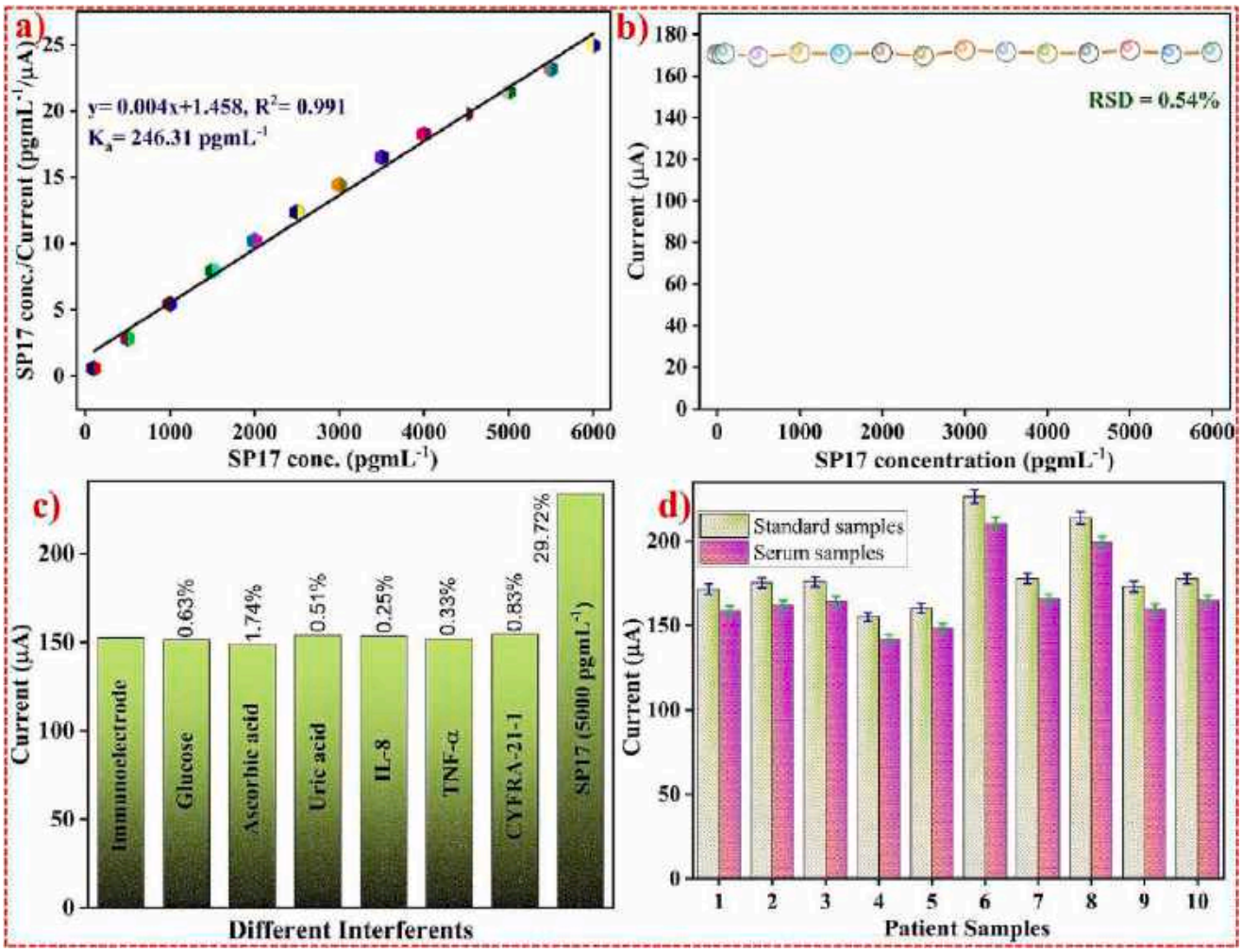

Fig. 7. (a) Measurement of Ka value using Hens-Wolf plot from developed biosensor; (b) Control studies depicting the electrochemical response of GPTMS@SAMs/ITO as a function of SP17 concentrations (100 pg mL^{-1}–6000 pg mL^{-1}), (c) Selectivity response performed utilizing the different analytes present in the blood of human in addition to SP17; and (d) Current comparison depicted by bar graph obtained using the CV of cancer patient samples and standard response.

electrodes were fabricated independently under similar experimental situations and used for evaluating the peak current response. The low relative standard deviation (RSD) was found at 3.42 %, as illustrated in Fig. 8(A). In addition, the repeatability of the proposed BSA/anti-SP17/GPTMS@SAMs/ITO immunoelectrode was assessed by taking 6 successive measurements for a specific SP17 concentration (6000 pg mL^{-1}) employing the CV technique [Fig. 8(B)]. A negligible difference in current was seen for repeatability with a % RSD of 0.93 %, which is quite acceptable. Both these results depicted capability and fair precision for providing repeatable and reproducible results.

In order to study the regeneration response of the immunosensor, the developed electrode was dipped in an acidic solution (HCl, 0.1 %, and ultra-pure water) after coupling of SP17 antigen, as well as again measuring the reading. The immunosensor electrochemical responses were recorded after each regeneration procedure. As depicted in Fig. 8 (C), the BSA/anti-SP17/GPTMS@SAMs/ITO immunosensor could be reutilized at least 5 times as 95 % retention of initial response was reported.

The long shelf-life is vital for its application as a biosensor. Thus, the shelf life of developed BSA/anti-SP17/GPTMS@SAMs/ITO immunoelectrode was measured in PBS (pH 7.0) at one-week intervals through CV analysis for 11 consecutive weeks [Fig. 8(D)]. The immunoelectrode depicts a 90 % response for 8 weeks, after which decrement of the peak current occurred abruptly. Hence, the obtained shelf-life of immunoelectrode was 6 weeks when kept at 4 °C.

3.7. Practical application in human blood samples

The practical utility of the immunosensor is vital for analyzing human biological samples [77,78]. SP17 is regarded as a tumor biomarker in an individual's serum; thus, SP17 concentration determination in the blood is vital. For this experiment, GPTMS@SAMs modified immunoelectrode was used to detect SP17 concentration in a complex biological medium, *i.e.*, human blood samples. We obtained ten serum samples of cancerous patients with swelling or lesions in the mouth produced by tobacco consumption over many years to determine SP17antigen. We quantified the concentration of SP17 through a quantitative sandwich ELISA kit (CUSABIO; Catalog No.- CSB-EL022451HU) and repeated it thrice. The wells of microtiter were precovered with FITC anti-SP17 antibody. After following all the steps according to manual instructions, a colorimetric reaction took place, and its absorbance at 450 nm was recorded in an ELISA plate reader. A sequence of SP17 concentration in blood samples found by ELISA was utilized for testing the accuracy of the developed biosensor.

After the quantification was done, incubation for 15 min was given to the blood samples, and the electrochemical response *via* CV method was checked for the fabricated BSA/anti-SP17/GPTMS@SAMs/ITO immunoelectrode. It was found that the peak current value measured for the real blood samples matched the standard concentration's current. We saw a brilliant co-relation between the CV current magnitude achieved for standard concentrations of SP17 and concentrations of SP17 in a real

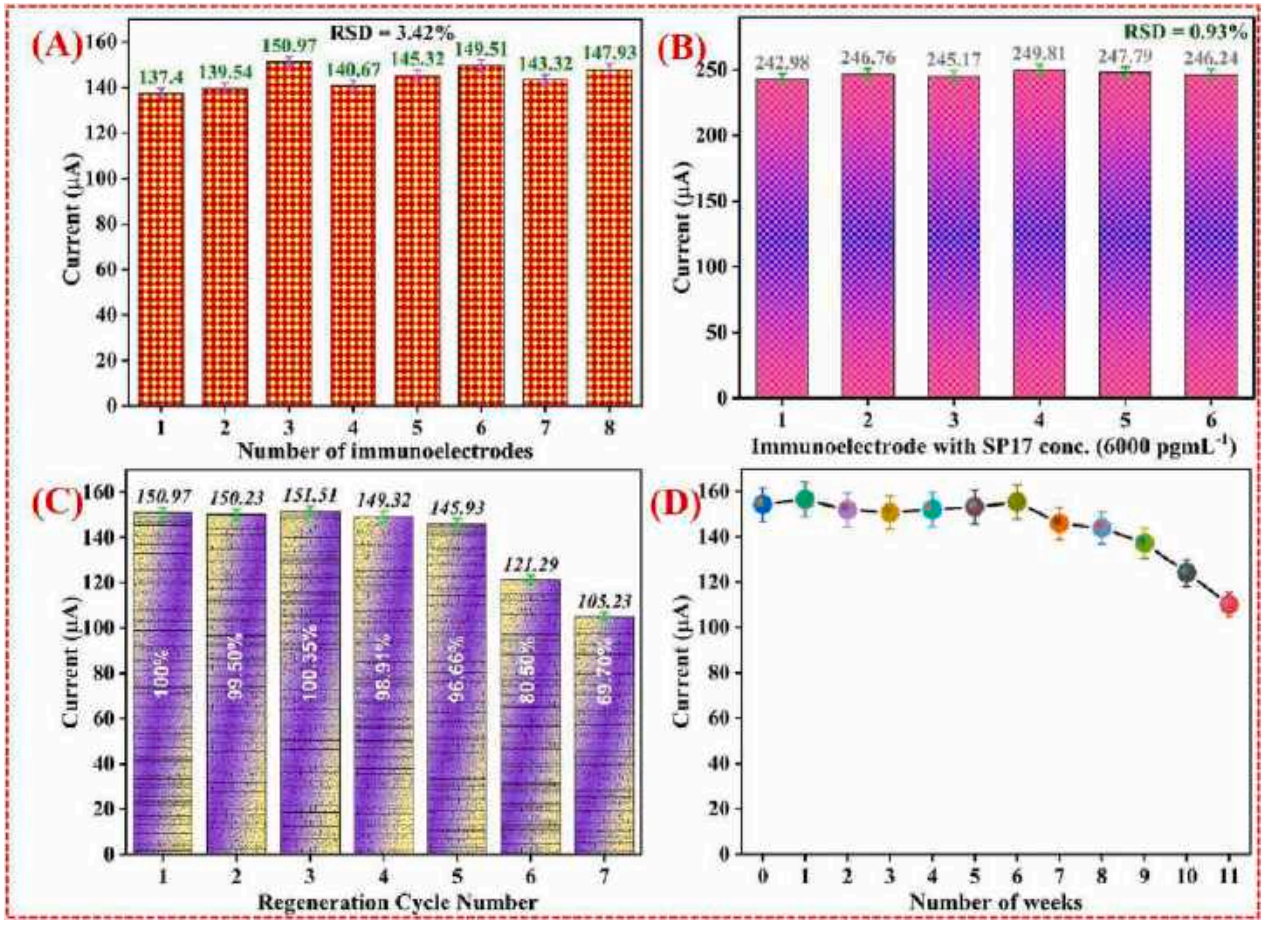

Fig. 8. Reproducibility (A) and Repeatability (B) examination of BSA/anti-SP17/GPTMS@SAMs /ITO immunoelectrode, respectively. Regeneration signal study of the BSA/anti-SP17/GPTMS@SAMs/ITO immunoelectrode (C); and Stability study of the fabricated SP17/GPTMS@SAMs/ITO immunoelectrode (D).

blood sample obtained *via* ELISA [Fig. 7(d)]. The observed results revealed ≤10 % of %RSD, indicating high accuracy of the fabricated biosensor that could detect the SP17 in human blood samples. Also, 97.89 % to 99.37 % (Table 1B) recovery rates were obtained that are quite satisfactory. Additionally, recovery results depict developed immunosensor robustness in examining the human blood samples. The developed immunosensor is a sensitive, reusable, and low-cost technique, while the ELISA needs a lengthy application procedure and is high-cost. Thus, the utilization of biosensors is more beneficial as compared to the ELISA kits.

Table 1B
Quantification of SP17 protein present in the serum of cancer patients through ELISA and its validation utilizing the developed BSA/anti-SP17/GPTMS@SAMs/ITO immunosensor.

S. No.	Sp17 concentration determined using ELISA (in pg mL^{-1})	Peak current (μA) obtained for standard Sp17 samples	Peak current (μA) obtained with patient's serum samples	% RSD	% Recovery
1.	58.94	171.63	168.93	1.12	98.42
2.	206.74	175.32	172.29	1.23	98.27
3.	336.97	176.12	175.02	0.443	99.37
4.	25.26	155.23	151.97	1.5	97.89
5.	52.21	160.45	157.97	1.1	98.45
6.	4480.41	226.38	223.93	0.769	98.91
7.	450.50	177.92	176.32	0.639	99.10
8.	3677.62	213.78	211.92	0.618	99.12
9.	275.2	173.07	170.12	1.22	98.29
10.	523.96	177.71	175.29	0.97	98.63

3.8. Statistical analysis

All bar plots show error bars and the arithmetic mean. Individual dots represent an average of experimental replicates. Unless noted, each experiment had three replicates (n = 3). A two-tailed Student t-test with GraphPad Prism8 was used to analyze the data. Results with p values <0.05 were significantly considered.

To verify the assay accuracy, coefficients of variation (CoV) and intra-test standard deviations (SD) at different SP17 standard concentrations were evaluated using the CV technique (100–6000 pg mL^{-1}). The studies were repeated thrice (n = 3), and three successive measurements were obtained after a specified optimal incubation period on a single day. As a result, the CoV was calculated using an average of three or nine observations. CV methods determined the entire mean intra-assay CoV (%) to be 0.06 %. The reported mean intra-assay CoV (%) values depict increased assay accuracy for clinical uses. Furthermore, for validating the results received using cancer patients' blood samples, the statistical examination was done employing students' F-test and *t*-test by associating its reaction with the electrochemical behavior of standard electrodes, *i.e.*, BSA/anti-SP17/GPTMS@SAMs/ITO. To do this, the average of anodic current of at least ten standard electrodes was measured before as well as after adding the serum samples, and every reading was taken thrice (n = 10 × 3). The paired t-test revealed a significant statistical variation within a 99.9 % (p 0.001) confidence interval between the two currents, suggesting that the variations did not attribute to arbitrary mistakes. Moreover, the F-test revealed a significant difference in the electrochemical response of standard electrodes before as well as after adding the blood samples, having p 0.001. These findings show that our manufactured immunosensor can accurately

detect SP17 in cancer patients' serum samples.

4. Conclusion

In summary, we fabricated a highly sensitive, selective, and reusable immunosensor for SP17 antigen detection in a human serum sample for the first time *via* GPTMS@SAMs modified low-cost and disposable ITO biosensing platform. For designing the immunosensor, anti-SP17 antibodies, as well as GPTMS@SAMs, were used as biorecognition molecules and immobilization matrices, respectively. The use of the GPTMS@SAMs provides the transfer of electrons between the working electrode surface and electrolyte and delivers binding sites for anti-SP17 bioreceptors. The proposed immunosensor depicts many benefits like simple, repeatability, selectivity, good reproducibility, low LOD (47.57 & 142.9 pg mL^{-1}), wide linear detection range (100–6000 & 50–5500 pg mL^{-1}), improved sensitivity (0.013 & 0.024 μA mL pg^{-1} cm^{-2}) by CV as well as DPV for detecting SP17 antigen. Additionally, the immunoelectrode could be repeated 5 times for the subsequent determination. These results provide a simple, stable, and reusable amperometric technique developed for SP17 detection, which will help in the early diagnosis of a cancer biomarker in real samples. This immunosensor can be used for widespread detection strategy for SP17 detection in the future. Moreover, the safety and biocompatibility of the GPTMS were in good agreement with the MTT assay findings, demonstrating the excellent efficacy of the GPTMS materials to be employed as the core electrode material for the futuristic fabrication of a biocompatible biosensing platform.

4.1. Live subject statement

All experiments were performed in accordance with Ethical Guidelines involving human subjects and approved by the All India Institute of Medical Sciences (AIIMS) and Jawaharlal Nehru University (JNU) Ethics Committee. Informed consent was obtained from human participants in this study. Experiments involving human blood were approved by the Institutional Human Ethics Committee of the Institute of Nuclear Medicine and Allied Science, Defence Research and Development Organization (INMAS/IIHEC/CT/2020/11).

Declaration of competing interest

The authors declare that they have no known competing financial interests or personal relationships that could have appeared to influence the work reported in this paper.

Data availability

The data that has been used is confidential.

Acknowledgment

All the authors greatly acknowledge Advanced Instrumentation Research Facility (AIRF), JNU, for providing the facilities for characterization. PRS is thankful to the Biomedical Device and Technology Development (BDTD) sponsored project No. TDP/BDTD/49/2021 General, Department of Science and Technology (DST), New Delhi, India; and Indian Council of Medical Research (ICMR) sponsored project No. 34/13/2019-TF/Nano/BMS, New Delhi, India for funding. Amit K. Yadav recognized the Ministry of Education, Govt. of India for the Prime Minister Research Fellowship for the financial assistants. We thank Prof. (Dr.) Alok Thakar and Prof. (Dr.) Amit Dinda from All India Institute of Medical Sciences (AIIMS), New Delhi, India, for the patient's sample collection and scientific discussion.

Appendix A. Supplementary data

Supplementary data to this article can be found online at https://doi.org/10.1016/j.ijbiomac.2023.124325.

References

[1] M. Piñeros, L. Mery, I. Soerjomataram, F. Bray, E. Steliarova-Foucher, Scaling up the surveillance of childhood cancer: a global roadmap, JNCI J. Natl. Cancer Inst. 113 (2021) 9–15.
[2] M. Pourmadadi, H. Soleimani Dinani, F. Saeidi Tabar, K. Khassi, S. Janfaza, N. Tasnim, M. Hoorfar, Properties and applications of graphene and its derivatives in biosensors for cancer detection: a comprehensive review, Biosensors 12 (2022) 269.
[3] H. Sung, J. Ferlay, R.L. Siegel, M. Laversanne, I. Soerjomataram, A. Jemal, F. Bray, Global cancer statistics 2020: GLOBOCAN estimates of incidence and mortality worldwide for 36 cancers in 185 countries, CA. Cancer J. Clin. 71 (2021) 209–249.
[4] D. Ou, D. Sun, X. Lin, Z. Liang, Y. Zhong, Z. Chen, A dual-aptamer-based biosensor for specific detection of breast cancer biomarker HER2 via flower-like nanozymes and DNA nanostructures, J. Mater. Chem. B 7 (2019) 3661–3669.
[5] A.C. Pereira, M.G.F. Sales, L.R. Rodrigues, Biosensors for rapid detection of breast cancer biomarkers, in: Adv. Biosens. Heal. Care Appl, Elsevier, 2019, pp. 71–103.
[6] X.Y. Wang, Y.G. Feng, A.J. Wang, L.P. Mei, P.X. Yuan, X. Luo, J.J. Feng, A facile ratiometric electrochemical strategy for ultrasensitive monitoring HER2 using polydopamine-grafted-ferrocene/reduced graphene oxide, Au@Ag nanoshuttles and hollow Ni@ PtNi yolk-shell nanocages, Sensors Actuators B Chem. 331 (2021), 129460.
[7] A.K. Yadav, P. Gulati, R. Sharma, A. Thakkar, P.R. Solanki, Fabrication of alkoxysilane substituted polymer-modified disposable biosensing platform: towards sperm protein 17 sensing as a new cancer biomarker, Talanta 243 (2022), 123376.
[8] C. Zhou, D. Liu, L. Xu, Q. Li, J. Song, S. Xu, R. Xing, H. Song, A sensitive label–free amperometric immunosensor for alpha-fetoprotein based on gold nanorods with different aspect ratio, Sci. Rep. 5 (2015) 1–7.
[9] D. Chauhan, Y. Kumar, R. Chandra, S. Kumar, 2D transparent few-layered hydrogen substituted graphdiyne nano-interface for unprecedented ultralow ANXA2 cancer biomarker detection, Biosens. Bioelectron. 213 (2022) 114433.
[10] M. Aydın, E.B. Aydın, M.K. Sezgintürk, Electrochemical immunosensor for CDH22 biomarker based on benzaldehyde substituted poly (phosphazene) modified disposable ITO electrode: a new fabrication strategy for biosensors, Biosens. Bioelectron. 126 (2019) 230–239.
[11] A. Kumar, B. Purohit, P.K. Maurya, L.M. Pandey, P. Chandra, Engineered nanomaterial assisted signal-amplification strategies for enhancing analytical performance of electrochemical biosensors, Electroanalysis 31 (2019) 1615–1629.
[12] P. Chandra, R. Prakash, Nanobiomaterial Engineering, Springer, 2020.
[13] K. Mahato, A. Prasad, P. Maurya, P. Chandra, Nanobiosensors: next generation point-of-care biomedical devices for personalized diagnosis, J. Anal. Bioanal. Tech. 7 (2016).
[14] J.M. Moon, D.M. Kim, M.H. Kim, J.Y. Han, D.K. Jung, Y.B. Shim, A disposable amperometric dual-sensor for the detection of hemoglobin and glycated hemoglobin in a finger prick blood sample, Biosens. Bioelectron. 91 (2017) 128–135.
[15] S. Chung, J.M. Moon, J. Choi, H. Hwang, Y.B. Shim, Magnetic force assisted electrochemical sensor for the detection of thrombin with aptamer-antibody sandwich formation, Biosens. Bioelectron. 117 (2018) 480–486.
[16] A.C. Sun, D.A. Hall, Point-of-care smartphone-based electrochemical biosensing, Electroanalysis 31 (2019) 2–16.
[17] H. Zeng, D.A.Y. Agyapong, C. Li, R. Zhao, H. Yang, C. Wu, Y. Jiang, Y. Liu, A carcinoembryonic antigen optoelectronic immunosensor based on thiol-derivative-nanogold labeled anti-CEA antibody nanomaterial and gold modified ITO, Sensors Actuators B Chem. 221 (2015) 22–27.
[18] A.K. Yadav, D. Verma, P.R. Solanki, Electrophoretically deposited L-cysteine functionalized MoS2@MWCNT nanocomposite platform: a smart approach toward highly sensitive and label-free detection of gentamicin, Mater. Today Chem. 22 (2021), 100567, https://doi.org/10.1016/J.MTCHEM.2021.100567.
[19] A.K. Yadav, D. Verma, G. Lakshmi, S. Eremin, P.R. Solanki, Fabrication of label-free and ultrasensitive electrochemical immunosensor based on molybdenum disulfide nanoparticles modified disposable ITO: an analytical platform for antibiotic detection in food samples, Food Chem. 363 (2021), 130245.
[20] D. Chauhan, A.K. Yadav, P.R. Solanki, Carbon cloth-based immunosensor for detection of 25-hydroxy vitamin D 3, Microchim. Acta 188 (2021) 1–11.
[21] A.K. Yadav, P. Gulati, R. Sharma, A. Thakkar, P.R. Solanki, Fabrication of alkoxysilane substituted polymer-modified disposable biosensing platform: toward sperm protein 17 sensing as a new cancer biomarker, Talanta 243 (2022) 123376.
[22] S.K. Mishra, A.K. Srivastava, D. Kumar, A. Mulchandani, Protein functionalized Pt nanoparticles-conducting polymer nanocomposite film: characterization and immunosensor application, Polymer 55 (2014) 4003–4011. Guildf.
[23] C.M. Pandey, S. Dewan, S. Chawla, B.K. Yadav, G. Sumana, B.D. Malhotra, Controlled deposition of functionalized silica coated zinc oxide nano-assemblies at the air/water interface for blood cancer detection, Anal. Chim. Acta 937 (2016) 29–38.
[24] D. Verma, A.K. Yadav, M. Das Mukherjee, P.R. Solanki, Fabrication of a sensitive electrochemical sensor platform using reduced graphene oxide-molybdenum

trioxide nanocomposite for BPA detection: an endocrine disruptor, J. Environ. Chem. Eng. 9 (2021), 105504.
[25] M. Aydın, E.B. Aydın, M.K. Sezgintürk, A highly selective poly (thiophene)-graft-poly (methacrylamide) polymer modified ITO electrode for neuron specific enolase detection in human serum, Macromol. Biosci. 19 (2019), 1900109.
[26] L.Y.S. Lee, T.C. Sutherland, S. Rucareanu, R.B. Lennox, Ferrocenylalkylthiolates as a probe of heterogeneity in binary self-assembled monolayers on gold, Langmuir 22 (2006) 4438–4444.
[27] D. Samanta, A. Sarkar, Immobilization of bio-macromolecules on self-assembled monolayers: methods and sensor applications, Chem. Soc. Rev. 40 (2011) 2567–2592.
[28] G. Demirel, Z. Rzaev, S. Patir, E. Pişkin, Poly (N-isopropylacrylamide) layers on silicon wafers as smart DNA-sensor platforms, J. Nanosci. Nanotechnol. 9 (2009) 1865–1871.
[29] S.M. Lee, H.J. Cho, J.Y. Han, H.J. Yoon, K.H. Lee, D.H. Jeong, Y.S. Lee, Silver nanoparticles preferentially reduced on PEG-grafted glass surfaces for SERS applications, Mater. Res. Bull. 48 (2013) 1523–1529.
[30] J.H.T. Luong, K.B. Male, J.D. Glennon, Biosensor technology: technology push versus market pull, Biotechnol. Adv. 26 (2008) 492–500.
[31] L. Yang, Y. Li, AFM and impedance spectroscopy characterization of the immobilization of antibodies on indium–tin oxide electrode through self-assembled monolayer of epoxysilane and their capture of Escherichia coli O157:H7, Biosens. Bioelectron. 20 (2005) 1407–1416.
[32] Y. Rai, R. Pathak, N. Kumari, D.K. Sah, S. Pandey, N. Kalra, R. Soni, B. S. Dwarakanath, A.N. Bhatt, Mitochondrial biogenesis and metabolic hyperactivation limits the application of MTT assay in the estimation of radiation induced growth inhibition, Sci. Rep. 8 (2018), https://doi.org/10.1038/s41598-018-19930-w.
[33] I. Gupta, A. Kumar, A.N. Bhatt, S. Sapra, S. Gandhi, Green synthesis-mediated silver nanoparticles based biocomposite films for wound healing application, J. Inorg. Organomet. Polym. Mater. 32 (2022) 2994–3011.
[34] A.N. Bhatt, A. Kumar, Y. Rai, N. Kumari, D. Vedagiri, K.H. Harshan, V. Chinnadurai, S. Chandna, Glycolytic inhibitor 2-deoxy-D-glucose attenuates SARS-CoV-2 multiplication in host cells and weakens the infective potential of progeny virions, Life Sci. 295 (2022), 120411.
[35] A. Kumar, D.K. Sah, K. Khanna, Y. Rai, A.K. Yadav, M.S. Ansari, A.N. Bhatt, A calcium and zinc composite alginate hydrogel for pre-hospital hemostasis and wound care, Carbohydr. Polym. 299 (2023), 120186.
[36] S. Kumar, J. Singh, V.V. Agrawal, M. Ahamad, B.D. Malhotra, Biocompatible self-assembled monolayer platform based on (3-glycidoxypropyl) trimethoxysilane for total cholesterol estimation, Anal. Methods 3 (2011) 2237–2245.
[37] A.K. Yadav, T.K. Dhiman, G. Lakshmi, A.N. Berlina, P.R. Solanki, A highly sensitive label-free amperometric biosensor for norfloxacin detection based on chitosan-yttria nanocomposite, Int. J. Biol. Macromol. 151 (2020) 566–575.
[38] G. Lakshmi, A.K. Yadav, N. Mehlawat, R. Jalandra, P.R. Solanki, A. Kumar, Gut microbiota derived trimethylamine N-oxide (TMAO) detection through molecularly imprinted polymer based sensor, Sci. Rep. 11 (2021) 1–14.
[39] J.M. Antonucci, S.H. Dickens, B.O. Fowler, H.H.K. Xu, W.G. McDonough, Chemistry of silanes: interfaces in dental polymers and composites, J. Res. Natl. Inst. Stand. Technol. 110 (2005) 541.
[40] Y. Gu, C.C. Chen, Eliminating the interference of oxygen for sensing hydrogen peroxide with the polyaniline modified electrode, Sensors 8 (2008) 8237–8247.
[41] P. Khullar, J.V. Badilla, R.G. Kelly, The use of a sintered Ag/AgCl electrode as both reference and counter electrode for electrochemical measurements in thin film electrolytes, ECS Electrochem. Lett. 4 (2015) C31.
[42] N. Yılmaz, E.B. Aydın, M.K. Sezgintürk, An epoxysilane modified indium tin oxide electrode for the determination of PAK 2: application in human serum samples, Anal. Chim. Acta 1062 (2019) 68–77.
[43] E.B. Aydın, M. Aydın, M.K. Sezgintürk, Construction of succinimide group substituted polythiophene polymer functionalized sensing platform for ultrasensitive detection of KLK 4 cancer biomarker, Sensors Actuators B Chem. 325 (2020), 128788.
[44] F.G.L.M. Borsagli, V.S.T. Ciminelli, C.L. Ladeira, D.J. Haas, A.P. Lage, H.S. Mansur, Multi-functional eco-friendly 3D scaffolds based on N-acyl thiolated chitosan for potential adsorption of methyl orange and antibacterial activity against Pseudomonas aeruginosa, J. Environ. Chem. Eng. 7 (2019), 103286.
[45] B. Riegel, S. Blittersdorf, W. Kiefer, S. Hofacker, M. Müller, G. Schottner, Kinetic investigations of hydrolysis and condensation of the glycidoxypropyltrimethoxysilane/aminopropyltriethoxy-silane system by means of FT-raman spectroscopy I, J. Non-Cryst. Solids 226 (1998) 76–84.
[46] I.M. Šapić, L. Bistričić, V. Volovšek, V. Dananić, K. Furić, DFT study of molecular structure and vibrations of 3-glycidoxypropyltrimethoxysilane, Spectrochim. Acta A Mol. Biomol. Spectrosc. 72 (2009) 833–840.
[47] M. Aydın, E.B. Aydın, M.K. Sezgintürk, A highly selective electrochemical immunosensor based on conductive carbon black and star PGMA polymer composite material for IL-8 biomarker detection in human serum and saliva, Biosens. Bioelectron. 117 (2018) 720–728.
[48] F.G.L.M. Borsagli, I.C. Carvalho, H.S. Mansur, Amino acid-grafted and N-acylated chitosan thiomers: construction of 3D bio-scaffolds for potential cartilage repair applications, Int. J. Biol. Macromol. 114 (2018) 270–282.
[49] K. Theerakittayakorn, T. Bunprasert, Differentiation capacity of mouse L929 fibroblastic cell line compare with human dermal fibroblast, Int. J. Med. Health Sci. 5 (2011) 51–54.
[50] M. Weber, H. Steinle, S. Golombek, L. Hann, C. Schlensak, H.P. Wendel, M. Avci-Adali, Blood-contacting biomaterials: in vitro evaluation of the hemocompatibility, Front. Bioeng. Biotechnol. 6 (2018) 99.
[51] Q. Qian, K.A. Nath, Y. Wu, T.M. Daoud, S. Sethi, Hemolysis and acute kidney failure, Am. J. Kidney Dis. 56 (2010) 780–784.
[52] D. Fischer, Y. Li, B. Ahlemeyer, J. Krieglstein, T. Kissel, In vitro cytotoxicity testing of polycations: influence of polymer structure on cell viability and hemolysis, Biomaterials 24 (2003) 1121–1131.
[53] D. Chauhan, V. Nirbhaya, C.M. Srivastava, R. Chandra, S. Kumar, Nanostructured transition metal chalcogenide embedded on reduced graphene oxide based highly efficient biosensor for cardiovascular disease detection, Microchem. J. 155 (2020), 104697.
[54] W. Huang, A.K. Diallo, J.L. Dailey, K. Besar, H.E. Katz, Electrochemical processes and mechanistic aspects of field-effect sensors for biomolecules, J. Mater. Chem. C 3 (2015) 6445–6470.
[55] Y. Chen, L.P. Mei, J.J. Feng, P.X. Yuan, X. Luo, A.J. Wang, Simple one-pot aqueous synthesis of 3D superstructured PtCoCuPd alloyed tripods with hierarchical branches for ultrasensitive immunoassay of cardiac troponin I, Biosens. Bioelectron. 145 (2019), 111638.
[56] S. Kumar, S. Kumar, S. Tiwari, S. Srivastava, M. Srivastava, B.K. Yadav, S. Kumar, T.T. Tran, A.K. Dewan, A. Mulchandani, Biofunctionalized nanostructured zirconia for biomedical application: a smart approach for oral cancer detection, Adv. Sci. 2 (2015), 1500048.
[57] N. Chaudhary, A.K. Yadav, J.G. Sharma, P.R. Solanki, Designing and characterization of a highly sensitive and selective biosensing platform for ciprofloxacin detection utilizing lanthanum oxide nanoparticles, J. Environ. Chem. Eng. 9 (2021), 106771.
[58] D. Verma, D. Chauhan, M. Das Mukherjee, K.R. Ranjan, A.K. Yadav, P.R. Solanki, Development of MWCNT decorated with green synthesized AgNps-based electrochemical sensor for highly sensitive detection of BPA, J. Appl. Electrochem. 51 (2021) 447–462.
[59] E. Spain, S. Carrara, K. Adamson, H. Ma, R. O'Kennedy, L. De Cola, R.J. Forster, Cardiac troponin I: ultrasensitive detection using faradaic electrochemical impedance, ACS Omega 3 (2018) 17116–17124.
[60] S. Srivastava, V. Kumar, M.A. Ali, P.R. Solanki, A. Srivastava, G. Sumana, P. S. Saxena, A.G. Joshi, B.D. Malhotra, Electrophoretically deposited reduced graphene oxide platform for food toxin detection, Nanoscale 5 (2013) 3043–3051.
[61] H. Bhardwaj, M.K. Pandey, G. Sumana, Electrochemical aflatoxin B1 immunosensor based on the use of graphene quantum dots and gold nanoparticles, Microchim. Acta 186 (2019) 1–12.
[62] V. Nirbhaya, D. Chauhan, R. Jain, R. Chandra, S. Kumar, Nanostructured graphitic carbon nitride based ultrasensing electrochemical biosensor for food toxin detection, Bioelectrochemistry 139 (2021), 107738.
[63] J. Okuno, K. Maehashi, K. Kerman, Y. Takamura, K. Matsumoto, E. Tamiya, Label-free immunosensor for prostate-specific antigen based on single-walled carbon nanotube array-modified microelectrodes, Biosens. Bioelectron. 22 (2007) 2377–2381.
[64] Y. Wei, C. Gao, F.L. Meng, H.H. Li, L. Wang, J.H. Liu, X.J. Huang, SnO2/reduced graphene oxide nanocomposite for the simultaneous electrochemical detection of cadmium (II), lead (II), copper (II), and mercury (II): an interesting favorable mutual interference, J. Phys. Chem. C 116 (2012) 1034–1041.
[65] S. Kumar, J.G. Sharma, S. Maji, B.D. Malhotra, Nanostructured zirconia decorated reduced graphene oxide based efficient biosensing platform for non-invasive oral cancer detection, Biosens. Bioelectron. 78 (2016) 497–504.
[66] Y. Wan, Y. Su, X. Zhu, G. Liu, C. Fan, Development of electrochemical immunosensors towards point of care diagnostics, Biosens. Bioelectron. 47 (2013) 1–11.
[67] S. Zhang, F. Zheng, Z. Wu, G. Shen, R. Yu, Highly sensitive electrochemical detection of immunospecies based on combination of Fc label and PPD film/gold nanoparticle amplification, Biosens. Bioelectron. 24 (2008) 129–135.
[68] S. Kumar, S. Kumar, C.M. Pandey, B.D. Malhotra, Conducting paper based sensor for cancer biomarker detection, in: J. Phys. Conf. Ser, IOP Publishing, 2016, p. 12010.
[69] D. Chauhan, Y. Kumar, R. Chandra, S. Kumar, Nanostructured zirconia@ reduced graphene oxide based ultraefficient nanobiosensing platform for food toxin detection, SensorsDiagnostics 1 (2022) 550–557.
[70] M.A. Sadique, S. Yadav, P. Ranjan, R. Khan, F. Khan, A. Kumar, D. Biswas, Highly sensitive electrochemical immunosensor platforms for dual detection of SARS-CoV-2 antigen and antibody based on gold nanoparticle functionalized graphene oxide nanocomposites, ACS Appl. Bio Mater. 5 (2022) 2421–2430.
[71] P.K. Gupta, Z.H. Khan, P.R. Solanki, One-step electrodeposited porous ZnO thin film based immunosensor for detection of vibrio cholerae toxin, J. Electrochem. Soc. 163 (2016) B309.
[72] S. Kumar, S. Kumar, S. Augustine, B.D. Malhotra, Protein functionalized nanostructured zirconia based electrochemical immunosensor for cardiac troponin I detection, J. Mater. Res. 32 (2017) 2966–2972.
[73] J. Bhardwaj, S. Devarakonda, S. Kumar, J. Jang, Development of a paper-based electrochemical immunosensor using an antibody-single walled carbon nanotubes bio-conjugate modified electrode for label-free detection of foodborne pathogens, Sensors Actuators B Chem. 253 (2017) 115–123.
[74] R. Singh, S. Kashyap, S. Kumar, S. Abraham, T.K. Gupta, A.M. Kayastha, B. D. Malhotra, P.S. Saxena, A. Srivastava, R.K. Singh, Excellent storage stability and sensitive detection of neurotoxin quinolinic acid, Biosens. Bioelectron. 90 (2017) 224–229.
[75] R. Singh, S. Hong, J. Jang, Label-free detection of influenza viruses using a reduced graphene oxide-based electrochemical immunosensor integrated with a microfluidic platform, Sci. Rep. 7 (2017) 42771.
[76] S. Kumar, S. Kumar, S. Tiwari, S. Augustine, S. Srivastava, B.K. Yadav, B. D. Malhotra, Highly sensitive protein functionalized nanostructured hafnium oxide

based biosensing platform for non-invasive oral cancer detection, Sensors Actuators B Chem. 235 (2016) 1–10.
[77] Y. Chen, X.Y. Ge, S.Y. Cen, A.J. Wang, X. Luo, J.J. Feng, Ultrasensitive dual-signal ratiometric electrochemical aptasensor for neuron-specific enolase based on Au nanoparticles@ Pd nanoclusters-poly (bismarck brown Y) and dendritic AuPt nanoassemblies, Sensors Actuators B Chem. 311 (2020), 127931.
[78] E.B. Aydın, M. Aydın, M.K. Sezgintürk, A novel electrochemical immunosensor based on acetylene black/epoxy-substituted-polypyrrole polymer composite for the highly sensitive and selective detection of interleukin 6, Talanta 222 (2021), 121596.

Talanta 243 (2022) 123376

Contents lists available at ScienceDirect

Talanta

journal homepage: www.elsevier.com/locate/talanta

Fabrication of alkoxysilane substituted polymer-modified disposable biosensing platform: Towards sperm protein 17 sensing as a new cancer biomarker

Amit K. Yadav [a], Payal Gulati [a], Rinu Sharma [b], Alok Thakkar [c], Pratima R. Solanki [a,*]

[a] Nano-Bio Laboratory, Special Centre for Nanoscience, Jawaharlal Nehru University, New Delhi, 110067, India
[b] Guru Gobind Singh Indraprastha University, Golf Course Rd, Sector 16 C, Dwarka, 110078, India
[c] Otolaryngology & Head Neck Surgery, All India Institute of Medical Sciences, New Delhi, 110029, India

ARTICLE INFO

Keywords:
(3-Aminopropyl) trimethoxysilane
Sperm protein 17
Cancer
Electrochemical immunosensor
Indium tin oxide

ABSTRACT

SP17 is a mammalian protein found in the testis and spermatozoa that have been identified as a tumor-associated antigen in a range of human cancers. A unique method for fabricating the first ultrasensitive, selective, and label-free immunosensor for the detection of SP17, a new cancer biomarker in complicated serum samples, is presented in this paper. This immunosensor was also the first biosensor built using a disposable ITO sheet modified with an aminosilane known as APTMS as an immobilization platform for fabricating the SP17 biosensor. The immobilization of chemical and biological species onto the electrode surface was cross-verified by various analytical and morphological techniques. Stepwise modifications done on the immunoelectrodes were also studied using electrochemical techniques. Selective interaction between anti-SP17 and SP17 with varying concentrations (100–5000 pg mL^{-1}) was measured with the DPV technique. The immunosensor exhibited low LOD and LOQ of 70.07 and 233.57 pg mL^{-1}, respectively, with a sensitivity of 0.013 μA mL pg^{-1} cm^{-2}. The fabricated immunosensor performance was analyzed by quantifying the SP17 concentrations in patient serum samples. The data obtained from the developed immunosensor demonstrated excellent reproducibility, repeatability, and selectivity among various interferants, including cancer biomarkers. Further, the observed results have been validated *via* ELISA, which showed good agreement with the electrochemical results. This could establish a new platform for detecting other cancer biomarkers and can be employed for clinical diagnostics applications.

Author contributions

Amit K. Yadav: Conceptualization, Investigation, Methodology, Validation, Writing - Original Draft, Review & Editing, **Payal Gulati**: Writing - Original Draft, Review & Editing, **Rinu Sharma**: Writing - Review & Editing, **Alok Thakkar**: Writing - Review & Editing, **Pratima R. Solanki**: Resources, Writing - Review & Editing, Visualization, Supervision, Project administration, Funding acquisition.

1. Introduction

Cancer is a group of diseases influencing human health worldwide with a leading cause of death. According to the recent cancer statistics data, the cancer growth rate is expected to increase in upcoming years due to deviant lifestyles, including diet, work, and environment. Biomarkers are considered as indicators of the diseased condition of the patient. The necessity for precise detection of tumor biomarkers is required to gather important disease-associated information for clinical diagnosis and prognosis [1]. There are various biomarkers reported in literature used to diagnose different cancer as of now, but to the best of my knowledge, this is the first paper discussing the role of sperm protein-17 (SP17) in the detection of certain cancers such as ovarian cancer, multiple myeloma, head and neck squamous cell carcinoma and non-small cell lung cancer immunotherapy [2–5].

SP17, an immunogenic protein whose sequence is highly conserved in the testicles and spermatozoon of mammals, belongs to the family of cancer-testis antigen (CTA). It has also been characterized as a tumor-associated antigen in various human malignancies [6]. Human SP17 is consists of 151 amino acids with a molecular mass of 24.5 kDa. SP17's function is unknown, although it is assumed to be involved in acrosomal

* Corresponding author.
E-mail address: partima@mail.jnu.ac.in (P.R. Solanki).

https://doi.org/10.1016/j.talanta.2022.123376
Received 28 September 2021; Received in revised form 31 January 2022; Accepted 8 March 2022
Available online 19 March 2022

activity, regulating sperm maturation, capacitation, and interactions with the egg zona pellucida throughout the fertilization process [7]. Combined with its cancer-specific expression, SP17 has therefore been suggested as a promising biomarker for various cancer. Detection of tumor biomarkers at their earliest with immense accuracy from body fluids can drastically decrease the mortality rate associated with cancer and demarcate a new strategy for cancer diagnosis [8]. Although several conventional techniques such as fluorescence immunoassay, radioimmunoassay, chemiluminescence immunoassay, and enzyme-linked immunoassay (ELISA) are being used for cancer diagnosis, but they have certain limitations [9,10]. Among these techniques, ELISA is the most widely used method in hospitals due to its reliability, sensitivity, specificity, and accurate quantification of biological species [11]. Despite several advantages of ELISA, it suffers from certain limitations such as laborious analysis procedure, insufficiency in sensitivity level towards challenging biomolecular species like miRNA, the requirement of central lab-based apparatus, labeled-antibody has shorter shelf-life, preparation, and consumption of excess reagents, costly and has restricted dynamic range [12]. Besides this, the ELISA method is also incapable of detecting specific protein biomarkers at their clinical threshold level, i.e., at nanomolar concentration level [13]. Developing the most sensitive and reliable point of care (POC) biosensing platform for early cancer diagnosis and monitoring treatment progress is urgently needed in developing and developed countries [14–16]. Due to several advantages of POC devices such as economic, less sample requirement, rapid monitoring, and relieving patient's anxiety, it stands out as a promising analytical platform in this new era of bio-nanotechnology [17–19]. Therefore, ultra-sensitive diagnosis of desired protein biomarkers is possible by utilizing electrochemical immunosensors in clinical diagnosis. Electrochemical immunosensor offers excellent merits such as a direct label-free antibody (Ab)-antigen (Ag) interaction-based detection phenomenon, rapid detection, economical, simple machinery, and controlled process [20,21].

The biosensing platform requires a stable and conductive substrate for biosensor fabrication to detect biomarkers. Therefore, indium tin oxide (ITO) serves the same purpose due to its unique conductivity, good optical transparency, wide working electrochemical potential window, highly stable, feasible, and miniaturized [22,23]. ITO is a planar electrode widely used in many applications such as optoelectronic devices and electrochemical biosensors. Thus, ITO is employed as a substrate for the electrochemical analysis of SP17 biomarkers in human serum in the proposed work. Another factor contributing to sensitive sensor formation is the stable immobilization of chemical/bio-recognition species onto the electrode surface. Although there are a variety of different methods for ITO electrode modification such as physical adsorption [24], electrophoretic/electrochemical deposition [25–27], self-assembled monolayers (SAMs) formation [28], silanization [29,30], and electro-polymerization [31–33] but silanization has caught significant attention of scientist, due to its uniform single layer formation and easy to use. Silanization is carried out on the hydroxylated ITO surface through SAMs formation, resulting in the generation of functional groups (-CN, –COOH, $–NH_2$, –SH) on the electrode surface, which acts as an active site for binding of biorecognition elements [34]. This functional group interaction with biomolecules facilitates electron transport between electrode surface and biomolecules.

The present study fabricates an ultra-sensitive, stable, regenerative, and novel immunosensor for SP17 biomarker detection. The steps involved in sensor fabrication are: modification of ITO electrode with APTMS, immobilization of NHS: EDC activated anti-SP17 antibody, and subsequently with BSA. The stepwise changes made on the electrode surface were studied through electrochemical measurements such as cyclic voltammetry (CV) and differential pulse voltammetry (DPV). DPV is a vital technique to gain information about SP17 antigen and anti-SP17 antibody interaction. Further, the characterization of modified ITO electrodes was performed *via* FT-IR and AFM to study functional groups and morphological characteristics. Investigation of specific immunosensor parameters was done, such as optimum operating conditions, calibration plot, and reproducibility of the SP17 biosensing platform. Sensing was performed in a linear range of 100–5000 pg mL^{-1}, and a low limit of detection (LOD) and limit of quantification (LOQ) of 70.07 and 233.57 pg mL^{-1}, respectively, were obtained from the calibration plot. The fabricated biosensor demonstrated a sensitivity of 0.013 μA mL pg^{-1} cm^{-2} with 30 min response time. To check the efficiency of the biosensor, real patient samples analysis was done, which suggested that the proposed biosensor has encouraging perspectives in the electro-analysis field. The developed immunosensor showed another crucial result in the regeneration of the biosensor. It can also be regenerated with the acidic solution, drastically decreasing the electrode's cost. The fabricated biosensor could be sensitively and quickly detect the SP17 antigen in human serum samples.

2. Experimental section

2.1. Materials and reagents

Bovine serum albumin (BSA), N-ethyl-N′-(3-dimethyl aminopropyl) carbodiimide hydrochloride (EDC), (3-aminopropyl) trimethoxysilane [APTMS], and N-hydroxysuccinimide (NHS) were purchased from Sigma-Aldrich. Sodium hydroxide pellets (NaOH), ethanol, hydrogen peroxide (H_2O_2), acetone, potassium ferricyanide ($K_3[Fe(CN)_6]^{3-/4-}$), and potassium ferrocyanide ($K_4[Fe(CN)_6]\cdot 3H_2O]^{3-/4-}$) were procured from Fisher Scientific, India. Sodium phosphate monobasic (NaH_2PO_4), sodium phosphate dibasic hydrous (Na_2HPO_4), ascorbic acid, oxalic acid, urea, uric acid, and sodium chloride (NaCl) were brought from SRL Pvt. Ltd., India. Sperm protein 17 (SP17), Cytokeratin 19 Fragment CYFRA-21-1, interleukin-8 (IL-8), Tumor necrosis factor-alpha (TNF-α), and anti-SP17 antibodies were purchased from MyBioSource, USA. Different concentrations of anti-SP17 antibody and Sperm protein 17 (SP17) antigen were reconstituted in PBS (pH 7.4) and 20 mM Tris, 150 mM NaCl buffer (pH 8.0), respectively. Human sperm surface protein SP17 (SPA 17) ELISA KIT (Catalog No.- CSB-EL022451HU) was procured from CUSABIO, USA. $NaHPO_4$ and NaH_2PO_4 were mixed in distilled water to prepare the electrolyte solution (PBS) of 0.2 M with pH = 7.0 and stored at 4 °C for further use. The ITO glass substrate was bought from Blazers, UK. All the chemicals utilized were of the analytical mark and used as such. Millipore water (MP H_2O) (18.25 M Ω/cm, Milli-Q) was used throughout the experiments.

2.2. Characterization tools

Electrochemical measurements like cyclic voltammetry (CV) and differential pulse voltammetry (DPV) were employed to study the immobilization process and monitor the immune-complex interaction among anti-SP17 antibody and SP17 antigen. The CV and DPV response of modified electrodes were carried out on an Autolab, Potentiostat/Galvanostat electrochemical analyzer (EcoChemie, The Netherlands) *via* a conventional three-electrode system; where a modified ITO sheet acted as a working electrode, a platinum wire as a counter electrode, and Ag/AgCl as a reference electrode and studied through the NOVA software of 1.10 version. These electrochemical measurements (CV and DPV) were carried out thrice (n = 3), and the amperometric measurements of the resulting biosensor were performed in PBS (0.2 M) as electrolyte with 5 mM potassium ferricyanide/ferrocyanide as redox mediators and 0.9% NaCl. CV measurements were carried out in a potential range of −0.8 to +0.8 V at a scan rate of 50 mVs^{-1}. Atomic force microscopy (AFM) of the WITEC system in the tapping mode utilizing the standard cantilevers were used to evaluate the surface modifications of the various fabrication steps. Fourier transform infrared spectroscopy (FT-IR) was done to monitor functional groups on modified electrode surfaces using the PerkinElmer spectrum 400 configuration of the FTIR spectrometer unit. FTIR was performed from 4000 to 400 cm^{-1} wavenumber with 4 cm^{-1} resolution and 16 scans per recording. The dispersive Raman

measurements were carried out in a range of 500–2000 cm^{-1} using Enspectr R532, USA laser of WITEC configuration system equipped with a confocal microscope having three objectives and a 780-nm excitation laser. Further, hydrophilicity and hydrophobicity of the fabricated electrodes were analyzed using a water-based contact angle through a drop shape analyzer [KRUSS, Germany].

2.3. Methodology

2.3.1. Preparation of working electrode

As reported in our previous work [35–37], initially, ITO electrodes of 1.5 × 0.5 cm dimensions were cleaned ultrasonically using acetone and DI water for 10 min each. After that, ITO electrodes were treated with $H_2O_2/NH_4OH/H_2O$ (1:1:5) solution for 90 min at 80 °C in an oven to obtain hydroxylated active sites onto the ITO surface. Eventually, electrodes were rinsed with ethanol and ultrapure water and dried at room temperature.

2.3.2. Fabrication of APTMS-modified SP-17 immunosensor

The hydroxylated ITO electrodes were treated with an APTMS (98%) solution overnight at room temperature (RT) to allow a P–O bond to cross-link between APTMS and hydroxylated ITO. The APTMS/ITO thin film was then rinsed with ultra-pure water to remove physically adsorbed silane molecules from the ITO film surface and further dried at RT. The SAMs formed through APTMS acts as an immune-sensing interface for biosensor construction. Additionally, anti-SP17 antibody solution of 50 μg mL^{-1} concentration was activated with the help of 0.1 M NHS (coupling agent) and 0.4 M EDC (activator) [prepared in PBS (pH 7.0)], in a ratio of 2:1:1 by incubating the mixture for 45 min before use. Subsequently, 30 μL of this activated anti-SP17 was immobilized onto APTMS/ITO electrode by incubating for 6 h in a humidified chamber (maintained at 25 °C) followed by washing with PBS (200 μL) of pH 7.0 to remove unbound anti-SP17 molecules. Before immobilization of anti-SP17 upon electrode surface, concentration optimization studies were performed. To prevent the leaching-out of anti-SP17 from the electrode surface, the carboxylic group (–COOH) present upon the Fc fragment of anti-SP17 was involved in covalent bond formation with the amine group (-NH_2) of APTMS silane molecules. EDC activated –COOH groups of anti-SP17, resulting in the generation of unstable O-acylisourea ester, which upon further reaction with the NHS, was converted to an amine-reactive NHS ester (a stable intermediate product). The anti-SP17 activation by NHS promotes the connection of –NH_2 groups of silane molecules (APTMS), resulting in amide bond formation. Finally, to minimize the non-specific interaction, the electrodes were blocked with 2% BSA for 4 h in the humid chamber to shield the terminal site, carboxylic groups. The electrodes were washed with PBS (pH 7.0; 100 μL) to remove excess unbound BSA, and the fabricated immunosensor (BSA/anti-SP17/APTMS/ITO) was ready for SP-17 detection was kept at 4 °C for further use [38]. The fabrication process of the amperometric immunosensor was illustrated in Scheme 1.

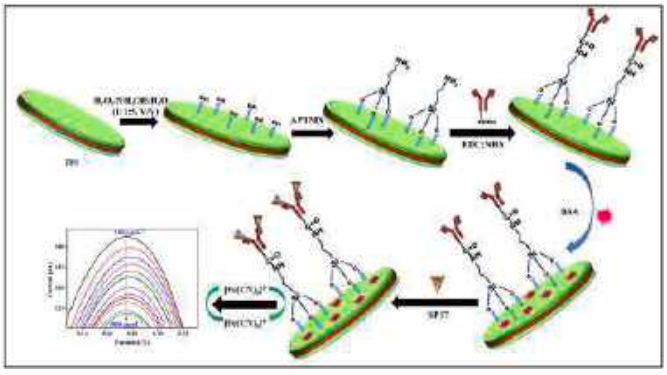

Scheme 1. Schematic illustration of SP17 cancer biomarker detection utilizing a novel APTMS self-assembled ITO based electrochemical biosensor.

2.4. Analyte (SP-17) sample preparation

The stock of SP17 protein was reconstituted in 20 mM Tris and 150 mM NaCl buffer (pH 8.0), and further various concentrations of SP17 (100 pg mL^{-1} to 5000 pg mL^{-1}) were prepared in 0.2 M PBS buffer with pH = 7.4. The developed immunosensor response was studied by utilizing the DPV measurement technique in a 0.2 M PBS (pH 7.0) having 5 mM $[Fe(CN)_6]^{3-/4-}$ containing 0.9% NaCl. The efficiency of the fabricated immunosensor was analyzed by testing real patient blood samples.

2.5. Blood sample collection

All the necessary ethical approvals were taken from the All India Institute of Medical Sciences (AIIMS), New Delhi, and Jawaharlal Nehru University (JNU), New Delhi, for patient samples collection. Patients too signed the consent form, confirming their participation at the time of blood sample collection. Blood samples were collected in a vial and allowed to stand for 20 min at 4 °C before processing. After that, blood was transferred to 5 mL centrifuge tubes and was centrifuged at 4 °C for 10 min at 3000 rpm. Eventually, serum was collected from the supernatant, and aliquots were made to avoid freeze-thaw cycles. The aliquots were stored at −80 °C until further use.

3. Results and discussion

3.1. Fourier transform infrared spectra (FT-IR) studies

FT-IR of the APTMS modified ITO electrode, i.e., APTMS/ITO electrode and anti-SP17 immobilized ITO electrode, i.e., anti-SP17/APTMS/ITO immunoelectrode, were obtained in the range of 400–4000 cm^{-1} as shown in Fig. 1A (a) and 1A (b), respectively. The –OH band broadens and shifts to 3353 cm^{-1} after APTMS interactions, with a single broad band at 3290 cm^{-1} arising from the stretching vibrations of the –N–H group of secondary amines, as illustrated in Fig. 1A (a). Two consecutive bands observed at 2925 and 2869 cm^{-1} correspond to symmetric and asymmetric stretching vibrations of the C–H bond of the APTMS alkyl chain. Moreover, one standard peak found in curves (a) and (b) around 1001 cm^{-1} wavenumber corresponds to the Si–O bond formation with the APTMS. On the contrary, Fig. 1A (b) curve represents two peaks at 1649 cm^{-1} and 1063 cm^{-1} wavenumber, obtained after anti-SP17 immobilization upon silane-modified ITO electrode. These peaks have originated from the amide bond present in proteins [39]. Additionally, curve (b) of Fig. 1A, also represents a band between 3000 and 3400 cm^{-1}, representing stretching vibrations of –OH and –N–H bonds of water molecules. One small peak observed at 1556 cm^{-1} corresponds to the amide II bond and –C═O stretching, which formed among the –NH_2 group of APTMS and –COOH group of the anti-SP17, confirming the attachment of anti-SP17 to the silane-modified ITO electrode.

3.2. Raman studies

Raman spectroscopy is usually employed to investigate the proteins' molecular structure. Raman spectra of APTMS silane molecules have been shown in Fig. 1B (a). The band observed at 383 cm^{-1} in the spectra corresponds to the bending vibration of the O–Si–O and Si–O–Si bond, whereas the band at 960 cm^{-1} results from vibration modes of -CH_3 and -NH_2 groups. The bands were seen at various frequencies such as 1070 cm^{-1} and 1306 cm^{-1}, attributed to stretching vibration of skeletal stretch and -CH_3, respectively. The peak at 1412 cm^{-1} corresponds to -CH_3 groups bending vibration involved in bond formation with Si atom (Si–CH_3). Peaks obtained at 1600 cm^{-1} and 278 cm^{-1} wavenumbers represent the bending vibration mode of the –NH_2 group and Ag–N adsorption behavior, respectively. Further, Raman spectroscopy has

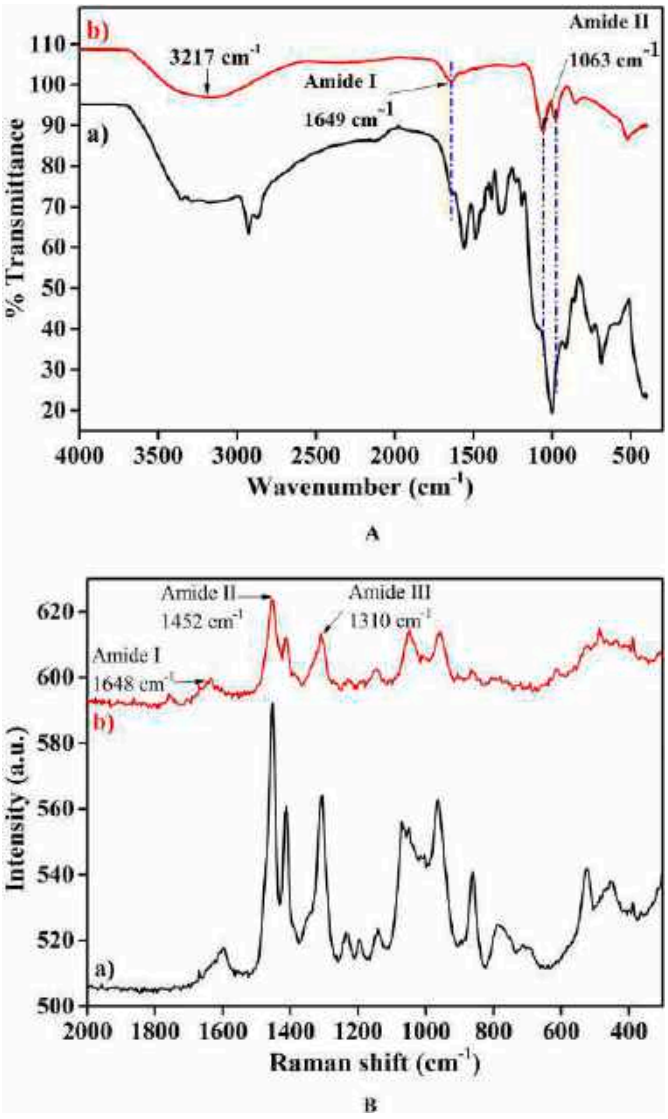

Fig. 1. A) FTIR spectrum of (a) APTMS/ITO electrode, and (b) anti-SP17/APTMS/ITO immunoelectrode. B) Raman spectra of (a) APTMS/ITO electrode, and (b) anti-SP17/APTMS/ITO immunoelectrode.

considered being the most convenient method to analyze amide bonds. Different amide bonds like amide I, amide II, and amide III are generally seen in the regions between 160 and 1680 cm^{-1}, 1480-1570 cm^{-1} and 1235-1300 cm^{-1}, respectively [40]. Fig. 1B (b) shows amide I, amide II, and amide III bonds at 1648 cm^{-1}, 1452 cm^{-1} and 1310 cm^{-1}, respectively, which confirmed the attachment of anti-SP17 onto the surface of the APTMS/ITO electrode.

3.3. Morphological characterization of the modified electrodes

Fig. 2 (A-D) demonstrates the AFM images to study morphological characteristics of the fabricated immunosensor and confirm stepwise changes performed on the sensing platform. Fig. 2A depicts the surface smoothness of the ITO electrode obtained after activation. Fig. 2B shows successful surface modification with APTMS as the AFM image represents the uniform distribution of APTMS, resulting in SAMs on the hydrolyzed ITO surface. The average roughness (RMS) values obtained after electrode surface modification with hydroxylation and APTMS were 2.85 nm and 6.08 nm, respectively. This confirms that highly ordered and dense SAMs is formed over the electrode surface. RMS value obtained after anti-SP17 immobilization was 118.11 nm on a 5 × 5 μm scale, confirming the change in electrode surface morphology, as represented in Fig. 2C. This increase in RMS magnitude also confirms the amide bond formation upon the APTMS modified electrode surface. Again, change in RMS value was obtained when non-binding sites (active terminal carboxyl groups) of the electrodes were blocked with BSA, and the RMS value obtained was 88.45 nm on a 5 × 5 μm scale.

3.4. Contact angle (CA) study

Sessile drop technique was employed for CA measurement to investigate the hydrophobicity or hydrophilicity behavior of the fabricated electrodes after each step-wise modification [Fig. 3 (a-d)]. As shown in Fig. 3 (a), Θ value is 81.0°, which indicates the hydrophilic nature of bare hydrolyzed ITO electrodes. After that, APTMS self-assembly onto the hydroxylated ITO electrode, Θ value was slightly decreased to 80.5° [Fig. 3 (b)], suggesting slight hydrophilic nature of the APTMS/ITO electrode, promoting a suitable platform for anti-SP17 antibodies immobilization. Further, the CA value was found to decrease, i.e., 31.0° [Fig. 3 (c)] and 18.3° [Fig. 3 (d)] after immobilization of bioactive molecules such as anti-SP17 and BSA molecules on APTMS/ITO electrode, indicating the increment in hydrophilic behavior of anti-SP17/APTMS/ITO and BSA/anti-SP17/APTMS/ITO immunoelectrode owing to the covalent association between the anti-SP17 and APTMS/ITO electrode. This hydrophilicity of the bio-electrode promotes significant enhancement in antigen (in PBS buffer) attachment, thereby improving the sensitivity of the immunosensor [35,37].

3.5. Experimental condition standardization

To increase the efficiency of fabricated immunosensor, certain experimental conditions are tuned such as APTMS volume, antibody concentration and incubation time, antigen incubation time, BSA concentration, the effect of redox species, and pH. These parameters are necessary to fabricate an immunosensor that is sensitive, stable, repeatable, and reproducible. Silane optimization is necessary as it provides the attachment sites for the biorecognition element. Therefore, five different APTMS volumes (1 μL, 5 μL, 10 μL, 15 μL, and 20 μL) were examined. The DPV current of 5 μL and 10 μL APTMS volumes were similar and higher than the current of 1 μL, 15 μL, and 20 μL APTMS volumes. Thus, 10 μL of APTMS volume was selected as the optimum value for functionalization due to economic sensor fabrication [Fig. 4 (a)]. Optimizing bio-recognition species quantity is also necessary to fabricate a successful biosensor with excellent performance. This factor contributes immensely to the detection capability of the immunosensor. The anti-SP17 quantity was tuned to get a maximum signal. Six different anti-SP17 concentrations from 10 to 60 μg mL^{-1} were tried, and the obtained results are shown in Fig. 4 (b). The DPV method was utilized to investigate the anti-SP17's optimum concentration, which is bounded to the APTMS/ITO electrode. It is observed in Fig. 4 (b), as the anti-SP17 concentration was increased from 10 to 50 μg mL^{-1}, peak current was also enhanced and got saturated at a concentration of 50 μg mL^{-1}. After that, no further increase in current intensity was obtained. The low concentration of anti-SP17 (10–40 μg mL^{-1}) induced a low signal, and the signals were the same in the increased concentration of anti-SP17 (50–60 μg mL^{-1}). Therefore, 50 μg mL^{-1} of anti-SP17 dilution was chosen to further immobilize the APTMS/ITO electrode. Additionally, bio-recognition species incubation time optimization is also necessary as it influences antibody immobilization efficacy. In this context, APTMS/ITO electrode was incubated with EDC: NHS activated antibodies (in PBS) for varying incubation hours, i.e., 1 h, 2 h, 3 h, 4 h, 5 h, 6 h, and 7 h. As the incubation time was increased from 1 to 5 h, peak current was also found to increase, suggesting this antibody binding time is insufficient. After that, as the time was increased further for 6 h and 7 h, peak current got saturated with the highest current value [Fig. 4 (c)], suggesting 6 h to be the most appropriate incubation time for binding bio-recognition molecule upon the sensing interface. Further, Fig. 4 (d)

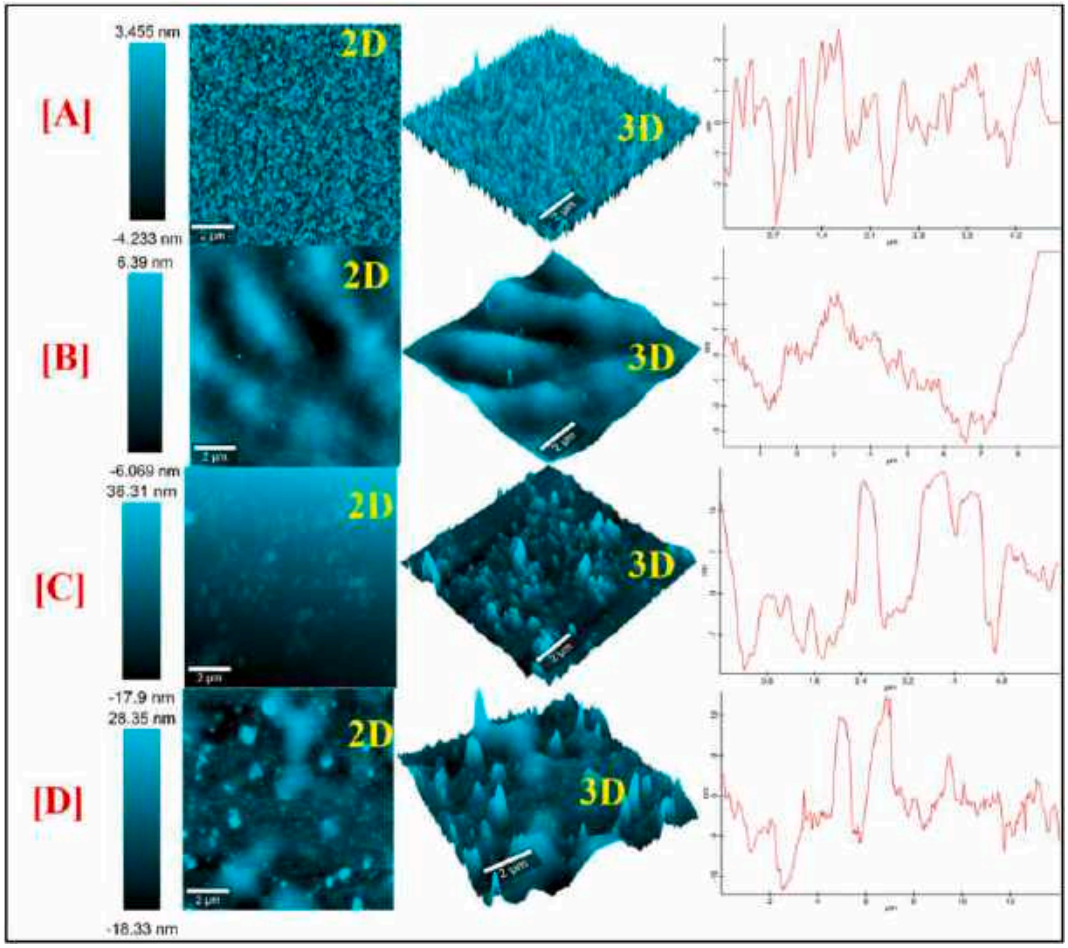

Fig. 2. AFM images of the immunosensor obtained after each immobilization step; ITO (A), APTMS/ITO (B), anti-SP17/APTMS/ITO (C), and BSA/anti-SP17/APTMS/ITO immunoelectrode (D).

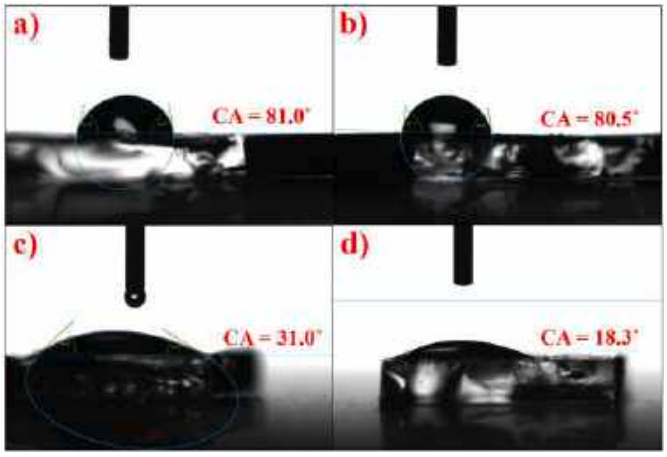

Fig. 3. Contact angle study of (a) bare ITO, (b) APTMS/ITO electrode, (c) anti-SP17/APTMS/ITO, and (d) BSA/anti-SP17/APTMS/ITO immunoelectrode.

shows changes in DPV peak current with varying BSA concentration (0.1 – 4%) on BSA/anti-SP17/APTMS/ITO immunoelectrode. As BSA concentration was increased, peak current was also enhanced but became saturated after 2%. Thus, 2% BSA concentration was considered most appropriate for subsequent experiments.

The effect of pH was studied on BSA/anti-SP17/APTMS/ITO immunosensor by measuring electrochemical response in an acidic and basic environment. This study has great significance as a change in pH can affect the activity and microstructure of the proteinaceous biological species such as Ab and BSA, immobilized onto the electrode surface. Thus, different pH response of PBS buffer was measured to analyze favorable pH. This study involves the electrochemical measurement of BSA/anti-SP17/APTMS/ITO immunoelectrode at 50 mVs^{-1} scan rate in an electrochemical cell containing $[Fe(CN)_6]^{3-/4-}$ as redox mediator in PBS (electrolyte) with varying pH range from 6.0 to 8.0. The conclusion drawn from the obtained results suggested that the surface charge of the proteinaceous biological species depends on the pH of buffer solution (i.e., utilized as electrolyte), which affects the electrochemical response [41]. Further, Fig. 4 (e) represents a graph where peak current (oxidation) is plotted v/s pH, and it depicts that maximum anodic peak current was attained at pH = 7.0. Thus, obtained results evidently suggest that proteinaceous molecule (antibody) is highly stable and active in its native form at neutral pH. The acidic and alkaline pH range causes denaturation of the protein-based biomolecules due to the H^+ or OH^- ions involvement on the amino acids of antibodies [42,43]. Although moderate pI adversely impacts the electrochemical response [41], it is a common assumption that biomolecules would display a significant current response at pI (isoelectric point). Therefore, considering this factor, subsequent electrochemical measurements have been carried out by utilizing a PBS buffer of pH = 7.0. The optimum results of experimental variables are summarized in Table 1.

3.6. Electrochemical characterization of the immunosensor

Electrochemical characterization of the fabricated immunosensor

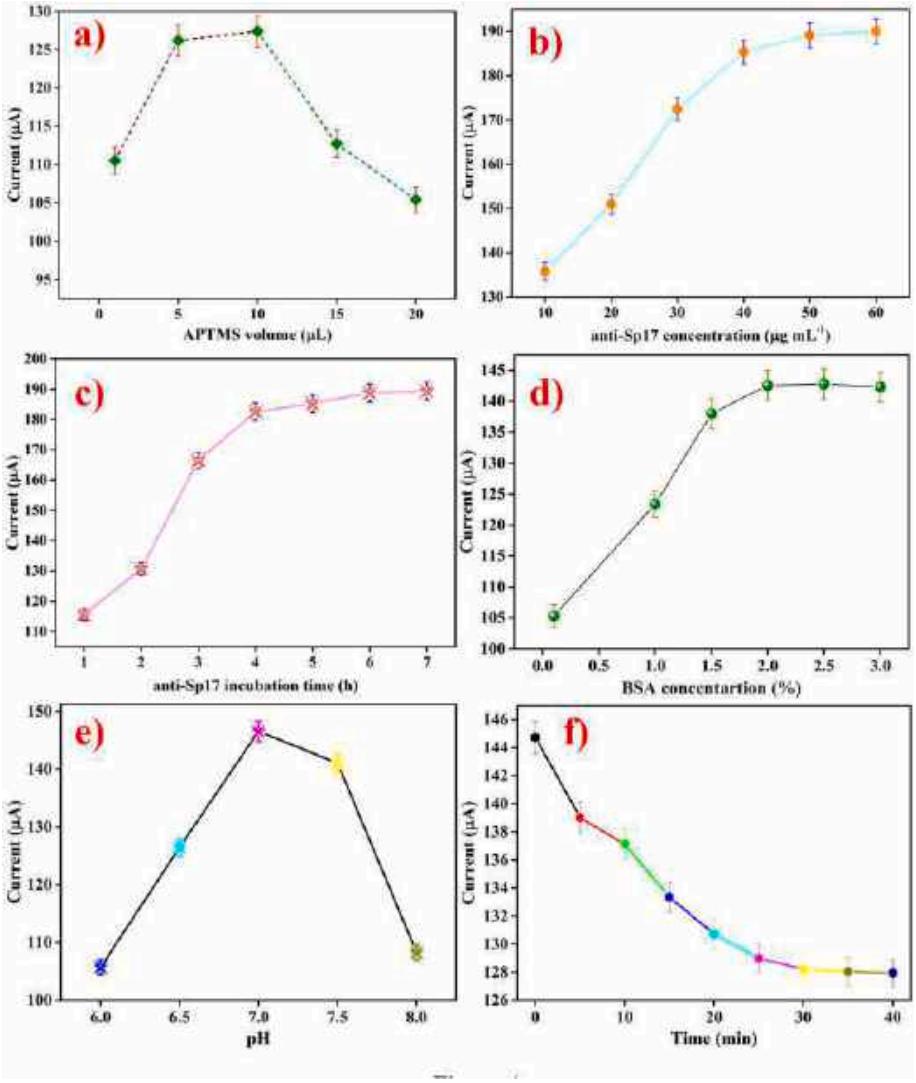

Fig. 4. Optimization of various parameters of a biosensor. (a) effect of APTMS volume on SAMs formation; (b) effect of different concentration of anti-SP17; (c) effect of incubation time of anti-SP17; (d) effect of different BSA concentration; (e) effect of pH onto immunoelectrode; and (f) effect of antigen-antibody (SP17-*anti*-SP17) interaction time.

Table 1
Optimized values of different experimental factors.

Variable	Tested	Selected
APTMS volume	1, 5, 10, 15, and 20 μL	10 μL
anti-SP17 concentration	10, 20, 30, 40, 50, 60 μg mL^{-1}	50 μg mL^{-1}
anti-SP17 incubation time	1, 2, 3, 4, 5, 6, and 7 h	6 h
BSA concentration	01, 0.5, 1, 2, 3, 4%	2%
anti-SP17-SP17 interaction time	5, 10, 15, 20, 25, 30, 35, and 40 min	30 min
pH	6.0, 6.5, 7.0, 7.5, 8.0	7.0

was conducted through CV and DPV measurement, as these methods are capable enough to study the redox behavior of an inorganic or organic chemical/biological species over a wide potential window. Effect of Ferri/ferrocyanide $[Fe(CN)_6]^{3-/4-}$ was studied using a three-electrode system where ITO coated glass substrate is selected as working electrode (WE), platinum works as an auxiliary/counter electrode (CE), and Ag/AgCl is taken as a reference electrode (RE). To study the effect of $[Fe(CN)_6]^{3-/4-}$, the cyclic voltammetry response of modified ITO electrodes were taken in two different conditions: first in 0.2 M phosphate buffer saline (PBS) and other is in PBS (0.2 M) containing $[Fe(CN)_6]^{3-/4-}$, at a scan rate of 50 mVs^{-1} as shown in Fig. 5 (a and b). The addition of Ferri/ferrocyanide in PBS resulted in enhancement of oxidation and reduction peak current in contrast to the poor signal obtained in the case of PBS without electroactive species ($[Fe(CN)_6]^{3-/4-}$). This is because electroactive species promote electron transfer and electronic amplification [37,44]. Therefore, subsequent electrochemical measurements were performed in 0.2 M PBS containing $[Fe(CN)_6]^{3-/4-}$ redox species.

CV and DPV are successful methods that can provide important information about current variation over the electrode surface [45,46]. Thus, these methods were employed to follow the proposed biosensor fabrication procedure and to study electrode (ITO) interface properties (curve i), APTMS/ITO (curve ii), anti-SP17APTMS/ITO (curve iii), and BSA/anti-SP17APTMS/ITO immunoelectrode (curve iv). The electrochemical CVs studies of the different modified surfaces were carried out in an electrochemical cell by using PBS as electrolyte with $[Fe(CN)_6]^{3-/4-}$, and currents were recorded at 50 mVs^{-1} within the potential range of −0.8 V to +0.8 V; as shown in Fig. 5c. Curve (i) depicted the lowest peak current of 254.67 μA along with redox peak couples, obtained in the case of hydroxylated ITO surface. The oxidation peak currents at the APTMS/ITO electrode increased drastically to 458.62 μA [curve (ii)] compared to OH^- modified ITO surface. APTMS increases peak current intensity due to the facilitated electron transport over the electrode surface. The activated amine groups increase peak currents as

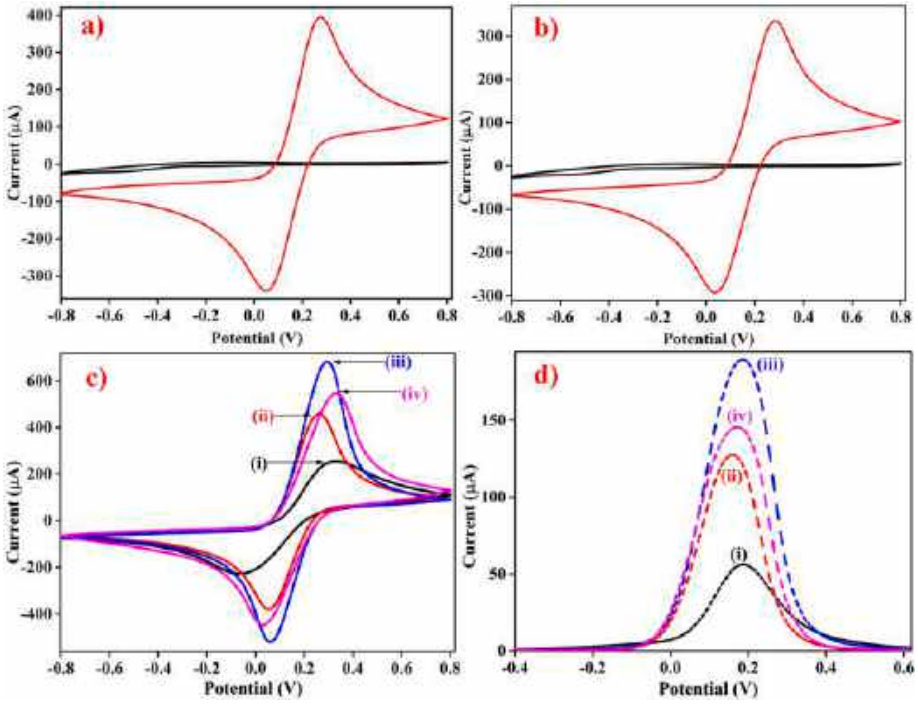

Fig. 5. Effect of Ferro-ferri on CV of APTMS/ITO (a) and BSA/anti-SP17/APTMS/ITO immunoelectrode (b); (c) CV and (d) DPV of ITO (curve i), APTMS/ITO (curve ii), anti-SP17APTMS/ITO (curve iii), and BSA/anti-SP17APTMS/ITO immunoelectrode (curve iv).

positively charged amino groups of APTMS facilitate the movement of negatively charged $[Fe(CN)_6]^{3-/4-}$. Further, an increase in current intensity was observed after anti-SP17 immobilization over the APTMS modified ITO electrode surface. These silane molecules act as mediators and promote a shorter electron tunneling distance between antibodies and the electrode. Therefore, the peak currents drastically increased to 682.37 μA [curve (iii)]. Additionally, free $-NH_3^+$ groups over anti-SP17/APTMS/ITO electrodes are non-binding sites and responsible for increasing electron transportation among anti-SP17/APTMS/ITO and APTMS/ITO electrodes [47,48]. The CV of BSA/anti-SP17/APTMS/ITO immunoelectrode exhibited decreased peak currents to 548.40 μA [curve (iv)] compared to anti-SP17/APTMS/ITO bioelectrode because of the non-conductive nature of proteinaceous BSA molecules and electron transfer is prevented towards the electrode surface. CV data were found in good agreement with the obtained DPV data thus, it confirmed a successful bio-sensing platform for biosensor fabrication [Fig. 5 (d)].

Fig. 6A and B shows the CV spectra of the scan rate study of APTMS/

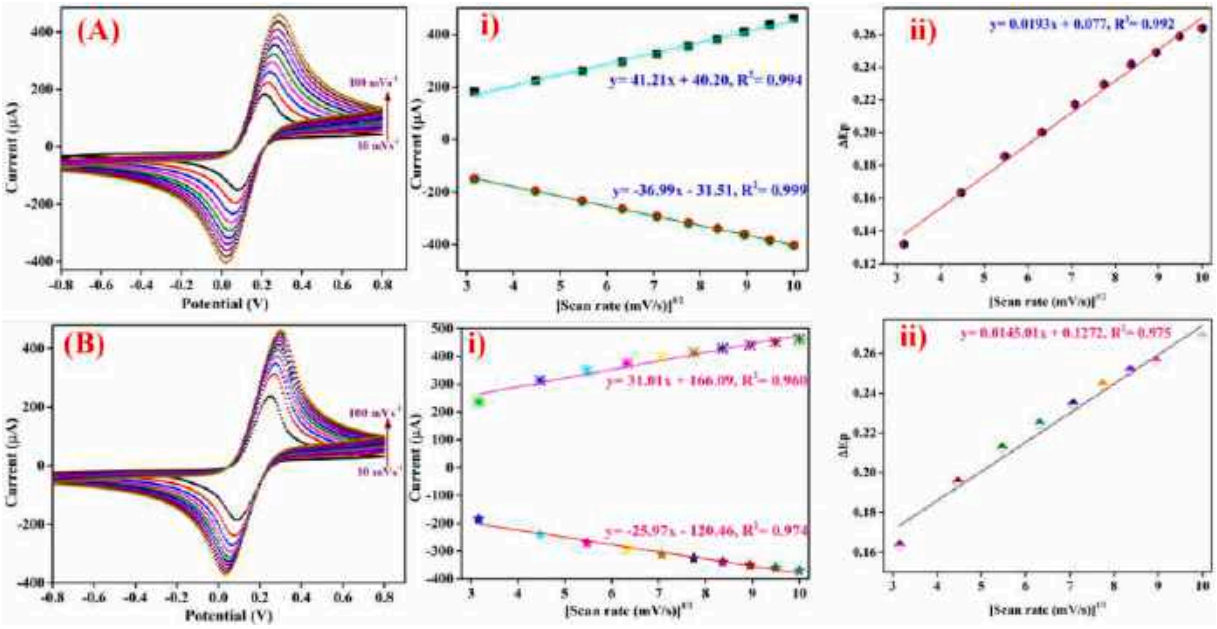

Fig. 6. Cyclic voltammetry (CV) of APTMS/ITO electrode (A) and BSA/anti-SP-17/APTMS/ITO immunoelectrode (B) as a function of scan rate (10-100 mVs^{-1}). The magnitude of oxidation and reduction current response as a function of scan rate (mV/s) [6A (i) and 6B (i)], and difference of cathodic and anodic peak potential (ΔEp) as a function of scan rate [6A (ii) and 6B (ii)].

ITO and BSA/anti-SP17/APTMS/ITO electrodes. The electrochemical response of both the electrodes was measured at the electrodes' surface interface, and electrolyte in a linear range of scan rate from 10 to 100 mVs^{-1} and within the potential window of −0.8 V to +0.8 V. The magnitudes of cathodic (Ipc) and anodic (Ipa) peak currents was found to increase linearly as the scan rate was increased from 10 to 100 mVs^{-1} for both the electrodes, thus, suggesting the diffusion-controlled electrochemical reaction [37,49].

Fig. 6A(i) and 6B (i) depict the variation in cathodic (Ipc) and anodic (Ipa) peak current v/s sq. root of scan rate. Results showed a linear increase in current magnitude with increasing scan rate for both the electrodes and follow Eqs. (1)–(4).

$$Ipa_{(APTMS/ITO)} = [41.21\ \mu A\ (s/mV) \times (\text{scan rate } [mV/s])^{1/2}] + 40.20\ \mu A,\ R^2 = 0.994 \quad \text{Eq.(1)}$$

$$Ipc_{(APTMS/ITO)} = -[36.99\ \mu A\ (s/mV) \times (\text{scan rate } [mV/s])^{1/2}] - 31.51\ \mu A,\ R^2 = 0.999 \quad \text{Eq.(2)}$$

$$Ipa_{(BSA/anti\text{-}SP17APTMS/ITO)} = [31.01\ \mu A\ (s/mV) \times (\text{scan rate } [mV/s])^{1/2}] + 166.09\ \mu A,\ R^2 = 0.960 \quad \text{Eq.(3)}$$

$$Ipc_{(BSA/anti\text{-}SP17APTMS/ITO)} = -[25.97\ \mu A\ (s/mV) \times (\text{scan rate } [mV/s])^{1/2}] - 120.46\ \mu A,\ R^2 = 0.974 \quad \text{Eq.(4)}$$

Moreover, with an increment in scan rate, the shift in peak-to-peak separation was observed, as shown in Fig. 6A (ii) and 6B (ii), suggesting the electrochemical process is quasi-reversible in nature [35,50]. A linear relationship was demonstrated by both APTMS/ITO and BSA/anti-SP17/APTMS/ITO electrodes, given in Eqs. (5) and (6), representing anodic (Epa) and cathodic (Epc) peak potential difference (ΔEp = Epa- Epc) as a function of the sq. root of scan rate. This indicated the facile transportation of electrons from the electrolyte towards the electrode surface.

$$\Delta Ep_{(APTMS/ITO)} = [0.0193\ V\ (s/mV) \times (\text{scan rate } [mV/s])^{1/2}] + 0.077\ V,\ R^2 = 0.992 \quad \text{Eq.(5)}$$

$$\Delta Ep_{(BSA/anti\text{-}SP17/APTMS/ITO)} = [0.0145\ V\ (s/mV) \times (\text{scan rate } [mV/s])^{1/2}] + 0.127\ V,\ R^2 = 0.975 \quad \text{Eq.(6)}$$

Randles-Sevcik equation is utilized for the estimation of diffusion coefficient (D) [51,52], at the interface of bioelectrode surface and an electrolyte containing $[Fe(CN)_6]^{3-/4-}$ as redox mediators:

$$Ip = (2.69 \times 10^5)\ C\ n^{3/2}\ D^{1/2}\ \upsilon^{1/2}\ A \quad \text{Eq.(7)}$$

Where I_p (I_{pa} or I_{pc}) represents electrodes peak current, n represents the number of electrons participating in the redox process, i.e., = 1 (in this electrochemical reaction), A represents the active area of the electrodes' surface, and its value is 0.25 cm^2 in this experiment, D represents diffusion coefficient (cm^2s^{-1}), C represents electrolyte redox species concentration which is 5 mM (here), and υ represents scan rate which is 50 mVs^{-1} for this experimentation.

The bio-electrode BSA/anti-SP17/APTMS/ITO demonstrated higher D value i.e., 1.93×10^{-11} $cm^2\ s^{-1}$ in comparison to APTMS/ITO electrode (0.216×10^{-11} $cm^2\ s^{-1}$) which indicated superior electron transfer at the electrolyte/electrode interface of the former electrode. This also suggests the excellent analytical efficiency of this immunosensor [53]. Thus, it can be concluded that the diffusion coefficient is dependent upon the working electrodes' surface area and electrolytic redox species concentration.

To calculate the value of the efficient and effective electroactive surface area (A_e) of the unmodified electrode APTMS/ITO and anti-SP17 and BSA modified BSA/anti-SP17/APTMS/ITO bioelectrode, the calculated value of D has been put in the following equation:

$$Ae = \frac{S}{(2.69 \times 10^5) n^3\ CD^{1/2}} \quad \text{Eq.(8)}$$

Where *S,* the slope of the linear curve obtained from the plot between Ipa versus square root of scan rate ($v^{1/2}$) [in $(mV/s)^{1/2}$]. The electroactive area (A_e) value of BSA/anti-SP17/APTMS/ITO bioelectrode is 1.36 mm^2, unveiling that it has more reactive sites per unit volume after biomolecules (i.e., BSA and antibody) immobilization. Therefore, this electrode is more suitable than the APTMS/ITO electrode with a 0.04 mm^2 electroactive area (A_e) value.

Additionally, the Brown-Anson equation [35] (mentioned in Eq. (9)), is used for the calculation of the surface concentration of electro-active ionic species (I* in mol cm^2) absorbed onto the electrode surface.

$$Ip = \frac{n^2F^2\gamma^*\ A\ \upsilon}{4\ R\ T} \quad \text{Eq.(9)}$$

Where I_p (I_{pa} or I_{pc}) denotes the peak current, A is the electrode surface area, γ is the concentration of electroactive species absorbed on the electrode surface, υ is the scan rate (Vs^{-1}), F- Faraday constant (96,485 C mol^{-1}), T- Room temperature (298 K), and R- Gas constant (8.314 $mol^{-1}\ K^{-1}$).

The estimated surface concentration (γ*) value of BSA/anti-SP17/APTMS/ITO bioelectrode obtained was 4.0×10^{-8} mol cm^2 which is higher than the APTMS modified electrode surface, i.e., (1.3×10^{-8} mol cm^2). The enhanced electrocatalytic behavior of the bio-electrode is because of the biomolecules and BSA presence which implies it be a successful biosensing platform.

The major contributing factors in electron transfer reversible kinetics are scan rate and heterogeneous electron transfer rate constant (K_s). The calculated K_s values for both APTMS/ITO electrode and BSA/anti-SP17/APTMS/ITO bioelectrode are 0.48 s^{-1} and 0.67 s^{-1}, respectively, using Laviron Equation [35]. The greater K_s value obtained in the case of bio-electrode indicated faster electron transfer among electrolytic redox species and the electrode surface.

$$Ks = \frac{mn\ Fv}{RT} \quad \text{Eq.(10)}$$

Where, m represents the potentials of peak-to-peak separation (V).

The calculated values of various electrochemical parameters; cathodic peak current (Ipc), anodic peak current (Ipa), charge transfer rate constant (K_s), diffusion coefficient (D), average surface concentration (γ*), electroactive surface area (A_e), of ionic species of the respective electrodes, were given in Table 2. The higher values of the interface kinetic parameters of the immunoelecrode compared to APTMS/ITO electrode suggest that biomolecules such as anti-SP17 and BSA are significantly involved in enhancing electron transfer at the interface of bioelectrode and electrolyte.

3.7. Analytical performance of the BSA/anti-SP17/APTMS/ITO biosensor

An antigen incubation time standardization was performed to determine the most appropriate binding time among antigen and antibody, subsequent study of fabricated biosensors' electrochemical response was carried out using optimized binding time. In this context, BSA/anti-SP17/APTMS/ITO immunoelectrode reaction was carried out with SP17 for the different binding duration (from 0 to 40 min), and the

Table 2
Projected values of electrochemical factors for electrodes.

Electrode	D ($cm^2\ s^{-1}$)	A_e (mm^2)	I*(mol cm^2)	K_s (s^{-1})	I_{pa} (A)	I_{pc} (A)
APTMS/ITO	1.93×10^{-11}	0.04	1.3×10^{-8}	0.48	$1.3626E^{-4}$	$1.564E^{-4}$
BSA/anti-SP17/APTMS/ITO	0.216×10^{-11}	1.36	4.0×10^{-8}	0.67	$4.2959E^{-4}$	$4.671E^{-4}$

DPV technique was employed to measure the changes in current values. Fig. 4f depicts the variation (decrease) in current with the change in time. It was observed that peak current was decreased till 30 min and beyond that, it got saturated. Thus, 30 min was considered the optimized binding time required for the reaction of SP17 with BSA/anti-SP17/APTMS/ITO immunoelectrode. Consequently, different concentration studies of SP17 biomolecule were carried out using 30 min incubation time, and the electrochemical response was taken respectively.

APTMS based immunosensor's analytical performance was evaluated by testing with varying SP17 concentrations with the help of the DPV technique, as represented in Fig. 7 (a and b). The electrochemical DPV technique is used for many purposes and is efficient enough to detect antigens from biosensing platforms. This method utilizes a three-electrode system in an electrochemical cell consisting of synthesized immunosensor as working electrode, platinum as an auxiliary electrode, and Ag/AgCl as a reference electrode. With standardized experimental conditions, the DPV spectra of the fabricated BSA/anti-SP17/APTMS/ITO immunoelectrode were measured upon incubation with different concentrations of SP17 antigen varies from 100 to 5000 pg mL^{-1} (100, 500, 1000, 1500, 2000, 2500, 3000, 3500, 4000, 4500 and 5000 pg mL^{-1}) using DPV technique at potential −0.2 to 0.5 V at a scan rate of 50 mVs^{-1}. Fig. 7 (a) displays the DPV response of immunoelectrode upon incubation with different concentrations of SP17 ranging from 100 to 5000 pg mL^{-1} for 30 min. It was found that as the concentration of SP17 increased from 100 to 5000 pg mL^{-1}, the peak current decreased linearly because of immune-complex formation among anti-SP17 and SP17 that prevented electron transfer [Fig. 7 (a)], and became constant after 5000 pg mL^{-1}. The reason behind the decrease in peak current after the addition of SP17 is a consequence of immune-complex formation between antigen and antibody, which is electrically insulating in nature and thereby preventing the electron transfer kinetics among immunoelectrode and electrolytic species $[Fe(CN)_6]^{3-/4-}$ [42,54]. This confirms the attachment of target SP17 over the surface of immunoelectrode, and the value of decrement in peak current corresponds to the amount of immune-complex on the immunoelectrode surface.

With optimized experimental conditions, excellent linearity was observed between change in current (ΔI) and SP17 antigen concentration in the range of 100–5000 pg mL^{-1}, as seen in Fig. 7 (c). The calibration plot between peak current v/s SP17 standard concentrations gives the following equation with a linear regression coefficient of 0.990.

$$Ip = [-0.003\ (\mu A\ mL\ pg^{-1}) \times \text{conc. of SP17 (pg } mL^{-1})] + 139.79\ \mu A,\ R^2 = 0.990 \quad \text{Eq.(11)}$$

The linear decrease in anodic peak current with a proportional increase in SP17 concentration concludes the immune-complex (antigen SP17 and anti-SP17 antibody) formation on the biosensing platform, i.e., BSA/anti-SP17/APTMS/ITO. Thus, providing fewer electro-active sites for free-electron transfer at the electrode surface, resulting in increased insulating layer thickness, is a reason for the decrease in the current [55, 56]. The fabricated biosensing electrode platform BSA/anti-SP17/APTMS/ITO showed a sensitivity of 0.013 μA mL pg $^{-1}$ cm^{-2} obtained by using the formula: the slope of calibration curve/-surface area (0.25 cm^{-2}) with linearity [i.e., regression coefficient (R^2)] of 0.990. The limit of detection (LOD) and limit of quantification (LOQ) were found as 70.07 pg mL^{-1} (3σ/m) and 233.57 pg mL^{-1} (10 σ/m), respectively (where σ is the standard deviation of intercept and m is the sensitivity of calibration plot). In addition, the immunosensor has a wide linear sensing range of 100–5000 pg mL^{-1}. The proposed immunosensor showed better results (detection limit and range) compared with the standard conventional technique known as ELISA kit (LOD = 16 pg mL^{-1} and linear range of 64–2400 pg mL^{-1}). The immunosensor demonstrated excellent sensitivity due to many contributing factors such as specific interaction of anti-SP17 antibody and SP17 antigen and highly ordered SAMs formation, suggesting that APTMS provides a strong matrix for antibody attachment *via* a well-known strong covalent bond, i.e., amide bond.

Further, the Hens-Wolf plot (SP17 concentration v/s SP17 concentration/current) was used for the calculation of association constant (K_a) value for BSA/anti-SP17/APTMS/ITO immunoelectrode, as given in Fig. 7 (d), and the value obtained was 123.15 pg mL^{-1}. K_a is dependent

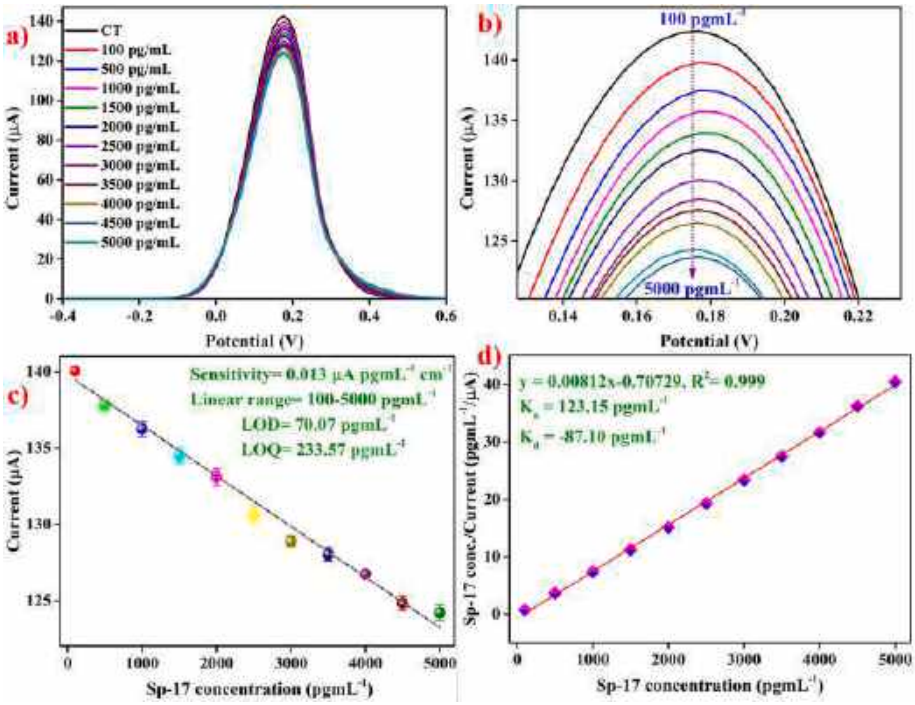

Fig. 7. (a) Electrochemical response analysis of BSA/anti-SP17/APTMS/ITO immunosensor versus concentration of GEN (100–5000 pg mL^{-1}); (b) the enlarged view of response study; (c) Calibration plot of BSA/anti-SP17/APTMS/ITO immunoelectrode between peak current v/s concentration of SP17; and (d) Hens-Wolf plot for BSA/anti-SP17/APTMS/ITO immunoelectrode.

upon certain immunosensor conditions such as attachment sites of biomolecules and how antibodies are attached to the surface of the electrode as it can cause conformational changes in the structure of antibodies present on the electrode surface. In this current work, the increased value of K_a represents constructive conformation of anti-SP17 and huge loading capacity on the electrode surface which directly contributes to the higher affinity of BSA/anti-SP17/APTMS/ITO immunoelectrode for SP17. Moreover, the determined dissociation constant (K_d) value was −87.10 pg mL^{-1}, demarcating a specific and robust affinity towards SP17. The calculation of K_a value was done from inverse values of slope acquired from the linear fitting of the Hanes-Wolf plot's, whereas the K_d value is obtained from the multiplication of K_a and the intercept value [37].

3.8. Control, specificity, reproducibility, repeatability, regeneration and stability studies

A control study was performed where the electrochemical response of the APTMS/ITO electrode was analyzed with the influence of SP17 concentration. DPV technique was utilized to study the change in current with a varying concentration range from 100 to 5000 pg mL^{-1} of SP17 biomolecules on the APTMS/ITO electrode, and obtained results are shown in Fig. 8 (a). This graph indicates no significant changes in ΔI values regarding the increasing concentration of SP17 biomolecules on the APTMS/ITO electrode. The conclusion drawn from the above results is that the electrochemical response obtained for BSA/anti-SP17/APTMS/ITO immunoelectrode and SP17 biomolecules is because of the immune-complex formation between anti-SP17 and SP17, whereas in the case of APTMS/ITO electrode, no reaction takes place with SP17 molecules.

The specificity test of the fabricated immunosensor was conducted by utilizing multiple control species. The interferent studies were performed on bioelectrode BSA/anti-SP17/APTMS/ITO using several human serum analytes such as glucose, urea, ascorbic acid, oxalic acid, uric acid, and in the presence of other cancer biomarkers like IL-8, TNF-α and CYFRA-21-1. Fig. 8 (b) shows significant variation in current intensity in the presence of SP17 alone and also in the presence of SP17 pre-mixed with various potential interferents as described above, resulting in antibody-antigen complex, confirming the specificity of the fabricated immunosensor. Moreover, the obtained % RSD (percentage relative standard deviation) value of the immunosensor was ~3.98%, which lies in an acceptable range. Since the sensor showed the selective response towards SP17 and mixture of proteins could not affect the SP17 signal, it is concluded that the fabricated BSA/anti-SP17/APTMS/ITO biosensing platform is highly specific for detecting SP17.

Reproducibility and repeatability are two vital parameters for practical utilization of immunosensors. Five different replicates of BSA/anti-SP17/APTMS/ITO immunoelectrode were prepared to investigate their reproducibility. The change in peak current response was monitored using the DPV technique while keeping the same experimental conditions [Fig. 8 (c)]. The reproducibility of immunoelectrode has also been examined through another electrochemical approach, i.e., cyclic voltammetry (CV), as shown in Fig. S1. CV also monitored the change in peak current response of immunoelectrode prepared at the same experimental conditions. Similarly, to investigate the repeatability of the immunoelectrode (BSA/anti-SP17/APTMS/ITO), six consecutive readings were taken using the DPV method at a specific concentration of SP17, data represented in Fig. 8 (d). The reproducibility and repeatability graph showed slight variation in peak current with % RSD of 0.99% and 0.47%, respectively. This value lies within an acceptable limit depicting good precision and capable enough to promote repeatable and reproducible outcomes.

Regeneration studies of BSA/anti-SP17/APTMS/ITO immunoelectrode were performed using acidic solution (HCl, 10 mM) to determine the electrode's reusability. This acidic treatment-based regeneration ability of the biosensor was tested by measuring the electrochemical response after anti-SP17 capture the SP17 on the electrode surface. The electrochemical response measured after four sequential regeneration processes of the fabricated immunosensor showed 75.73% of its initial response, indicating the biosensor can be reused four times [Fig. 9 (a)].

Further, the storage stability of fabricated immunoelectrode (BSA/anti-SP17/APTMS/ITO) was measured for ten week at an interval of one

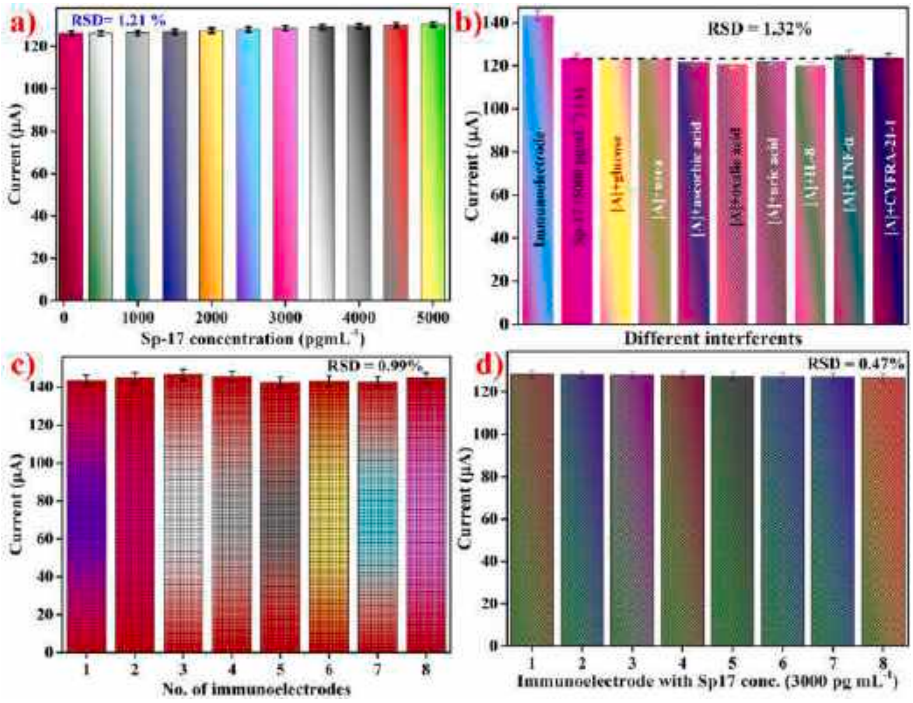

Fig. 8. (a) Control study of APTMS/ITO versus SP17 concentration (100–5000 pg mL^{-1}); (b) specificity analysis of BSA/anti-SP17/APTMS/ITO immunoelectrode; (c) Reproducibility study for BSA/anti-SP17/APTMS/ITO immunoelectrode prepared under similar condition; and (d) Repeatability study of BSA/anti-SP17/APTMS/ITO immunoelectrode.

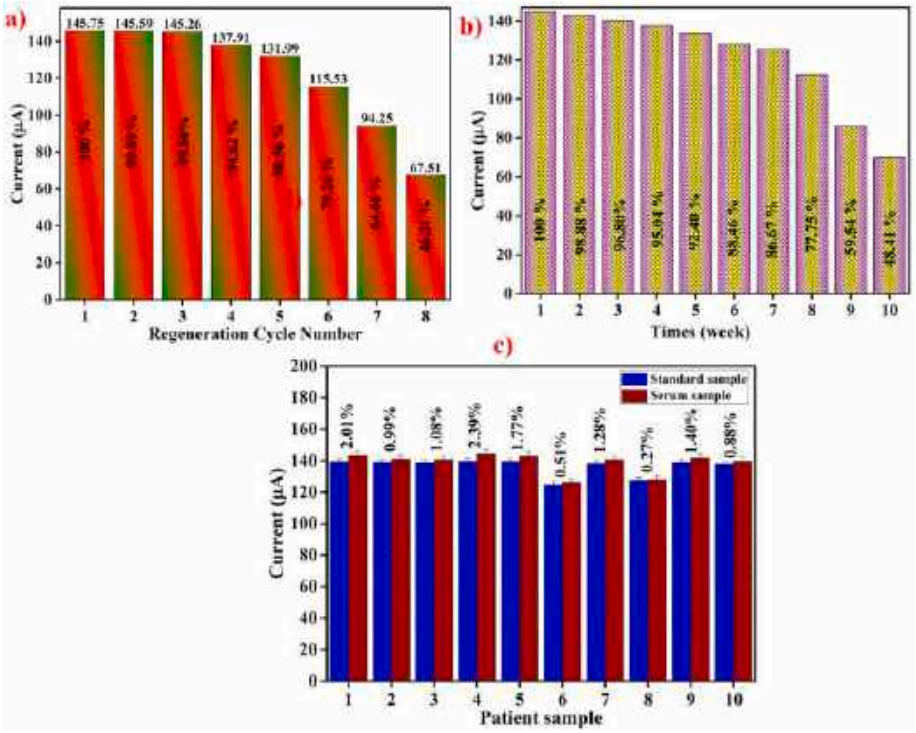

Fig. 9. (a) Effect of regeneration, signal response of the BSA/anti-SP17/APTMS/ITO immunoelectrode; (b) Shelf-life of the fabricated BSA/anti-SP17/APTMS/ITO immunoelectrode; and (c) Comparative analysis of current response with % RSD between the standard sample and cancer patient sample through fabricated BSA/anti-SP17APTMS/ITO immunoelectrode.

week. This study was conducted in 0.2 M PBS (pH 7.0, 5 mM redox species), and the experiment was carried out for 10 successive weeks [Fig. 9 (b)]. DPV technique was employed to know the changes in peak current response. This immune-electrode demonstrated up to 95% of the same current response for 6 weeks, after which peak current was reduced unexpectedly. Therefore, the immunoelectrode was found stable for 6 weeks at 4 °C.

3.9. Clinical sample analysis

Fabricated immunosensor applicability was measured by analyzing human samples obtained from the biological fluid, which is important [57–59]. For this purpose, patient real serum samples were tested for SP17 determination. We received blood samples of ten cancer patients with lesions or swelling in the mouth caused by tobacco consumption to determine SP17 antigen over several years. Blood samples were centrifuged at 3000 rpm for 10 min at 4 °C to get the serum from the supernatant, and aliquots were prepared to avoid freeze-thaw cycles. Serum was stored at −80 °C for further use. Patients' blood samples were collected from the All India Institute of Medical Sciences (AIIMS), New Delhi, India, and processed to acquire serum from them and analyzed *via* standard technique ELISA. We quantified SP17 concentration in triplicate by sandwich ELISA kit (CUSABIO; Catalog No.- CSB-EL022451HU). This kit was obtained with a pre-coated FITC anti-SP17 in microtiter wells. The steps were followed according to manual instructions, followed by colorimetric reaction and absorbance measurement at 450 nm using an ELISA plate reader. ELISA technique was used to obtain the series of SP17 concentrations for various serum samples to validate the results of the fabricated immunosensor. After that, the electrochemical response of fabricated BSA/anti-SP17/APTMS/ITO immunoelectrode was measured *via* DPV technique after 30 min incubation with serum samples. Subsequently, the current value obtained for real serum samples was correlated with standard samples of the same concentration. We found an excellent correlation between the magnitudes of the DPV current obtained for SP17 concentration in the real sample determined by ELISA and SP17 concentration in the standard sample [Fig. 9 (c) and Table 3]. In this case, the fabricated immunosensor showed less than 10% of % RSD, which means the biosensor could detect SP17 antigen in human serum samples with huge accuracy.

4. Conclusion

The proposed research work presents the development of a facile, label-free, and sensitive immunosensor for SP17 cancer biomarker detection based on the APTMS sensing platform. This is a novel biomarker (SP17) for cancer detection. The developed immunosensor was synthesized by anti-SP17 immobilization upon self-assembled (APTMS) modified ITO electrode surface. The amperometric signals of the immunosensor were decreased by increasing the concentration of the SP-17. The synthesized immunosensor could detect SP17 biomarker in a range from 100 to 5000 pg mL^{-1}, a limit of detection and limit of quantification of 70.07 pg $mL^{-1}$and 233.57 pg mL^{-1} respectively with a

Table 3
Determination of % relative standard deviation between peak current obtained for the standard sample and cancer patient samples of SP17 concentration determined through ELISA using BSA/anti-SP17APTMS/ITO immunoelectrode.

S. No.	SP17 concentration determined using ELISA (in pg mL^{-1})	Peak current (μA) obtained for standard SP17 samples	Peak current (μA) obtained with Patients serum samples	% RSD
1.	58.94	139.31	143.32	2.01
2.	206.74	138.83	140.78	0.99
3.	336.97	138.41	140.54	1.08
4.	25.26	139.42	144.21	2.39
5.	52.21	139.33	142.86	1.77
6.	4480.41	124.96	125.86	0.51
7.	450.50	138.04	140.56	1.28
8.	3677.62	127.57	128.06	0.27
9.	275.2	138.61	141.39	1.40
10.	523.96	137.79	139.52	0.88

sensitivity of 0.013 μA mL^{-1} pg^{-1} cm^{-2} having a good response time of 30 min, which was lower than ELISA. The SAMs-based amperometric immunosensor was employed to analyze human serum samples to determine the SP17 biomarker successfully, and the biosensor exhibited satisfactory recovery results. Therefore, we could conclude that the developed immunosensor is highly sensitive, stable, specific, and cost-effective for quantifying SP17 antigen concentration. As a result, this is a promising device for timely cancer detection at its earliest. This work opens a new window in designing and developing efficient label-free and disposable biosensing platforms for infectious, non-infectious, food pathogen, and airborne virus detection. Lastly, more efforts can be put to synthesize sensors with more defined SAMs to increase the efficiency and sensing range for cancer biomarkers detection. Despite fabrication of electrochemical immunosensors as analytical devices in detection of cancer biomarkers is very encouraging, but limitations still persist, showing challenges in development of biosensors. The fundamental challenge in the immobilization process of an electrochemical immunosensor is properly positioning and aligning the biological recognition element (i.e., immobilized antibodies or antigens) on a surface of the electrode. Further, one of the key challenges associated with biosensor's development is its stability [60,61].

Live subject statement

All experiments were performed in accordance Ethical Guidelines involving human subjects of and approved by All India Institute of Medical Sciences (AIIMS) and Jawaharlal Nehru University (JNU) Ethics Committee. Informed consents were obtained from human participants of this study.

Declaration of competing interest

The authors declare that they have no known competing financial interests or personal relationships that could have appeared to influence the work reported in this paper.

Acknowledgment

All the authors greatly acknowledge Advanced Instrumentation Research Facility (AIRF), JNU, to provide the facilities for characterization. PRS is thankful to the Biomedical Device and Technology Development (BDTD) sponsored project No.TDP/BDTD/49/2021 General, Department of Science and Technology (DST), New Delhi, India; and Indian Council of Medical Research (ICMR) sponsored project No. 34/13/2019-TF/Nano/BMS, New Delhi, India for funding. Amit K. Yadav recognized the Ministry of Education, Govt. of India for the Prime Minister Research Fellowship for the financial assistants. We thank Prof. (Dr.) Amit Dinda from All India Institute of Medical Sciences (AIIMS), New Delhi, India, for the scientific discussion.

Appendix A. Supplementary data

Supplementary data to this article can be found online at https://doi.org/10.1016/j.talanta.2022.123376.

References

[1] E.B. Aydın, M.K. Sezgintürk, Bioelectrochemistry 138 (2021) 107698.
[2] M. Chiriva-Internati, F. Grizzi, J.A. Weidanz, R. Ferrari, Y. Yuefei, B. Velez, M. H. Shearer, D.B. Lowe, E.E. Frezza, E. Cobos, J. Immunol. Methods 321 (2007) 86–93.
[3] M. Chiriva-Internati, Z. Wang, E. Salati, K. Bumm, B. Barlogie, S.H. Lim, Blood, J. Am. Soc. Hematol. 100 (2002) 961–965.
[4] M. Chiriva-Internati, Y. Yu, L. Mirandola, M.R. Jenkins, C. Chapman, M. Cannon, E. Cobos, W.M. Kast, PLoS One 5 (2010), e10471.
[5] L. Mirandola, J.A. Figueroa, T.T. Phan, F. Grizzi, M. Kim, R.L. Rahman, M. R. Jenkins, E. Cobos, C. Jumper, R. Alalawi, Oncotarget 6 (2015) 2812.
[6] A.K. Yadav, D. Verma, R. Sharma, A. Thakkar, P.R. Solanki, SPAST Abstracts 1 (2021).
[7] F.Q. Li, Q. Liu, Y.L. Han, B. Wu, H.L. Yin, BMC Cancer 10 (2010) 1–8.
[8] E.B. Aydın, M. Aydın, M.K. Sezgintürk, J. Pharmaceut. Biomed. Anal. 190 (2020) 113517.
[9] M. Aydın, E.B. Aydın, M.K. Sezgintürk, Biosens. Bioelectron. 126 (2019) 230–239.
[10] V. Espina, E.C. Woodhouse, J. Wulfkuhle, H.D. Asmussen, E.F. Petricoin III, L. A. Liotta, J. Immunol. Methods 290 (2004) 121–133.
[11] A.K. Yadav, D. Verma, N. Chaudhary, A. Kumar, P.R. Solanki, Mater. Lett. 308 (2022) 131239.
[12] C. Zhou, D. Liu, L. Xu, Q. Li, J. Song, S. Xu, R. Xing, H. Song, Sci. Rep. 5 (2015) 1–7.
[13] S.K. Arya, P. Estrela, Sensors 18 (2018) 2010.
[14] S.A. Soper, K. Brown, A. Ellington, B. Frazier, G. Garcia-Manero, V. Gau, S. I. Gutman, D.F. Hayes, B. Korte, J.L. Landers, Biosens. Bioelectron. 21 (2006) 1932–1942.
[15] M. Urdea, L.A. Penny, S.S. Olmsted, M.Y. Giovanni, P. Kaspar, A. Shepherd, P. Wilson, C.A. Dahl, S. Buchsbaum, G. Moeller, Nature 444 (2006) 73–79.
[16] N. Chaudhary, A.K. Yadav, J.G. Sharma, P.R. Solanki, J. Environ. Chem. Eng. 9 (2021) 106771.
[17] Y. Shen, T.T. Tran, S. Modha, H. Tsutsui, A. Mulchandani, Biosens. Bioelectron. 130 (2019) 367–373.
[18] R. Sista, Z. Hua, P. Thwar, A. Sudarsan, V. Srinivasan, A. Eckhardt, M. Pollack, V. Pamula, Lab Chip 8 (2008) 2091–2104.
[19] A.K. Yadav, D. Verma, A. Kumar, P. Kumar, P.R. Solanki, Mater Today Chem (2021) 100443.
[20] B.V. Chikkaveeraiah, A.A. Bhirde, N.Y. Morgan, H.S. Eden, X. Chen, ACS Nano 6 (2012) 6546–6561.
[21] Y. Li, Z. Zhang, Y. Zhang, D. Deng, L. Luo, B. Han, C. Fan, Biosens. Bioelectron. 79 (2016) 536–542.
[22] X.R. Cheng, B.Y. Hau, T. Endo, K. Kerman, Biosens. Bioelectron. 53 (2014) 513–518.
[23] E.B. Aydın, M.K. Sezgintürk, Trac. Trends Anal. Chem. 97 (2017) 309–315.
[24] C.M. Pandey, S. Dewan, S. Chawla, B.K. Yadav, G. Sumana, B.D. Malhotra, Anal. Chim. Acta 937 (2016) 29–38.
[25] I. Tiwari, M. Singh, C.M. Pandey, G. Sumana, Sensor. Actuator. B Chem. 206 (2015) 276–283.
[26] A. Sharma, D. Baral, H. Bohidar, P.R. Solanki, Chem. Biol. Interact. 238 (2015) 129–137.
[27] A.K. Yagati, J.C. Pyun, J. Min, S. Cho, Bioelectrochemistry 107 (2016) 37–44.
[28] E.B. Aydın, M. Aydın, M.K. Sezgintürk, Biosens. Bioelectron. 97 (2017) 169–176.
[29] L. Yang, Y. Li, Biosens. Bioelectron. 20 (2005) 1407–1416.
[30] M.B. Dos Santos, S. Azevedo, J. Agusil, B. Prieto-Simón, C. Sporer, E. Torrents, A. Juárez, V. Teixeira, J. Samitier, Bioelectrochemistry 101 (2015) 146–152.
[31] S. Komathi, A.I. Gopalan, K.P. Lee, Biosens. Bioelectron. 24 (2009) 3131–3134.
[32] W. Chu, Q. Zhou, S. Li, W. Zhao, N. Li, J. Zheng, Appl. Surf. Sci. 353 (2015) 425–432.
[33] N. Prabhakar, Z. Matharu, B. Malhotra, Biosens. Bioelectron. 26 (2011) 4006–4011.
[34] H. Törer, E.B. Aydın, M.K. Sezgintürk, Anal. Chim. Acta 1024 (2018) 65–72.
[35] A.K. Yadav, T.K. Dhiman, G. Lakshmi, A.N. Berlina, P.R. Solanki, Int. J. Biol. Macromol. 151 (2020) 566–575.
[36] G. Lakshmi, A.K. Yadav, N. Mehlawat, R. Jalandra, P.R. Solanki, A. Kumar, Sci. Rep. 11 (2021) 1–14.
[37] A.K. Yadav, D. Verma, G. Lakshmi, S. Eremin, P.R. Solanki, Food Chem. 363 (2021) 130245.
[38] A. Yadav, D. Verma, A. Kumar, P. Kumar, P. Solanki, Mater. Today 20 (2021) 100443.
[39] J. Kong, S. Yu, Acta Biochim. Biophys. Sin. 39 (2007) 549–559.
[40] T. Kitagawa, S. Hirota, Handbook of Vibrational Spectroscopy, 2006.
[41] W. Huang, A.K. Diallo, J.L. Dailey, K. Besar, H.E. Katz, J. Mater. Chem. C 3 (2015) 6445–6470.
[42] S. Kumar, S. Kumar, S. Tiwari, S. Augustine, S. Srivastava, B.K. Yadav, B. D. Malhotra, Sensor. Actuator. B Chem. 235 (2016) 1–10.
[43] D. Chauhan, A.K. Yadav, P.R. Solanki, Microchim. Acta 188 (2021) 1–11.
[44] S. Kumar, J.G. Sharma, S. Maji, B.D. Malhotra, Biosens. Bioelectron. 78 (2016) 497–504.
[45] H. Bagheri, R. Talemi, A. Afkhami, RSC Adv. 5 (2015) 58491–58498.
[46] Y. Chen, L.P. Mei, J.J. Feng, P.X. Yuan, X. Luo, A.J. Wang, Biosens. Bioelectron. 145 (2019) 111638.
[47] S. Kumar, S. Kumar, S. Tiwari, S. Srivastava, M. Srivastava, B.K. Yadav, S. Kumar, T.T. Tran, A.K. Dewan, A. Mulchandani, Adv. Sci. 2 (2015) 1500048.
[48] D. Chauhan, V. Nirbhaya, C.M. Srivastava, R. Chandra, S. Kumar, Microchem. J. 155 (2020) 104697.
[49] A. Kaushik, P.R. Solanki, M. Pandey, S. Ahmad, B.D. Malhotra, Appl. Phys. Lett. 95 (2009) 173703.
[50] N. Elgrishi, K.J. Rountree, B.D. McCarthy, E.S. Rountree, T.T. Eisenhart, J. L. Dempsey, J. Chem. Educ. 95 (2018) 197–206.
[51] D. Verma, A.K. Yadav, M.D. Mukherjee, P.R. Solanki, J. Environ. Chem. Eng. 9 (2021) 105504.
[52] D. Verma, D. Chauhan, M.D. Mukherjee, K.R. Ranjan, A.K. Yadav, P.R. Solanki, J. Appl. Electrochem. 51 (2021) 447–462.
[53] C. Singh, S. Srivastava, M.A. Ali, T.K. Gupta, G. Sumana, A. Srivastava, R. Mathur, B.D. Malhotra, Sensor. Actuator. B Chem. 185 (2013) 258–264.
[54] P.K. Gupta, Z.H. Khan, P.R. Solanki, J. Electrochem. Soc. 163 (2016) B309.
[55] S. Srivastava, V. Kumar, M.A. Ali, P.R. Solanki, A. Srivastava, G. Sumana, P. S. Saxena, A.G. Joshi, B. Malhotra, Nanoscale 5 (2013) 3043–3051.

[56] H. Bhardwaj, M.K. Pandey, G. Sumana, Microchim. Acta 186 (2019) 1–12.
[57] Y. Chen, X.Y. Ge, S.Y. Cen, A.J. Wang, X. Luo, J.J. Feng, Sensor. Actuator. B Chem. 311 (2020) 127931.
[58] E.B. Aydın, M. Aydın, M.K. Sezgintürk, Sensor. Actuator. B Chem. 325 (2020) 128788.
[59] E.B. Aydın, M. Aydın, M.K. Sezgintürk, Talanta 222 (2021) 121596.
[60] R.K. Sen, P. Prabhakar, N. Bisht, M. Patel, S. Mishra, A.K. Yadav, D.V. Venu, G. K. Gupta, P.R. Solanki, S. Ramakrishnan, Current Medicinal Chemistry, 2021.
[61] R. Jalandra, A.K. Yadav, D. Verma, N. Dalal, M. Sharma, R. Singh, A. Kumar, P. R. Solanki, Biomed. Pharmacother. 129 (2020) 110446.